44(1/2)

LIBRARY

JUL 28 1994

National Marine Fisheries Service
2570 Dole Street
Honolulu, Hawaii

気象庁欧文海洋報告

第44巻　第1−2号

THE OCEANOGRAPHICAL MAGAZINE

Vol. 44 Nos. 1-2

CONTENTS

SAKURAI K., T. MATSUBARA and H. MINAMI : The air-sea heat exchange in the sea south of Kyushu and around Japan 1

MIYAO T. : The fractal dimension analysis applied to the eddies in the Sea of Japan 13

KANO Y. and K. HAYASHI : Seasonal variation of carbon dioxide partial pressure in sea surface water around Japan 31

KANEKO I., Y. TAKATSUKI, T. TASHIRO and SUN X. : Characteristics of interannual variation of water temperature in the East China Sea and Yellow Sea 45

IMAI M., K. FUSHIMI, J. OHYAMA and K. OGAWA : Distributions and behaviors of chemical substances in the East China Sea and Yellow Sea 59

Published by the Japan Meteorological Agency

March. 1994

投稿規定

1　資　格

原則として，気象庁職員に限る。ただし，気象庁職員との連名の場合は，この限りではない。

2　論文及び報文（以下「論文等」という）の内容

未発表の欧文原稿で，海洋（物理・化学・生物・地質など）及び海上気象（波浪・海氷・海気相互関係など）に関する論文並びに気象庁における海洋・海上気象業務の活動，そのために開発された測器及び方法に関する報文など。

3　書き方

(1) 用語は，欧文（原則として英文）とする。

(2) 論文等には，英文（300語以内）及び和文（800字以内）の要約を付ける。要約は，方法・測器・実験・観測の結果・仮定・理論などの中味が読みとれるように留意し，なるべく指定の長さで簡潔に書く。

(3) 論文等の始めには，題名・著者名・所属機関名及び住所を明記する。和文の要約にも同様のことを（住所を除く）明記する。

(4) 原稿は，A 4 用紙にダブルスペースでタイプする。

(5) 図は，白紙又は青方眼紙に墨入れし，図及び図中の文字の大きさは，印刷の際の縮小率を考えて作成する。特に重要な図は，投稿者が大きさを指定する。（印刷の都合上，希望どおりにならないこともある）

(6) 図（写真を含む）及び表には，必ず説明を付ける。図の説明文は，別紙にタイプする。折り込みの図及び表は，なるべく避ける。図及び表のそう入箇所を本文の欄外に記入する。

(7) 数式は，2行取りに書き，数式の文字及び記号をはっきりと説明する。

(8) 論文等の中に文献を引用する場合は，「ALLEN (1927)」又は「(ALLEN, 1927)」のように書く。

(9) 引用文献は，最後にまとめて付け，著者名のアルファベット順に並べる。書き方は次のようにする。

ALLEN, W.E. (1927): Surface catches of marine diatoms and dinoflagellates made by U.S.A. Pioneer in Alaskan waters in 1923. *Bull. Scripps Inst. Oceanogr., Tech. Ser.* **1**, 39—48.

BUDYKO, M.I. (1956): *The heat balance of the earth's surface*. Hydrometeorological Publishing House, Leningrad, pp. 254.

VERONIS, G. and H. STOMMEL (1956): The action of a variable wind stresses on a stratified ocean. *J. Mar. Res.*, **15**, 43-75.

4　提出方法

投稿票を付け，本稿のほかにコピー（図及び表を含む）2部を添える。

5　送付先

気象庁海洋気象部海洋課

6　その他

論文等1編につき別刷り50部を著者に無料で送付する。

Oceanographical Magazine

編集委員長　Editor

宇　治　豪，T. UJI*

編集委員　Editorial Board

麻　生　　正，T. ASOH*
網　野　正　明，M. AMINO*
植　野　耕　治，K. UENO***
石　崎　　廣，H. ISHIZAKI**
大　山　準　一，J. OHYAMA*
金　子　郁　雄，I. KANEKO*
桜　井　邦　雄，K. SAKURAI*
重　原　好　次，K. SHIGEHARA**
西　沢　純　一，J. NISHIZAWA*
伏　見　克　彦，K. FUSHIMI*
上　橋　　宏，H. JOBASHI*

*気　象　庁　JAPAN METEOROLOGICAL AGENCY
**気象研究所　METEOROLOGICAL RESEARCH INSTITUTE
***気象大学校　METEOROLOGICAL COLLEGE

The Oceanographical Magazine
Vol. 44. Nos. 1-2. pp. 1 to 12, March 1994

The Air-sea Heat Exchange in the Sea South of Kyushu and around Japan

Keizo SAKURAI
Observations Department, Japan Meteorological Agency
1-3-4 Otemachi, Chiyoda-ku, Tokyo 100, Japan
Takeo MATSUBARA
Forecast Department, Japan Meteorological Agency
1-3-4 Otemachi, Chiyoda-ku, Tokyo 100, Japan
and
Hideto MINAMI
Kobe Marine Observatory
7-14-1 Nakayamate-dori, Chuo-ku, Kobe 650, Japan

(Received November, 1993; Accepted January 14, 1994)

Abstract: Latent and sensible heat fluxes from the sea surface in the sea south of Kyushu are estimated by meteorological data observed in November 1990 by four research vessels. Sum of latent and sensible heat fluxes from the sea surface in the Kuroshio area is about 40 % larger than that out of the Kuroshio area.

Oceanic heat transports are estimated by acoustic current-meter data and oceanographical data across the Tokara strait. Relations between oceanic heat transports and latent and sensible heat fluxes along the observation lines are studied. The area where larger values of latent and sensible heat fluxes are appeared roughly corresponds to the Kuroshio current axis.

Furthermore, latent and sensible heat fluxes around Japan are estimated based on the data obtained by four marine meteorological buoys from 1982 to 1991. Sum of latent and sensible heat fluxes in the east China Sea is 1.4 times larger than other three sea areas (that is, east of Japan, the Japan Sea and south of Shikoku). Especially, the latent heat flux in winter in the east China Sea shows the largest value among other seasons and other sea areas.

1. Introduction

The heat exchange through the sea surface is one of the important elements to control the atmospheric and the oceanic circulations, therefore it is very important to elucidate the mechanism and variation. The Kuroshio area is the greatest heat source area from the sea surface to the atmosphere in the north Pacific Ocean (IWASAKA and HANAWA, 1990).

One of the object to analyse the air-sea interaction is to elucidate the effect of the ocean on the weather and the climate, especially in the Kuroshio area over the east China Sea. Heat fluxes in the east China Sea around the Kyushu were analysed by SAKURAI (1990, 1992) and SAKURAI *et al.* (1991). Heat fluxes from south of Japan to the equator along the long observation line (137° E) were also analysed by MINAMI *et al.*(1993). In this report, not only the influence to heat fluxes by existence of the Kuroshio current but features of heat fluxes in the east China Sea compared to other sea areas are analysed. In

other words, the following four subjects are discussed based on the data of maritime meteorological and oceanographical observations around the Tokara strait in the sea south of Kyushu in November 1990, and on the data of four marine meteorological buoys between 1982 and 1991.

Four subjects are as follows.

1) The relation between air pressure pattern and heat fluxes from the sea surface.
2) The comparison between heat fluxes in and out of the Kuroshio area.
3) The relation between heat fluxes from the sea surface and oceanic heat transports.
4) Comparison of heat fluxes between in the east China Sea and in other sea areas.

2. Data and the method of analyses

2.1 Data

Research vessels "*Keifu-maru*", "*Chofu-maru*", "*Shumpu-maru*" and "*Seifu-maru*" of the Japan Meteorological Agency carried out observations in the sea south of Kyushu in November 1990. Fig. 1 shows the sea surface current distribution in November 1990 after the Japan Meteorological Agency.

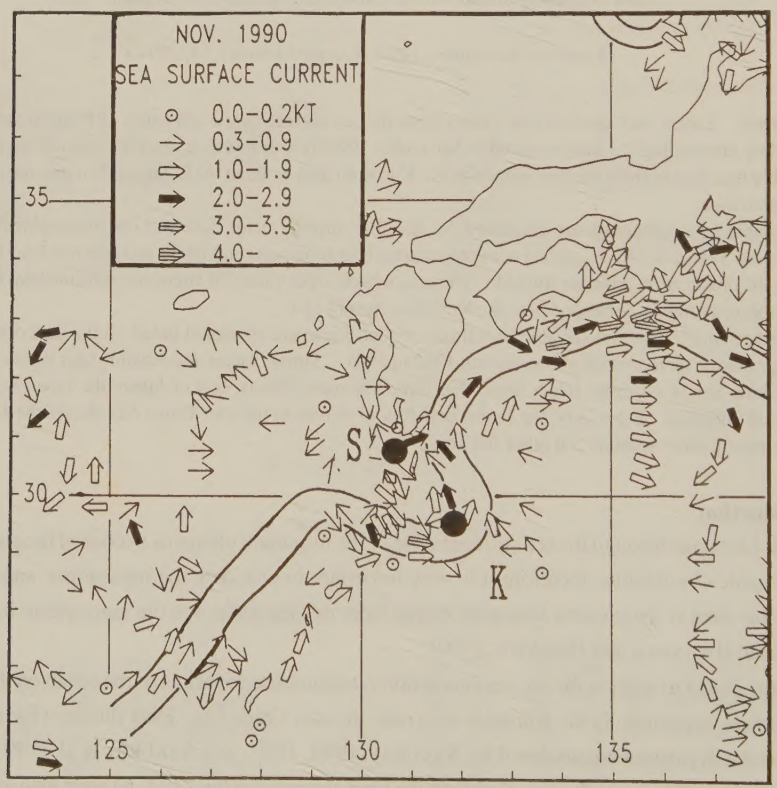

Fig. 1 Surface current distribution in November 1990 (after the Japan Meteorological Agency, 1990). S and K indicate the fixed observation stations.

The Kuroshio flows through the Tokara strait from the east China Sea into the sea south of Kyushu. *Shumpu-maru* and *Seifu-maru* observed at station S located out of the Kuroshio area (*i.e.* in the coastal region), and *Keifu-maru* observed at station K located in the Kuroshio area. The details of this observations and obtained data are shown in Table 1 and Fig. 2 (a).

Table 1 Observations and obtained data in November 1990 by four research vessels of the Japan Meteorological Agency. Maritime meteorological data were got 24 times by a day (hourly).

Type of observation	Station / line	Obtained data	Period	R/V
Fixed point observation	S	meteorological	Nov.18-26, 1990	*Shumpu-maru / Seifu-maru*
	K	meteorological and radiation	Nov.18-26, 1990	*Keifu-maru*
Line observation	Y	meteorological, ACM* and X-BT	Nov.27,07-17h, 1990	*Keifu-maru*
	TK	meteorological and CTD	Nov.25,15h-26,24h, 1990	*Chofu-maru*

ACM*: Acoustic subsurface Current-Meter, or so called ADCP

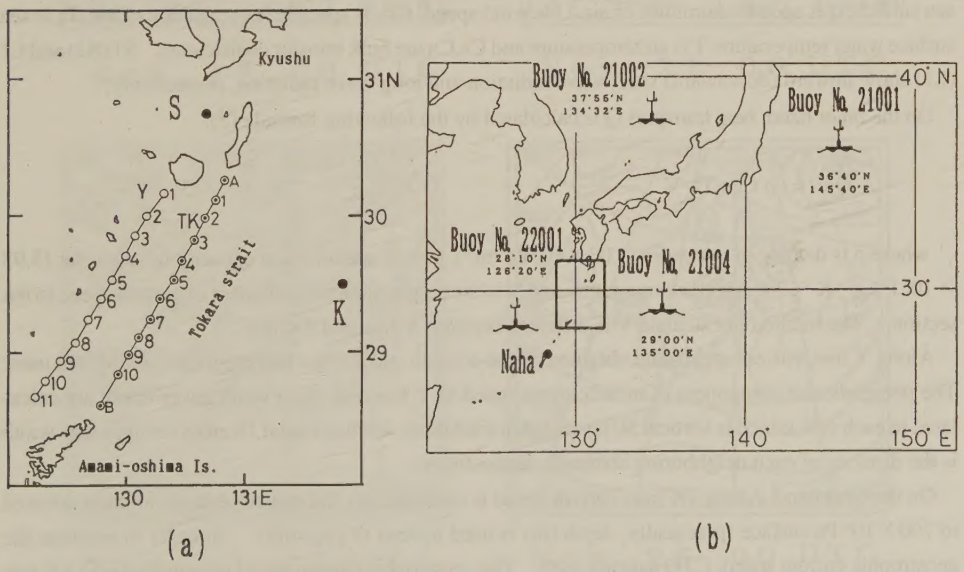

Fig. 2 a) Observation stations and lines. Marks "●", "○" and "⊙" indicate fixed stations S and K, X-BT observation stations and CTD observation stations, respectively. Y and TK lines are observation lines. Figure (b) shows the location of four marine meteorological buoys.

Data used for analyses of the subject 4 are three-hourly maritime meteorological observations from marine meteorological buoys around Japan (that is, east of Japan, the Japan Sea, south of Shikoku and the east China Sea) from 1982 to 1991. The location of these buoys is shown in Fig.2 (b).

2.2 The method of analyses

Latent and sensible heat fluxes from the sea surface are estimated by the bulk method using air temperature, dew point temperature, water temperature, air pressure and wind speed. Bulk transfer coefficients are calculated by the scheme suggested by KONDO (1975). The downward radiations of long wave and short wave are observed by the long wave radiometer and the pyranometer on board *Keifu-maru*, respectively. The upward short wave radiation is estimated from the downward short wave radiation using the constant value 0.1 as the reflecting coefficient. And the upward long wave radiation is calculated by the Stefan-Boltzmann's law using the constant value 0.95 as the emissivity to the black body.

The net heat budget HB through the sea surface and the net radiation RB are calculated as follows.

$$HB = \iota E + H + RB \quad (1)$$

$$\iota E = \iota \rho C_E (qs - q) U \quad (2)$$

$$H = \rho C_{PA} C_H (Ts - T) U \quad (3)$$

$$RB = S\uparrow - S\downarrow + L\uparrow - L\downarrow \quad (4)$$

where, upward heat flux (released from the sea surface) is indicated as positive values. ιE is latent heat flux, and H is sensible heat flux. ι is latent heat of water, ρ is air density, qs is specific humidity at the sea surface, q is specific humidity of air, U is wind speed, C_{PA} is specific heat capacity of air, Ts is sea surface water temperature, T is air temperature and C_E,C_H are bulk transfer coefficients. $S\uparrow$ ($S\downarrow$) and $L\uparrow$ ($L\downarrow$) show upward (downward) short wave radiation and long wave radiation, respectively.

On the other hand, heat transport Q is calculated by the following formula (5).

$$Q = \rho C_{PW} Tw V \quad (5)$$

where ρ is density of sea water (1.03×10^3 kg·m^{-3}), C_{PW} is specific heat capacity of sea water (3.93×10^3 J·kg^{-1}·K^{-1}), Tw is water temperature and V is the perpendicular component of current speed to the section. The method to calculate V is different between Y line and TK line.

Along Y line, current speed data obtained by the acoustic subsurface current-meter (ACM) are used. The perpendicular component of mean current speed to Y line and mean water temperature are calculated in each cell, which is vertical 50 layers (16m thickness) and horizontal 10 cross sections (the width is the distance of each neighboring stations), respectively.

On the otherhand, Along TK line, current speed is calculated by the geostrophic assumption referred to 700×10^4 Pa surface (practically, depth (m) is used instead of pressure). In order to estimate the geostrophic current speed, CTD data are used. The geostrophic current speed perpendicular to TK line and mean temperature are calculated in each cell divided by neighboring two stations horizontally and by so called standard depths vertically (JAPAN METEOROLOGICAL AGENSY, 1970).

3. Results of analyses

3.1 The relation between air pressure patterns and heat fluxes

Air pressure patterns on the surface weather map (Fig. 3) during the observation period are classified into following three types. The classification of these pattern is divided by the unit of a day.

Type Ⅰ : a low pressure in the Japan Sea (18-20th and 25-26th November)

Type Ⅱ : winter monsoon outbreak (21st November)

Type Ⅲ : covered by a high pressure (22-24th November)

Time sequences of meteorological elements (wind direction, wind speed, air pressure and sea surface temperature) at station K are shown in Fig. 4. Weak southerly wind blows during type Ⅰ. During type Ⅱ, strong northerly wind blows and air temperature falls down. During type Ⅲ, air temperature rises up gradually.

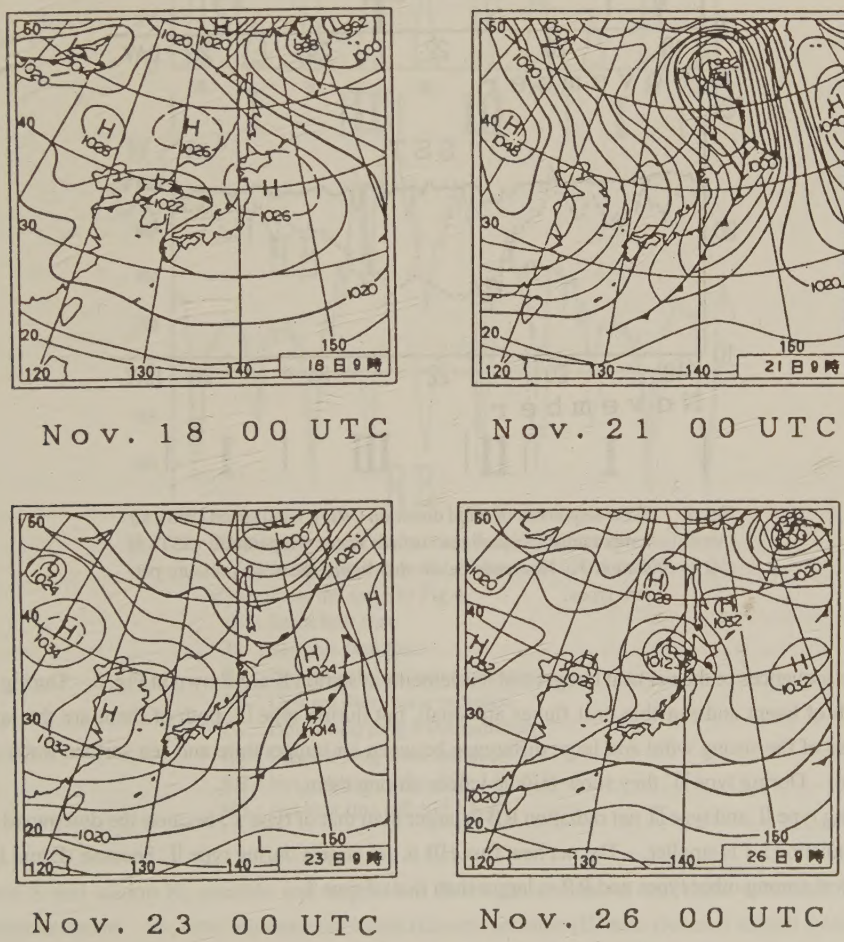

Fig. 3 Surface weather maps at every 00 UTC from November 18th to 26th (after "Kishou", 1990).

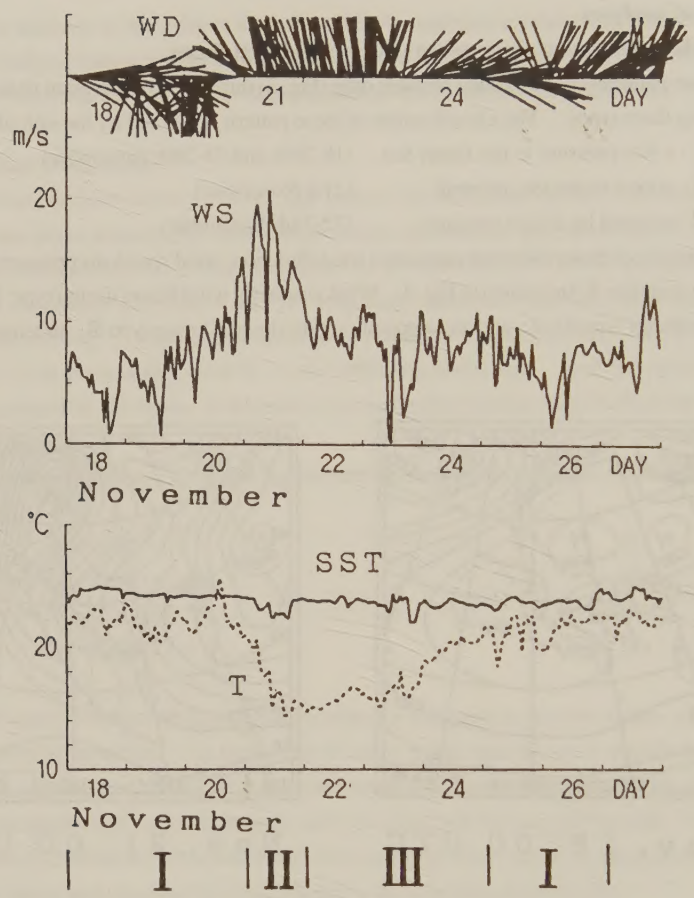

Fig. 4 Time sequences of wind direction (WD), wind speed (WS), air temperature (T) and sea surface water temperature (SST) at station K. Numerals below this figure show air pressure pattern types.

Time sequences of the net heat budget and its elements at station K are shown in Fig. 5. During type Ⅰ, both of latent and sensible heat fluxes are small, but during type Ⅱ, both of them are the largest beacause of the strong wind and large difference between air temperature and sea surface water temperature. During type Ⅲ, they show middle values among them.

During type Ⅱ and type Ⅲ net radiation RB is larger than that of type Ⅰ, because the downward long wave radiation L↓ is smaller. The net heat flux HB is the largest during type Ⅱ, because ιE and H are the largest among other types and RB is larger than that of type Ⅰ.

3.2 The comparison between heat fluxes in and out of the Kuroshio area

Station S locates out of the Kuroshio and station K locates in the Kuroshio area shown in Fig. 1. At

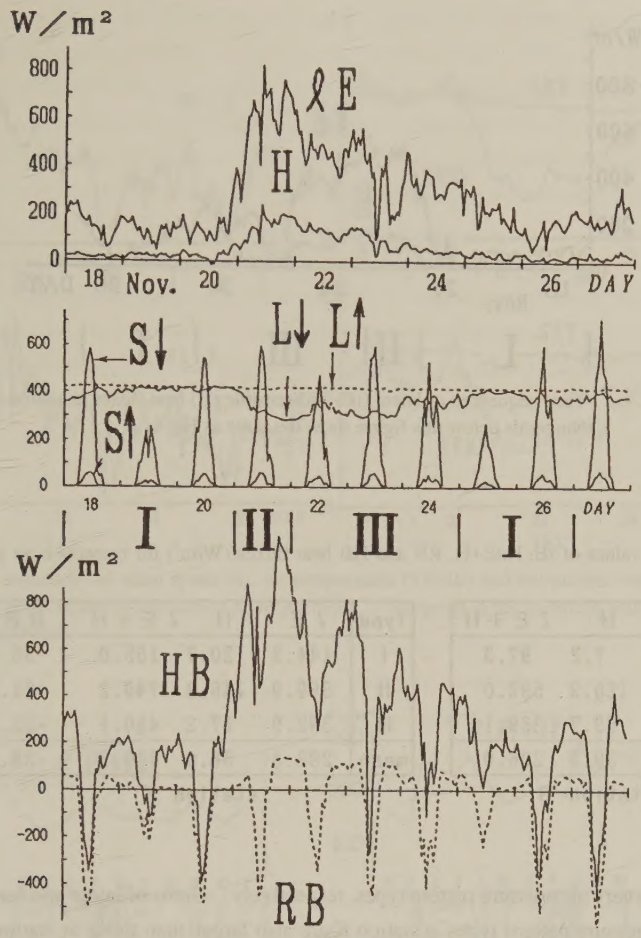

Fig. 5 Time sequences of the net heat budget and its elements (shown in followings) at station K. Numerals in the middle of this figure show the same as Fig.4.

ιE : latent heat flux
H : Sensible heat flux
S↓ : Downward short wave radiation
S↑ : Upward short wave radiation
L↓ : Downward long wave radiation
L↑ : Upward long wave radiation
RB : Net radiation (S↑−S↓+L↑−L↓)
HB : Net heat flux (ιE+H+RB)

station S and station K, sensible and latent heat fluxes are estimated, and those at station K were mentioned above. So, time sequences of latent (ιE) and sensible (H) heat fluxes at station S are shown in Fig. 6. Moreover, mean heat fluxes in every air pressure pattern types at station S and station K are shown in Table 2. Latent (ιE) and sensible (H) heat fluxes at station S are smaller than those at station

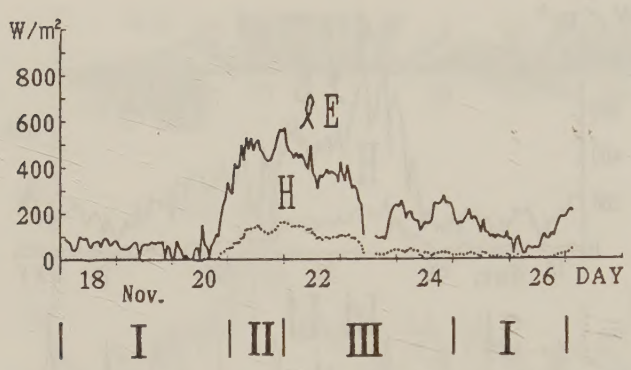

Fig. 6 Time sequences of latent (ιE) and sensible (H) heat fluxes at station S. Numerals below this figure show the same as Fig.4.

Table 2 Mean values of ιE, H,ιE+H, RB and HB heat fluxes (W/m^2) for respective air pressure pattern types.

Type	ιE	H	ιE+H
I	90.1	7.2	97.3
II	471.1	120.9	592.0
III	299.4	69.7	369.1
mean	196.7	39.3	236.0

station S

Type	ιE	H	ιE+H	RB	HB
I	144.3	20.7	165.0	-33.0	132.0
II	599.9	146.3	746.2	-21.4	724.8
III	392.9	87.2	480.1	-23.0	457.1
mean	282.3	58.0	340.3	-28.4	311.9

station K

K (see Fig. 5) in every air pressure pattern types, respectively. Sums of latent and sensible heat fluxes ιE+H of every pressure pattern types at station K are also larger than those at station S, *i.e.* during type I ιE+H at station K is 70 % larger than that at station S and during type II and type III at station K it is 20-30 % larger than that at station S. Generally, mean value of ιE+H at station K is about 40 % larger than that at station S.

In order to study above difference, time sequences of wind speed, sea surface water temperature and air temperature at station S and station K are shown in Fig. 7. There is not so remarkable difference between wind speed data at two stations, except for during type II. Also air temperature, there is almost no difference. However, sea surface water temperature at station K is about 2 degrees higher than that at station S throughout the observation period. This leads to the conclusion that latent and sensible heat fluxes show larger value due to the heat supply from the Kuroshio at station K located in the Kuroshio area than that at station S located in the coastal region.

3.3 The relation between heat fluxes and oceanic heat transports

Fig. 8 shows cross sections of oceanic heat transports along Y and TK lines shown in Fig. 2 (a), and changes of latent and sensible heat fluxes along each observation line. Heat transports in subsurface

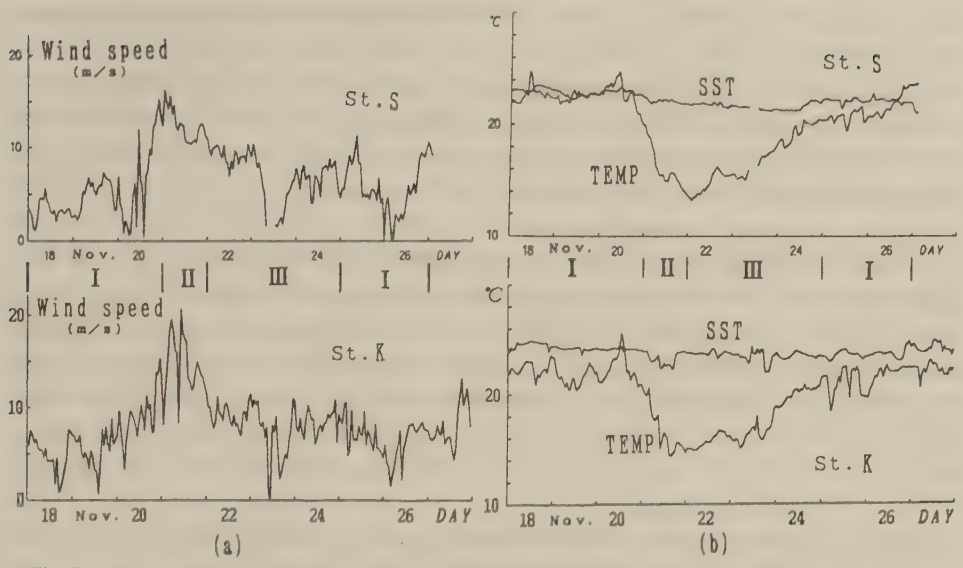

Fig. 7 Time sequences of wind speed (a), air temperature (TEMP) and sea surface water temperature (SST) (b) at station S and station K, respectively. Numerals in the middle of this figure show the same as Fig.4.

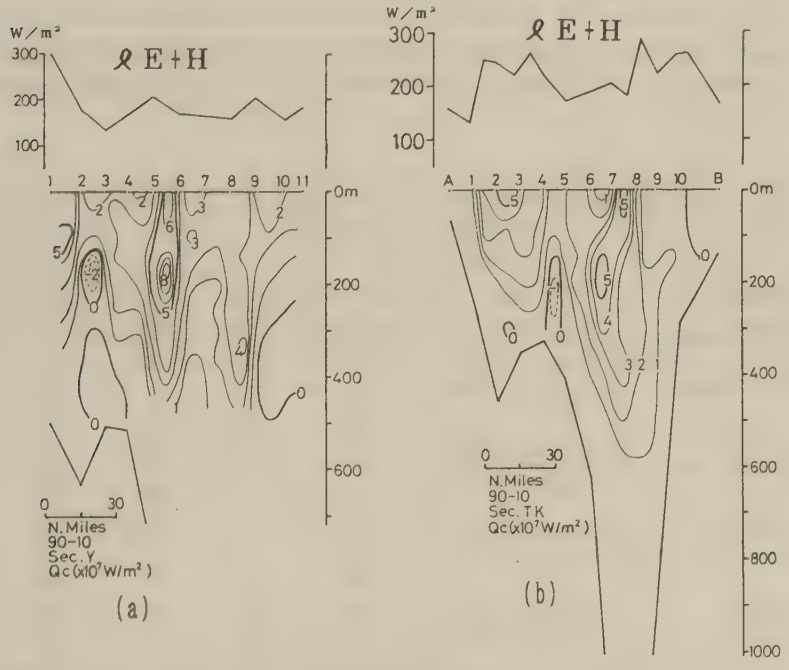

Fig. 8 Sum of latent and sensible heat fluxes (upper, ℓE+H) and the cross sections of the oceanic heat transport (lower) along Y line (a) and TK line (b), respectively.

layer show larger value at station 1-2, station 5-6 and station 6-8 on Y line, and at station 2-3 and station 7-8 on TK line.

The area where larger heat transport values appear corresponds roughly to regions where heat fluxes show larger values, but they do not exactly correspond. Because this analysis is based on only one-time observation data, if same observations are carried out many times, larger values of heat fluxes may be shown exactly around the Kuroshio current axis.

3.4 Comparison of heat fluxes between the east China Sea and other sea areas

Latent and sensible heat fluxes in east of Japan, the Japan Sea, south of Shikoku and the east China Sea are compared. Those values are calculated in each season shown in Table 3. Whole year is divided into Dec.-Feb. as winter, Mar.-May as spring, June-Aug. as summer and Sept.-Nov. as autumn. Latent and sensible heats were calculated by several authors (ex., in the Japan Sea: MAIZURU MARINE OBSERVATORY (1972), in the east China Sea: ISHII and KONDO (1987), in the north Pacific Ocean: IWASAKA and HANAWA (1990)). These estimation was used statistical and/or ship reported data, but buoy data has been got 8 times/day continuously.

Annual mean value of the sum of latent and sensible heat fluxes in the east China Sea is 1.4 times larger than that in other sea areas. That value in other three sea areas is almost the same value. Beacause main contribution to the net value comes from latent heat flux, and the largest latent heat flux observed in the east China Sea. Otherwise, the maximum sensible heat flux is estimated in the Japan Sea, and the second one is in the east China Sea.

From Table 3 latent heat flux shows seasonal variation, and the maximum latent heat appears in winter except in the Japan Sea. Especially the winter latent heat flux in the east China Sea is the largest among other seasons and other sea areas. Furthermore, the maximum (minimum) sensible heat flux

Table 3 Latent and sensible heat fluxes (W/m^2) of four marine meteorological buoys of the Japan Meteorological Agency around Japan. Those values are calculated as follows. Daily mean values are calculated from sensible and latent heat fluxes estimated from three hourly observation data. And then, seasonal mean values are calculated from monthly mean values through daily mean values.

Buoy	element	winter	spring	summer	autumn	annual
No.21001 (east of Japan)	latent heat	171	133	49	140	123
	sensible heat	85	41	4	38	42
	sum	256	174	53	178	165
No.21002 (the Japan sea)	latent heat	169	58	43	190	115
	sensible heat	112	23	3	56	49
	sum	281	81	46	246	164
No.21004 (south of Shikoku)	latent heat	219	100	86	166	143
	sensible heat	52	14	4	19	22
	sum	271	114	90	185	165
No.22001 (east China Sea)	latent heat	308	151	96	209	191
	sensible heat	105	40	5	34	46
	sum	413	191	101	243	237

appears in winter (summer) in all sea areas.

The reason why latent and sensible heat fluxes in the east China Sea are larger than those of other sea areas may be as follows (see Table 4). The difference between sea surface water temperature and air temperature (Ts-T), and the defference between specific humidity at the sea surface and air specific humidity (qs-q) are larger than those of other sea areas or almost the same. These larger differences are caused by the warmer sea surface due to the existence of the Kuroshio current and the dry and cold winter monsoon which generally blows from the continent.

In order to compare latent and sensible heat fluxes with solar radiation in the east China Sea, solar radiation observed at Naha which locates southeastern of the buoy (see Fig. 2 (b)) is used. Daily mean net solar radiation in January at Naha is 8.4 MJ/m^2 (that is 97 W/m^2) according to the Japan climatic table. Sum of latent and sensible heat fluxes by the bulk method at the buoy in the east China Sea is released to the atmosphere 4.2 times larger than the absorption of solar radiation in January.

Table 4 Seasonal mean values of marine meteorological elements at four buoys.
T: air temperature Ts: sea surface water temperature U: wind speed
q_s-q: difference of the specific humidity at sea surface and specific humidity of air

Buoy	element	winter	spring	summer	autumn
No.21001 (east of Japan)	T (℃)	7.0	13.4	21.6	17.4
	Ts (℃)	11.7	16.0	21.9	20.0
	q_s-q (g/kg)	3.8	3.8	2.1	4.1
	U (m/s)	9.7	7.7	5.5	7.2
No.21002 (the Japan sea)	T (℃)	4.6	9.7	21.9	16.4
	Ts (℃)	11.5	11.4	22.3	20.4
	q_s-q (g/kg)	4.3	2.0	2.0	6.0
	U (m/s)	8.0	6.0	4.9	6.7
No.21004 (south of Shikoku)	T (℃)	17.0	19.8	26.6	24.6
	Ts (℃)	20.8	20.9	27.0	26.3
	q_s-q (g/kg)	6.8	3.7	4.0	6.5
	U (m/s)	7.4	6.5	6.0	6.3
No.22001 (east China Sea)	T (℃)	14.4	19.2	27.1	23.4
	Ts (℃)	21.1	22.0	27.7	26.0
	q_s-q (g/kg)	8.3	4.9	4.4	6.9
	U (m/s)	8.0	6.6	6.1	7.0

References

ISHII,T. and J.KONDO (1987) : Seasonal variation of the heat balance of the East China Sea. *Tenki*, 34, 517-415.

IWASAKA,N. and K.HANAWA (1990) : Climatologies of marine meteorological variables and surface fluxes in the North Pacific computed from COADS. *Tohoku Geophys. Journ.*, 33, 185-239.

JAPAN METEOROLOGICAL AGENCY (1970) : Water sampling and water temperature measurement. 9-54. The guide of the oceanographical observation.

KONDO,J. (1975) : Air-sea bulk transfer coefficients in diabatic conditions. *Report of National Res. Inst. Disaster Prev.*, 10, 41-65.

MARITIME METEOROLOGICAL DIVISION, MAIZURU MARINE OBSERVATORY(1972) : Marine Meteorological Study of the Japan Sea. *Technical report of the JMA*, 80, 1-116.

MINAMI,H., Y.TAKATSUKI and T.MATSUBARA (1994) : The heat budget around Japan and along 137° E observation line. *Umi to Sora*, 69, 231-244.

SAKURAI,K. (1990) : A research on the heat balance in the oceanic mixed layer in the western sea area of Kyusyu. *KER annual contribution*, 1988. 206-215.

SAKURAI,K., H.NAKANE and Y.HARAGUCHI (1991) : The heat balance of the oceanic mixed layer in the sea north of Kyusyu. *KER annual contribution*, 1989. 173-181.

SAKURAI,K. (1992) : The air-sea heat exchange in the sea south of Kyusyu. *KER annual contribution*, 1990. 121-132.

九州南海上及び日本周辺における海気熱交換

櫻井 敬三(気象庁観測部)・**松原 竹男**(気象庁予報部)・**南 秀人**(神戸海洋気象台)

九州南海上における潜熱・顕熱フラックスを，4観測船によって1990年11月に行われた観測の気象データによって見積もった．黒潮海域における潜熱・顕熱フラックスの和は，黒潮域外におけるより約40%大きい．

トカラ海峡を横切る海洋熱輸送量を，表層海流計及び海洋データから見積もった．観測船上における海洋熱輸送と潜熱・顕熱フラックスの関係を調べた．潜熱・顕熱フラックスのより大きい値を示す海域は，ほぼ黒潮流軸に一致する．

さらに，日本周辺の潜熱・顕熱フラックスを，1982年～1991年までの4海洋気象観測ブイにより得られたデータから見積もった．東シナ海における潜熱・顕熱フラックスの和は，他の3海域（本州東方，日本海，四国南方）におけるよる1.4倍大きい．特に，東シナ海における冬の潜熱フラックスは，季節中最大で，全ての海域中で最大である．

The Oceanographical Magazine
Vol. 44. Nos. 1-2. pp. 13 to 30, March 1994

The fractal dimension analysis applied to the eddies in the Sea of Japan

Takashi MIYAO

Maizuru Marine Observatory

901 Shimofukui, Maizuru 624, Japan

(Received November 13, 1993 ; Accepted January 14,1994)

Abstract : The method of the fractal dimension analysis is applied to the zonal distribution of the sea surface temperature extracted from the NOAA images and to the time sequence of the coastal water temperature observed at some stations around the Sea of Japan in order to estimate the characteristic spatial/temporal scale of eddy fields.

The dominant diameter of warm eddies is estimated to be from 50 to 70 km in the southern region and larger than 200 km in the northern cold water region, respectively. This diameter has a tendency which becomes larger in the cooling season in the regions south of the Polar Front. This can be explained by means of the vertical mixing process in the cooling season which reveals the subsurface field to the surface.

The characteristic period of the alternation of the coastal water temperature is estimated commonly to be three weeks around the Sea of Japan. On the other hand, the period caused by meteorological conditions has a tendency which becomes longer at higher latitude.

The characteristic speed can be derived from the characteristic spatial/temporal scales. It is shown, however, that the value is not always coincident with the propagation speed of the warm eddy which is obtained from the monthly mean analysis of the oceanographic conditions.

1. Introduction

The Sea of Japan is characterized by its peculiar structure. The surface layer is divided into the northern part and the southern part with the Polar Front, which lies nearly along the 40° N parallel. The northern part is covered with the cold water almost all the year around. In the southern part, the warm/cold eddies, which appear almost in the entire region, make the oceanographic conditions complex.

Therefore, those who investigate the oceanographic conditions of the Sea of Japan are always interested in the warm/cold eddies. The 10-day or monthly analytical maps of the oceanographic conditions have been often used in order to pursue the warm/cold eddies. Furthermore, many of the investigations on the warm eddies have described about their behavior and the process of mixing between the warm and the cold waters.

MINAMI and ANDO (1982), who applied the method of "Structure Function" to the concurrent oceanographic observational data, indicated that the spatial scale and the strength of the warm eddies are different between the northern part and the southern part of the Sea of Japan. MATSUYAMA *et al.* (1990) tried to explain the reason why the dominant spatial scale of warm eddies is 100 km by the

baroclinic Rossby wave theory. ISODA and NISHIHARA (1992) pointed out that there are several regions where the warm eddies tend to be stationary.

NISHIYAMA *et al.* (1990) suggested that the cooling of the warm and saline eddies which move into the northern cold water region causes the formation of the Japan Sea Proper Water. ISODA *et al.* (1992) clarified that the doughnut-like flow structure around the warm eddy above the Yamato Rise play an important role in the northward transport of warm and saline water in summer.

However, the horizontal distributional maps of the water temperature which are used in many of these investigations on the eddies cannot help being smoothed out in a certain sense. First, some data are omitted if they do not coincide with neighbouring data. Also, when the grid point values are used, they represent the mean temperature of regions greater than the grid size. Moreover, since the spatial intervals of the observational data are usually larger than several ten kilometers, the phenomena smaller than that can be hardly analyzed.

Most of the past investigations have been obliged to treat the phenomena larger than that. Inevitably, the smoothed distributional maps of the temperature have been used to explain the mixing process at the boundary between the two different waters. It is unlikely, however, that any significant mixing are brought about at such smooth boundaries.

It can be easily found that the sea surface temperature (SST) field always has a random minute structure almost everywhere. The zonal SST distributions taken out from the NOAA satellite AVHRR image data on April 20th, 1992, are shown in Fig. 1. There are several gaps of the SST larger than 1 $^{\circ}$C between pixels next to each other. Since the width of the pixel is 2.44 km at the latitude of 35° N, the spatial scales of these gaps are too small to be detected by traditional oceanographical observations. Furthermore, the NOAA images show that the boundary between the warm and the cold waters are always complex (see Plates 1). This complex minute structure is considered to be a nest-set-like structure, and is the so called "fractal structure".

The "length" of the fractal curve is strikingly longer than that of the smooth curve along it. As might be expected, the mixing process at fractal boundaries could be prompt and effective enough to cause the formation of some water masses.

So, it is neccessary to study the behavior of eddies and the structure of the boundaries between the different water masses for the purpose of the elucidation of the mixing process. In this paper, the "Fractal Dimension Analysis" method is applied to the SST data taken out from the NOAA images in order to evaluate the characteristic spatial scale of the SST field in the Sea of Japan. Also, the similar method is applied to the characteristic time scale of the SST variations around the Sea of Japan. Then, the correspondance between the behavior of the warm eddies and the characteristic scales is discussed with some examples.

2. The method of "Fractal Dimension Analysis"

The characteristic temporal scales of the given time sequence data can be analized, for example, with the FFT (Fast Fourier Transformation) method. The FFT method is always used under the implicit assumption of the continuity and the periodicity of the phenomena. But the assumption might not be always valid, because many of the natural phenomena can hardly be represented by continuous functions of time and does not have any periods. Consequently, the method based on the fractal dimension

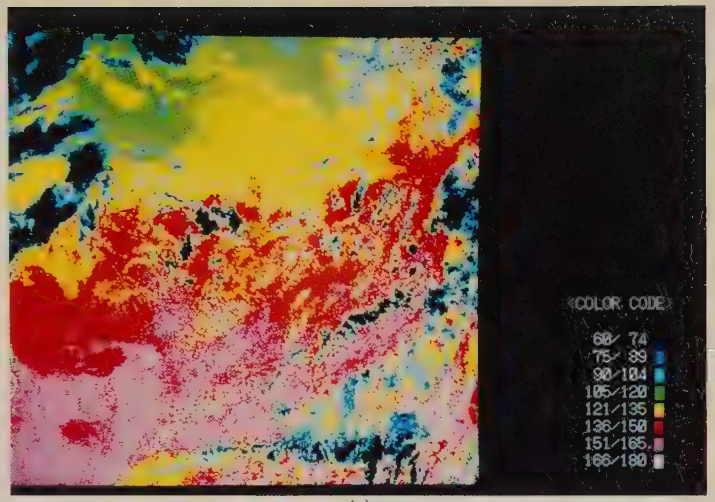

(a)

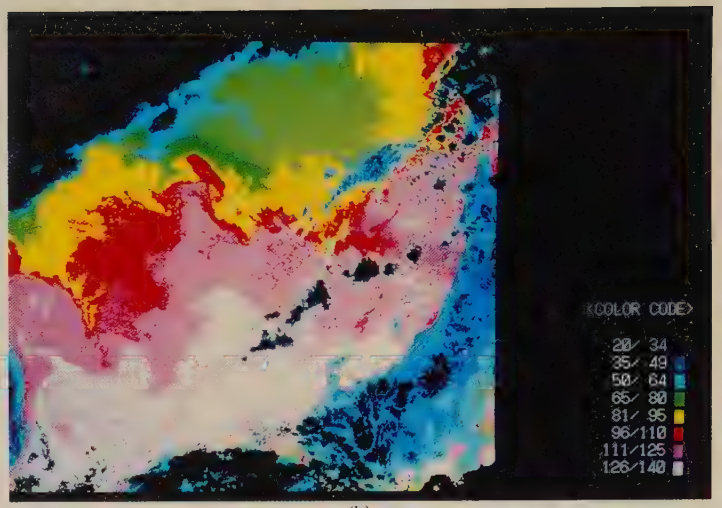

(b)

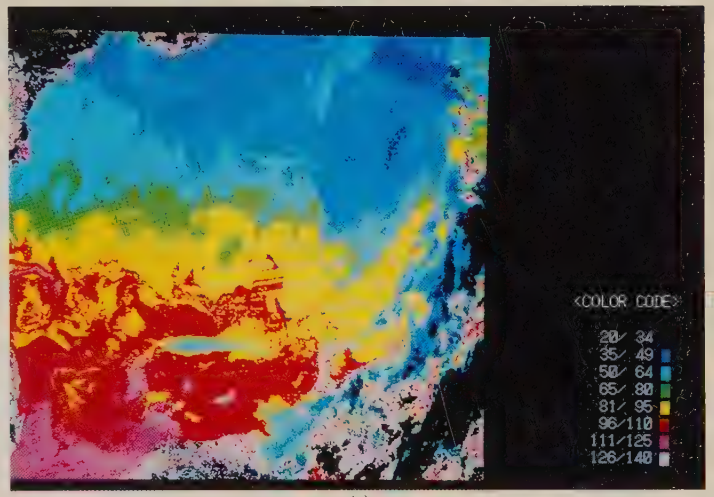

(c)

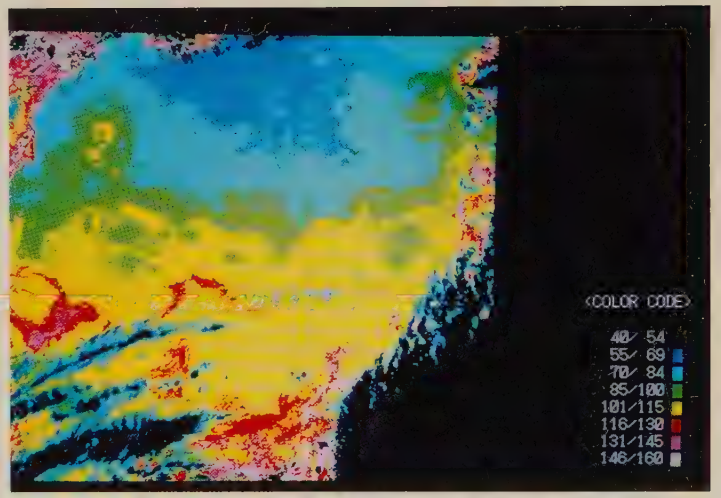

(d)

Plates 1. The sea surface temperature (SST) field can be viewed by NOAA cloud-free images. The shape of the boundary between the warm and the cold waters is always very complicated. Each plate shows the SST field of (a) October 18th, 1991, (b) December 5th, 1991, (c) April 2nd, 1992, and (d) May 10th, 1992, respectively.

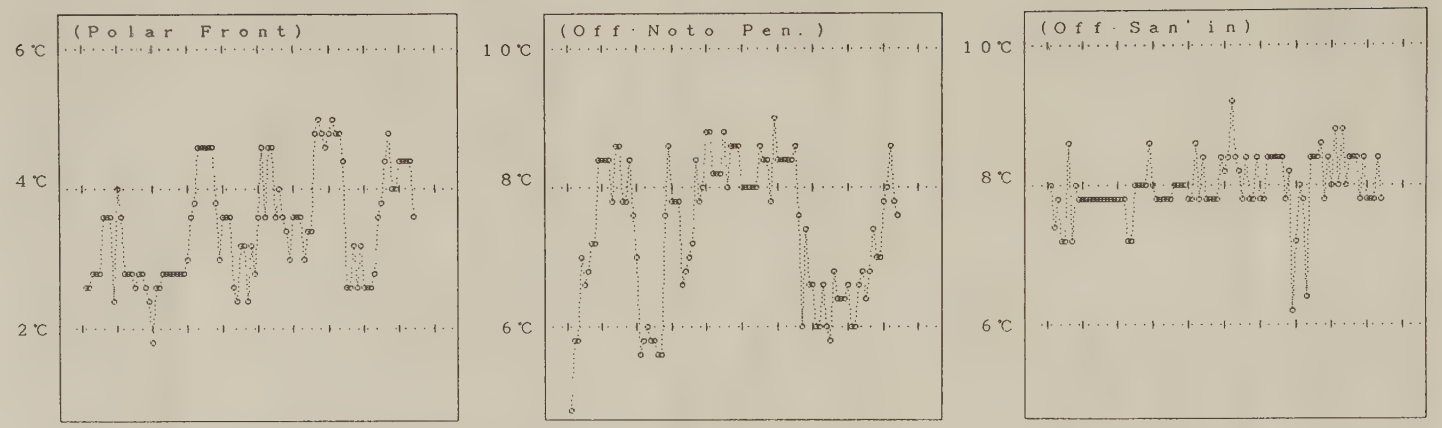

Fig. 1 The zonal cross section of SST extracted from the NOAA image data of April 20th, 1992. Each section shows the distribution of SST
(a) near the Polar Front, (b) off Noto Peninsula,
(c) off San'in Coast, respectively.
The horisontal axis represents the parallel of latitude of the center of respective region.

of the data, which needs to assume neither the continuity nor the periodicity of the phenomena, should be adopted.

When the time sequence data $\{X_i\}$ (i=1,2,...,n) is given, the fractal dimension can be defined as the dimension of the line of the graph based on the data. The fractal dimension of the data is calculated as follows:

① The line is divided in an equal time interval ε.

② L(k,ε), which is the sum of the data variation at the interval of ε after k (k=1,2,...,k_{max} :k_{max}=30 in this paper), is calculated by

$$L(k,\varepsilon) = \frac{n}{m\varepsilon} \cdot \sum_{j=1}^{m} \left| X_{k+j\varepsilon} - X_{k+(j-1)\varepsilon} \right|,$$

where

$$m = \left[\frac{n-k}{\varepsilon} \right] \quad ([\cdot] : \text{Gauss sign}).$$

This L(k,ε), which is normalized by the coefficient (n/mε), represents the total length of the line graph in the direction of the vertical axis.

③ L(k,ε) is averaged over k, and L(ε), which represents the length of the line, is given by

$$L(\varepsilon) = \frac{1}{k_{max}} \sum_{k=1}^{k_{max}} L(k, \varepsilon) .$$

④ Δ(ε), which is the number of division of the graph for the fixed ε, is given by

$$\Delta(\varepsilon) = \frac{L(\varepsilon)}{\varepsilon} .$$

The definition of the fractal dimension is described in appendix. Henceforth, this procedure to obtain the fractal dimension is called the "Fractal Dimension Analysis", abbreviated FDA. Of course, FDA can be applied not only to the time sequence data but also to any single valued function including the spatial sequence data.

The application of FDA often define two distinct fractal dimensions for the different ranges of the spatial/temporal scale. In this paper, ε represents the spatial/temporal scale. Also, the primary dimension for the smaller ε and the secondary one for the larger ε are represented D_1 and D_2, respectively. Furthermore, ε_t represents the sandwiched range of ε between two regions in which respective fractal dimensions are defined, and it is called the "transitional scale range".

3. The data

3.1 The SST data from the NOAA image

The complexity of the SST field are represented by the fractal dimension of the isotherms. But the SST field is too complex to draw the isotherms. Consequently, FDA will be applied to the zonal distribution of SST, not to the figure of the isotherms, for the purpose of studying the charasteristic spatial scale of the SST field. The SST data of five regions in the Sea of Japan (Fig. 2) were scanned

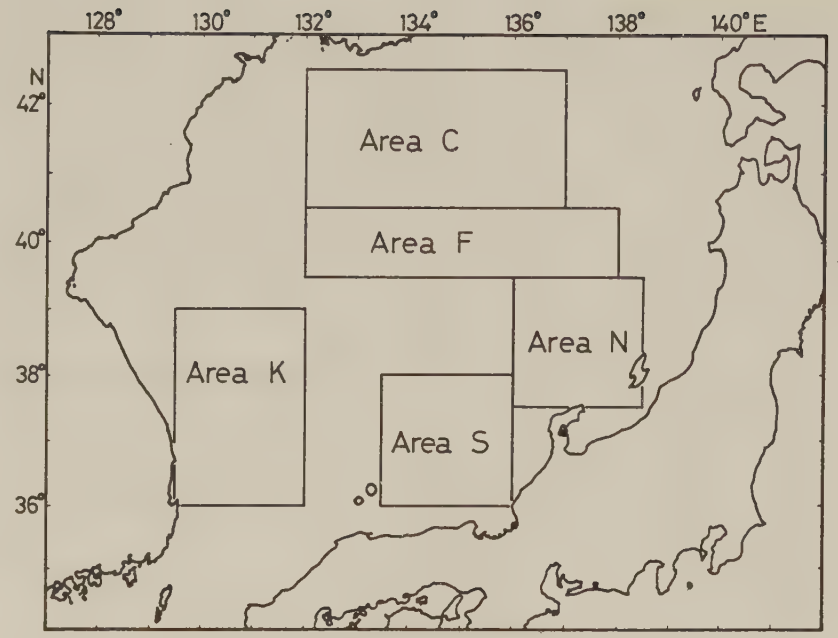

Fig. 2 The regions selected to prepare the data files of SST.
C : the cold water region
F : the region near the Polar Front
K : the region east of Korea Peninsula
N : the region off Noto Peninsula
S : the region off San'in Coast

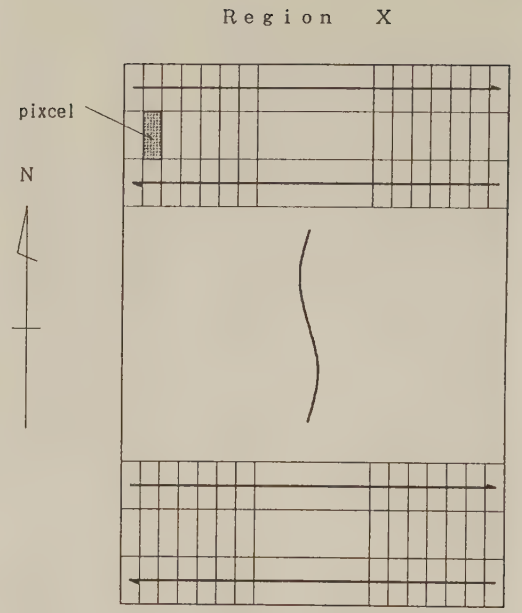

Fig. 3 The conception of the scanning method to extract the SST data from the rectangular region. The region is scanned back and forth sevaral times and the sufficient number of the data is obtained.

Table 1 The selected five regions with the regional mean and the non-biassed standard deviation of SST. Each data file is named by one captal letter and number of six figures, which signify the region and observed date, respectively.

		Range of the region in latitude and in longitude		1991				1992		
				Oct. 18	Nov. 6	Nov. 25	Dec. 5	Apr. 2	Apr. 20	May 10
C	Cold Water Region	42°30'— 40°30' N	mean SST	14.2		5.9	4.6			4.2
		132°00'—137°00' E	σ_{n-1}	1.16		1.64	1.70			1.14
F	Near the Polar Front	40°30'— 39°30' N	mean SST		12.8	10.3	9.5		5.1	7.5
		132°00'—138°00' E	σ_{n-1}		1.94	1.93	2.31		1.62	1.53
K	East of Korear Peninsula	39°00'— 36°00' N	mean SST	19.0	15.3		13.4	9.9	7.2	
		129°30'—132°00' E	σ_{n-1}	1.38	1.66		2.36	1.32	1.57	
N	Off Noto Peninsula	39°30'— 37°30' N	mean SST		16.3			6.9	8.3	10.7
		136°00'—138°30' E	σ_{n-1}		1.19			1.73	0.95	0.82
S	Off San'in Coast	38°00'— 36°00' N	mean SST		17.6		15.8	9.9	8.5	
		133°30'—136°00' E	σ_{n-1}		0.93		0.73	0.87	0.70	

from the NOAA cloud-free images to prepare the data files for the application of FDA. The scanned images and regions are shown accompanied with the regional mean SST and the non-biassed standard deviation in Table 1. Each data file is named by one capital letter and six numerals, which signify the scanned region and the observed date, respectively. For example, the file name "C911125" means that the data were extracted from the Cold Water Region by scanning the NOAA image observed on November 25th, 1991.

Though it is desirable that the prepared file contains more than 1000 data to be applied with FDA, there are less than 250 pixels in the zonal widths of the selected regions in the NOAA images. To get the sufficient number of data, the regions were scanned in the zonal direction back and forth several times (Fig. 3).

Since some reiterational variations which have the period of the multiple of number of pixels contained in the width of the regions might result from this method of scanning, FDA was performed over the range of $\varepsilon \leqq 90$ which is smaller than the width of each region for fear of the variations. Deservedly, the pixels disturbed by cloud were omitted. After that, if more than 80% of the data remained, the file was applied with FDA.

3.2 Coastal water temperature data

FDA was applied to the coastal water temperature data during four years (1982 to 1985) at six stations (Fig. 4) facing or neighbouring the Sea of Japan in order to presume the characteristic time scale of the

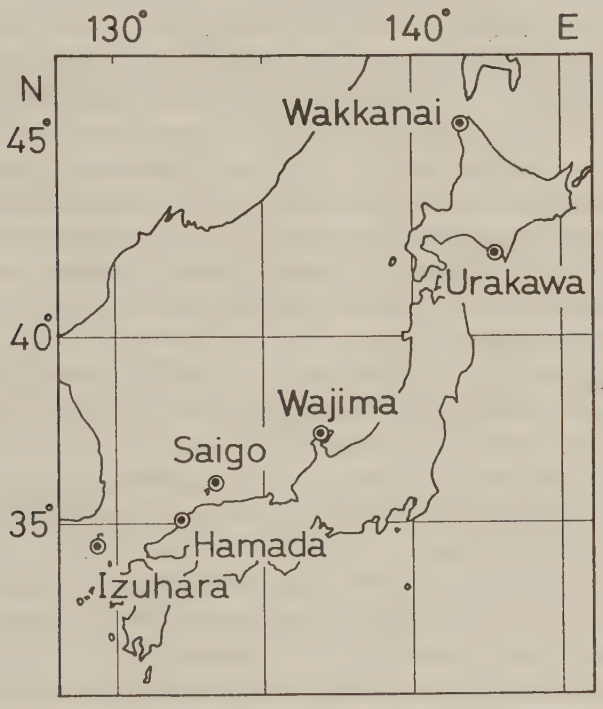

Fig. 4 The observational stations of the coastal water temperature.

SST field. The data files are shown accompanied with the 4-year mean temperature and the non-biassed standard deviation in Table 2. Missing data were linearly interpolated using the data before and after.

It is quite plain that the coastal water temperature has the seasonal variation. Moreover, NAGANUMA (1987) showed that the temperature variation of the surface layers has the dominant period of a half year. Consequently, the analysis was performed within the range not to exceed 90 days, which is about a quarter year, for fear that the variations of annual and a half year period should be picked up.

4. Results

4.1 The spatial distribution of the SST

The fractal dimensions D_1 , D_2 and the transitional scale range ε_t of the SST data are shown in Table 3. Here, each ε_t, in the unit of the number of pixels, is the characteristic spatial scale of the data.

The appearence of two distinct fractal dimensions implies that the SST distribution might be under the influence of two factors which correspond with the respective spatial scale. On the other hand, ε_t represents the spatial scale of the border at which the dominant factor changes, and can be considered as the average diameter of eddies.

Each data except "C911018" and "C911125" has the two different dimensions and the distinct transitional scale range ε_t. In each pair of the dimensions, D_2 is always larger than D_1. Since D_2 is obtained for larger ε, it means that the stronger randomness of the SST distribution appears when the pixel interval is taken larger than ε_t.

It can be found that the transitional scale ranges in each region are larger in the cooling season (October to December) than in the warming season (April and May), except the region off San'in Coast.

In the cold water region (C), "C911018" and "C911125" have the uniform dimensions of 1.75 and 1.64 over the range of $\varepsilon \leqq 90$, respectively. Moreover, the difference between the two dimensions of "C920510" (D_1=1.75 and D_2=1.80) might not be significant. Therefore, the fractal dimension of the zonal SST distribution is considered to be almost uniformly about 1.7, which is the mean value of D_1 in this region. It follows that the specific character of the SST variation is uniform over the spatial scale range of 90 pixels (about 200 km) and that the characteristic diameter of the eddy fields are considered to be larger than 200 km in this region. On the other hand, the two dimensions of "C911205" (D_1=1.66, D_2=1.92) are separated distinctly at ε_t=24.

In the region near the Polar Front (F), the two dimensions, D_1 and D_2, of each SST data are scattered over the range of 1.55 to 1.70 and 1.78 to 1.99, respectively. D_1=1.55 of "F911205" is the smallest of all D_1, while D_2=1.78 of "F920510" is also the smallest of all D_2.

In the region east of Korea Peninsula (K), D_1 of the data except "K911018" are within the range of 1.60 to 1.67, while D_2 of the data except "K911205" are within the range of 1.92 to 2.00. As for the case of "K911106", ε_t=33 is fairly large.

In the region off Noto Peninsula (N), D_1 of the data are within the range of 1.68 to 1.74, while D_2 of the data are within the range of 1.90 to 2.00. The two dimensions and the transitional scale range of "N920420" are almost the same to those of "N920510", respectively.

In the region off San'in Coast (S), the two different dimensions of all SST data are almost the similar, $D_1 \fallingdotseq 1.8$ and $D_2 \fallingdotseq 2.0$ appear distinctly, but the transitional scale ranges are scattered between 18 to 31.

Table 2 The observational stations with the 4-year mean and the non-biassed standard deviation of the coastal water temperature.

Station	Location	4-year mean	σ_{n-1}
Wakkanai	45°25'N 141°41'E	10.0	7.38
Urakawa	42°10'N 142°47'E	8.2	6.53
Wajima	37°23'N 136°54'E	16.6	6.58
Saigo	36°12'N 133°20'E	17.7	5.49
Hamada	34°54'N 132°04'E	18.2	5.82
Izuhara	34°12'N 129°18'E	18.5	4.96

Table 3 The results of FDA applied to the data files of SST.
ε_t : the trasitional scale (spatial scale),
D_1 : the primary fractal dimension for smaller ε,
D_2 : the secondary fractal dimension for larger ε.

		1991				1992		
		Oct. 18	Nov. 6	Nov. 25	Dec. 5	Apr. 2	Apr. 20	May 10
C	ε_t	—		—	24			15
	D_1	1.75		1.69	1.66			1.75
	D_2	—		—	1.92			1.80
F	ε_t		29	26	33		15	15
	D_1		1.68	1.70	1.55		1.62	1.70
	D_2		1.82	1.91	1.99		1.92	1.80
K	ε_t	20	33		28	14～16	14～16	
	D_1	1.84	1.67		1.60	1.67	1.67	
	D_2	1.95	2.00		1.80	1.98	1.92	
N	ε_t		28～36			18	25	24～28
	D_1		1.72			1.68	1.74	1.74
	D_2		1.99			1.90	1.97	2.00
S	ε_t		18～23		20	25	31	
	D_1		1.82		1.83	1.79	1.80	
	D_2		1.99		1.98	1.99	1.99	

4.2 The time dependent variations of the coastal water temperature

The results of FDA applied to the time sequence of the coastal water temperature data are shown in Table 4. Here, each ε_t, in the unit of days, represents the characteristic time scale of the data.

The time variation of the coastal water temperature, besides being under the influence of the air temperature, the solar radiation, or so, can be considered to represent the motion of the SST field. But some attention have to be paid when the data is used, because the observational spot is too near to the land to presume the good representation of SST.

For all the cases, two different dimensions D_1 and D_2 are defined clearly. The smallest and the largest values of D_1 are 1.52 and 1.64, which are obtained from the data of Wakkanai and Izuhara, respectively. As for the value of D_2, the smallest and the largest ones are 1.17 and 1.35, which are obtained from the data of Izuhara and Urakawa, respectively.

The lower ends of ε_t range between 7 and 19, while the upper ends of them are almost uniform, of 19 to 23. The lower ends of ε_t show a tendency which becomes longer at higher latitude.

As for the data of Wakkanai, Urakawa and Wajima, the fractal dimension cannot be defined for the time scale shorter than 2 days, because the logε-logΔ plots are noticeably off the straight lines of the

Table 4 The results of FDA applied to the time sequences of the coastal water temperature.
ε_t : the transitional scale (time scale),
D_1 : the primary fractal dimension for smaller ε,
D_2 : the secondary fractal dimension for larger ε.

Station		
Wakkanai	ε_t	16～21
	D_1	1.52
	D_2	1.25
Urakawa	ε_t	19
	D_1	1.63
	D_2	1.35
Wajima	ε_t	7～19
	D_1	1.63
	D_2	1.25
Saigo	ε_t	11～22
	D_1	1.60
	D_2	1.27
Hamada	ε_t	9～23
	D_1	1.55
	D_2	1.19
Izuhara	ε_t	8～22
	D_1	1.64
	D_2	1.17

region of ε where D_1 were defined. This implies that the variation of the coastal water temperature of these stations might be under the influence of some factors which vary in the short period.

5. Discussion

5.1 The results of FDA applied to the SST data

The surface layers of the northen part of the Sea of Japan are covered with cold water almost all the year around. FDA results indicate that the fractal dimension is usually about 1.7, almost uniform over the region C. This means that the zonal trend of the SST distribution in this region is very weak, and that the average diameter of the eddy field is larger than about 200 km (90 pixels in the NOAA image) if it exists. This is consistent with the characteristic diameter of 350 to 400 km in the corresponding area, which is indicated by MINAMI and ANDO (1982).

As for "C911205", which is the exceptional data in the region C, the two different dimensions are distinguished. The standard deviation (σ) of this data is 1.70, which is larger about one and a half times than those of "C911018" and "C920510". Moreover, D_1=1.66 and D_2=1.92 of this data corresponds to mean dimension pairs in the regions F, K and N. On the other hand, the uniform small dimension of 1.64 was obtained from "C911125", which also has the large σ of 1.64. These facts suggest that the zonal trend and the scattering of SST in "C911205" was caused by the warm water which came into from the southern region.

It can be easily ascertained whether the warm water comes into the cold water region by using the NOAA images (see Plates 1 again). On December 5, 1991, the warm water penetrated into the cold water region, reaching about 41°N on the north. On the contrary, the region was almost uniformly covered with cold water on October 18, 1991 and May 10, 1992.

Considering the transitional scale range ε_t in the regions of F, K and N, there is the tendency that the larger value appears in the cooling season than in the warming season. Though the SST field must be easily disturbed by the condition of the air temperature, the wind speed and the solar radiation, the subsurface water temperature field cannot be under the direct influence of such factors. Consequently, the field of the subsurface water temperature is expected to be not so complex (i.e. ε_t is large) as that of the SST. Therefore, the tendency mentioned above can be explained naturally by means of the vertical mixing process which is active in the cooling season and reveals the subsurface field to the surface.

Conversely, the transitional scale ranges of the data in the region S are slightly larger in the warming season than in the cooling season. But the difference between the two fractal dimensions of each data does not exceed 0.20. Accordingly, the variation of ε_t in the region S might not be significant. Since the upper layers of the region S is considered to be usually occupied by the Tsushima Warm Current Water, no variation can be expected to result from the vertical mixing process which is active in the cooling season.

After all, the average scale of eddies in the southern region of the Sea of Japan can be supposed to be in the range of 50 to 75 km (20 to 30 pixels in the NOAA images). This scale is small compared with the diameter of 125 to 160 km, which is indicated by MINAMI and ANDO (1982).

The values of dimension which are defined within the scale smaller than ε_t might be under the influence of the meteorological conditions. This idea will be discussed later.

5.2 The results of FDA applied to coastal water temperature data

The results of FDA applied to coastal water temperature data suggest that stronger randomness appears in the short time scale than in the long one. This implies that the daily coastal water temperature does not represent the offshore SST in the time scale which is shorter than ε_t, and that the smooth periodical variations become clear in the time scale of which is longer than ε_t.

The values of the lower end of ε_t have a tendency of becoming larger at higher latitude. This can be explained by means of meteorological conditions as follows.

The transit of the extratropical cyclones and anticyclones, which characterize the climate of Japan, causes the quasi-periodical weather variation. In general, the climate of Japan can be roughly divided into the north and the south regions at the latitude of about 38° N (WADACHI, 1958). The northern region is frequently covered with the cold air masses which come from the Sea of Okhotsk or the Asia continent, while the air masses often change in the southern region.

As is shown in Table 5, TAKAHASHI (1955) indicated that the transit frequency of the anticyclones between the latitude of 36° N and 38° N is about twice larger than that of north of 40° N. In the meantime, the mean number of the extratropical cyclones which pass the Sea of Japan can be considered to be about 3 per month, as is shown in Table 6 (WADACHI, 1958). Consequently, the dominant period of the weather variation in the southern region is expected to be about 10 days, while that of the northern region might be fairly long.

On the other hand, the upper end of ε_t is about 3 weeks, which is common to the six stations, and this period can be considered to represent the characteristic time scale of the SST variations around the Sea of Japan.

It may be natural that these explanation based on the meteorological conditions can also be applied to the characteristic spatial scale of eddies, because the respective values of D_t, which is given to the zonal SST distribution and the coastal water temperature, are uniformly about 1.6, but for some expectional cases. So, the phenomena which are smaller than the characteristic spatial/temporal scales might be considered to be under the influence of the meteorological conditions.

After all, it is suggested that the long period variation of the coastal water temperature can be regarded to represent the motion of the SST field, while the short period variation might be under the direct

Table 5 The frequency of the transit of anticyclones at the longitude of the 140°E (after Takahashi, 1955).

Latitude (°N)	22	24	26	28	30	32	34	36	38	40	42	44	46	48	50	52
frequency	2	5	17	26	18	23	33	81	89	44	24	24	13	9	2	1

Table 6 The number of the extratropical cyclones which passed the Sea of Japan each month during 1931 to 1935 (after Wadachi, 1958).

Month	Jan.	Feb.	Mar.	Apr.	May	June	July	Aug.	Sept	Oct.	Nov.	Dec.	averrage
frepuncy	2.6	2.6	3.4	4.0	3.4	2.0	2.4	1.6	2.4	2.4	2.6	3.2	2.8

influence of the weather changes.

5.3 The correspondance between the characteristic scales and the propagation speed of warm eddies

① The warm eddy off Noto Peninsula

The warm eddy which appeared off Noto Peninsula in 1981 is followed in Fig. 5. The propagation speed of the eddy is estimated to be about 1.4 nautical miles (2.6 km) per day. Considering the result of FDA applied to the coastal water temperature of Wajima, the characteristic time scale in this region is about 19 days from the upper end of ε_1. These follow that the spatial scale of the eddy is about 27 nautical miles (50 km).

Since the actual radius of the eddy is about 50 km either from the results of FDA appllied to the NOAA image or from analysis of the depth of 200 m, it is roughly consistent with the scale estimated above.

② The stagnant warm eddy east of the Oki Islands

The track of the center position of the warm eddy which had stagnated east of the Oki Islands for a long period is shown in Fig. 6. The eddy was almost stationary, within the region of the south-west edge of Yamato Basin or Oki Basin during 1989 to 1991, staying over the coldest season twice.

According to the result of FDA applied to the NOAA SST data in this region and the coastal water temperature data at Saigo and Hamada, the characteristic time scale and spatial scale in this region are estimated to be about 10 days and 50 to 60 km (20 to 25 pixels in the NOAA image), respectively.

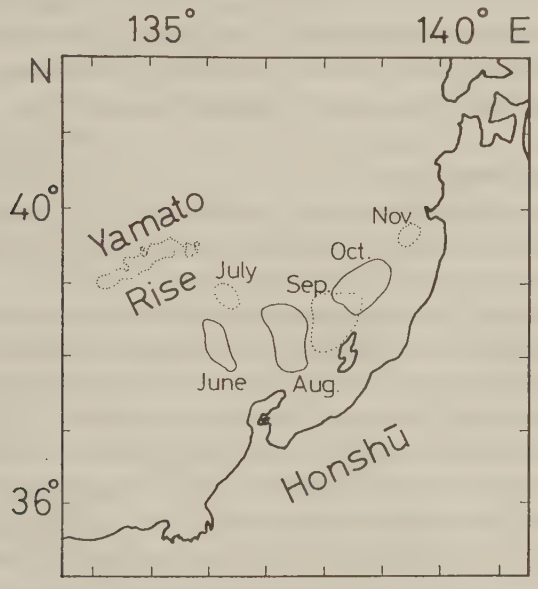

Fig. 5 The shape of the warm eddy at the depth of 200m, from June to November, 1981.

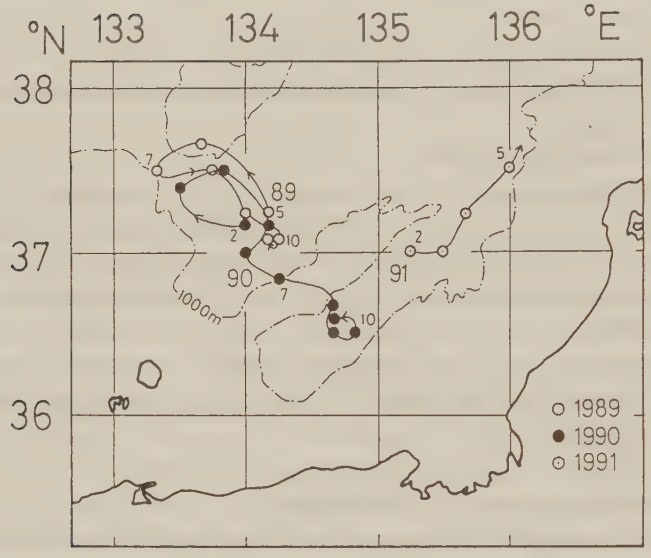

Fig. 6 The track of the center position of the warm eddy, which had stagnated east of the Oki Ilands for a long period of time from 1989 to 1991. The eddy had kept its position almost stationary and wintered twice.

Consequently, the propagation speed of eddies in this region is expected to be about 3 nautical miles (5 to 6 km) per day. The eddy started to move in Feburary, 1992, and the propagation speed after that is about 0.7 nautical miles (1.2 km) per day, which is only about a quarter of that calculated from the characteristic spatial/temporal scales. It follows that the behavior of the warm eddy can be explained neither in stationary stage nor in moving stage by means of the results of FDA.

6. Summary and concluding remarks

The transitional scales, which can be obtained from the results of FDA applied to the spatial SST distribution and the time sequence of the coastal water temperature, were considered to represent the average diameter and the characteristic time period of eddies.

It is found that the diameter of eddies becomes smaller in the cooling season in the southern region of the Sea of Japan. This fact can be explained by means of the vertical mixing process in the cooling season which reveals the subsurface field to the surface. It is also suggested that the average diameter of eddies might have a tendency of becoming larger at higher latitude.

The characteristic time period of about three weeks, which is obtained as the upper end of the transitional scales, is common in all regions around the Sea of Japan. On the other hand, the lower end of the transitional scales, which are considered as the dominant period of meteorological conditions, have a tendency of becoming longer at higher latitude. These facts suggest that the alternation of the water temperature which has the time scale longer than about three weeks might be regarded as much predictable as the seasonal variation.

But some attention must be paid to interpret the values of the dimension of the coastal water temperature variation which are defined for the time scale longer about 3 weeks, because the coastal water temperature may not represent the SST.

The characteristic spatial/temporal scales are compared with the propagation speed of the warm eddies. The value which is derived from the characteristic spatial/temporal scales can be regarded as the characteristic speed. It is shown, however, that the value is not always coincident with the propagation speed of the warm eddy which is obtained from the monthly mean analysis of the oceanographic conditions.

Acknowledgement

I wish to offer my cordial thanks to Mr. Kumio Komura, the head of Oceanographical Division of Maizuru Marine Observatory (MMO), for his encouragement and linguistic help. I would also like to express my heartfelt gratitude to Mr. Takanori Mizuno and Mr. Akiyoshi Wada of MMO for their earnest help on programming and profitable suggestions. I would like to acknowledge Mr. Tsutomu Tohmine and Mr. Masato Ichikawa of Hakodate Marine Observatory for their offering the coastal water temperature data.

Appenndix
The definition of the fractal dimension and its meaning

A1. The definition of the length of a curve

Let us think how to measure the length of a curve $C(P_s \rightarrow P_e)$, which is given within the two-dimensional Euclidean space.

First, arbitrary points P_1, P_2, ..., P_{n-1} are taken on C. Next, the neighbouring points are joined with a straight line one after another, and the line C_n ($P_s=P_0$, P_1, ..., P_{n-1}, $P_n=P_e$) is made up with the sum of a segment $P_i P_{i+1}$ ($i=0,1,2,...,n-1$) which is a straight line. Consequently, we can think that the curve C is approximated in some sense by C_n when the number n is large enough.

L_n, the length of whole C_n, is

$$L_n = \sum_{i=0}^{n-1} P_i P_{i+1} = \sum_{i=0}^{n-1} l_i \qquad \text{.....(A-1),}$$

where $l_i=P_i P_{i+1}$ ($i=0,1,2,...,n-1$) is the length of each segment.

Generally, L_n is dependent on the number n and the position of P_i ($i=0,1,2,...,n-1$), but it has always the finite decided value.

Then, if the limit value of L_n for $n \rightarrow \infty$

$$L = L_\infty = \lim_{n \rightarrow \infty} L_n = \lim_{n \rightarrow \infty} \sum_{i=0}^{n-1} l_i \qquad \text{.....(A-2)}$$

exists, we can define L as the length of a curve C. Pay attention to the fact that the limit value L does not always exist.

A2. The definition of the fractal dimension of a curve

P_i can be placed as each $l_i=P_i P_{i+1}$ (i=0,1,2,..., n-1) has the same length. Then, the curve C is approximated by the line which is divided into n of the minute straight line segments.

Let ε be the size of the division, which is the length of the minute segments, and let Δ be the number of the division. Of course, as ε becomes smaller, Δ increases. But Δ is not always inversely proportional to ε.

Now, let Δ_1, Δ_2 be the value of Δ at $\varepsilon=\varepsilon_1$, ε_2, respectively. If there is a linear relation between log ε and log Δ within the range of $\varepsilon_1 \leqq \varepsilon \leqq \varepsilon_2$, the fractal dimension of the curve C can be defined by the equation

$$D = \left| \frac{\log \Delta_2 - \log \Delta_1}{\log \varepsilon_2 - \log \varepsilon_1} \right| \qquad \text{.....(A-3).}$$

This means that the fractal dimension is given by the absolute value of the slope of the straight portion of the logε-logΔ graph. It follows that the fractal dimension itself depends on neither the expansion nor the reduction of the curve. Also, if the logε-logΔ graph has two straight portions which have the different slope, the two distinct dimensions are defined for the respective portions.

The conception of the fractal dimension is given as the extension of the topological dimension. Since equation (A-3) gives the fractal dimension of the one-dimensional set in the two-dimensional Euclidean space, it is represented by the value within the range between 1 and 2.

A3. The meanings of the fractal dimension

In general, the line graph based on the data (x_i, y_i) (i=0,1,2,..., n-1) can be regarded as a curve given within the two-dimensional Euclidean space. It follows that the fractal dimension of the graph, which is not smaller than 1 and does not exceed 2, can be defined and expected to represent some characteristics of the data. So, it can be regarded as the dimension of the data.

For example, if (x_i, y_i) (i=0,1,2,..., n-1) satisfies y=ax, then the dimension of the data is 1, which is the dimension of a straight line. If the data satisfies y=sin x, then the asymptotic dimension of the data is 1, because sine curves can be approximated with straight line segments in the microscopic limit. On the other hand, if the data represents some kind of noise, then the dimension is nearly 2. Particularly, if the noise has a spectrum inversely proportional to the frequency f, i.e. $S(f) \sim 1/f$, then the dimension is just equal to 2. On the fact mentioned above, the fractal dimension can be regarded as an index of the complexity or the randomness of the data.

The log ε-log Δ graphs based on the sample data, which are made of the linear trend data and the periodical data (sine function) with random noises, are shown in Fig. A-1 and Fig. A-2, respectively. In each case, the dimension for the larger ε is about 1 and the one for the smaller ε is nearly equal to 2. This can be explained that the randomness is dominant in microscopic scales and the regularity is revealed in macroscopic scales. Concequently, the data which has the two distinct fractal dimensions is considered to be under the influence of two different factors for respective scales.

The phenomena which satisfy the elementary function can be easily predicted, but the random variation of noise can hardly predicted. Since the meanings of the fractal dimension of the data is connected with the predictability of the phenomena as mentioned above, it is of wide application in various fields

which are concerned with the prediction problem.

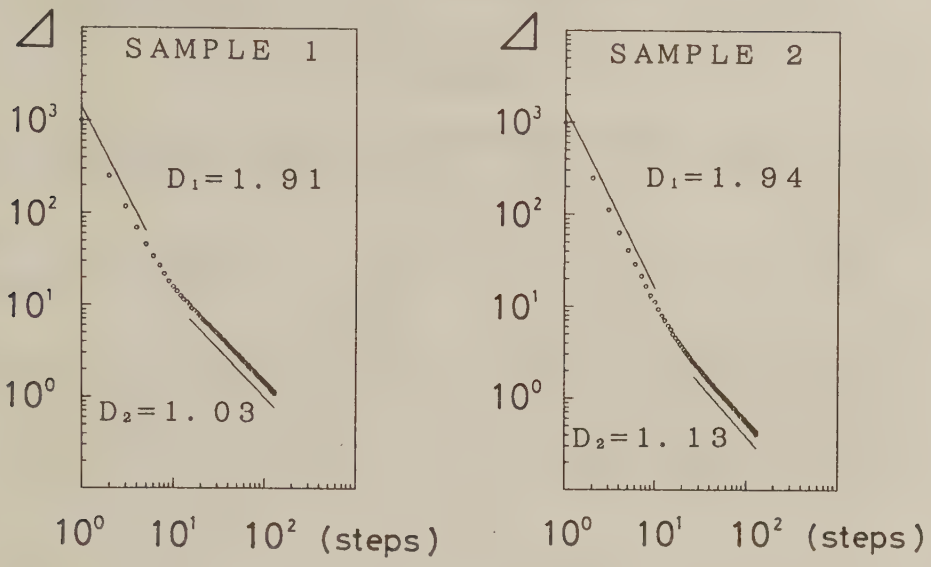

Fig. A The results of "Fractal Dimension Analysis (FDA)" applicated to the sample data. The ransom noise are added to the data of (1) the linear function and (2) the periodical (sine) function, respectively. Two different fractal dimensions are obtained in both of the cases.

References

ISODA, Y. and M. NISHIHARA (1992) : Behavior of warm eddies in the Japan Sea. *Umi to Sora*, **67**, Special Issue, 231-243.

ISODA, Y., M. NAGANOBU, H. WATANABE and K. NUKATA (1992) : Horizontal and vertical structure of a warm eddy above the Yamato Rise. *Umi no Kenkyu*, **1**, No.4, 141-151.

MATSUYAMA, M., Y. KURITA, J. YOSHIDA, K. INOUE, I. KASUGA and S. TAKEDA (1988) : The warm eddy observed east of Oki Islands in the Japan Sea. *Journal of the Tokyo Univercity of Fisheries*, **75**, 247-255.

MATSUYAMA, M., Y. KURITA, T. SENJYU, Y. KOIKE and T. HAYASHI (1990) : The warm eddy observed east of Oki Islands in the Japan Sea (2). *Umi to Sora*, **66**, 67-75.

MINAMI, H and T. ANDO (1982) : Characteristics of eddy fields in the Japan Sea. *Journal of Meteorological Research*, **34**, 277-287.

NAGANUMA K. (1987) : Some areas of fluctuations of the seasonal water temperature in the Tsushima Warm Current Region in the Japan Sea. *Bulletin of the Japan Sea Regional Fisheries Research Laboratory*, **37**, 1-11.

NISHIYAMA, K., S. KAWAE and H. SASAKI (1990) : The Japan Sea Proper Water and the Japan Sea Warm Eddy. *Bulletin of Kobe Marine Observatory*, **209**, 1-10.

TAKAHASHI, K. (1955) : *The dynamical climatology*. Iwanami Co., Ltd.,122.

WADACHI, K. (ed.) (1958) : *The climate of Japan*. Tokyodo Co., Ltd.,33-35.

The Oceanographical Magazine Vol. 44 (1994)

フラクタル次元解析の日本海の渦への適用

宮　尾　　孝
（舞鶴海洋気象台）

フラクタル次元解析の手法をＮＯＡＡ衛星画像から抽出した緯度線方向の海面水温分布と日本海周辺の幾つかの観測点における沿岸水温時系列に適用し，渦場の特徴的な空間的・時間的スケールを見積もった．

暖水渦の卓越半径は，南部海域で50～70km，北部海域で200km以上と見積もられた．この半径は極前線よりも南の海域においては海面が冷却される季節に大きくなる傾向を示す．この事実は冬季鉛直混合の作用により下層の場が海面に現れることで説明できる．

沿岸水温変動の特徴的な周期は，日本海周辺では共通してほぼ3週間と見積もられた．一方，気象条件による周期は高緯度ほど長くなる傾向を示す．

渦場の特徴的な空間的・時間的スケールから特徴的な速度が計算できる．しかし，その値は月平均の海況解析から求めた暖水渦の移動速度とは必ずしも一致しない．

The Oceanographical Magazine
Vol. 44. Nos. 1-2. pp. 31 to 44, March 1994

Seasonal Variation of Carbon Dioxide Partial Pressure in Sea Surface Water around Japan

Yuji KANO and Kazuhiko HAYASHI
Hakodate Marine Observatory
3-4-4 Mihara, Hakodate 041, Japan

(Received October 20, 1993; Accepted January 14, 1994)

Abstract: Seasonal variation of carbon dioxide partial pressure in sea surface water around Japan is investigated from the data on temperature, hydrogen ion concentration (pH) and phosphate obtained by the Japan Meteorological Agency and the four Marine Observatories for five years. Carbon dioxide partial pressures around Japan are calculated by pH and alkalinity based on chemical equilibrium of carbonate system in sea water. They are also calculated by phosphate concentration based on the relation among nutrient, total carbonate and total alkalinity. The results by the two calculations both show that the carbon dioxide partial pressure in the Oyashio region is higher in winter than in summer in contrast with the other seas around Japan. It is concluded that water quality is more dominant than water temperature to carbon dioxide partial pressure in the Oyashio region in contrast with the other seas around Japan.

A simple model consisting of atmosphere and two layers of sea water is introduced to explain the results. The model output is in good agreement with the actual data in both the Oyashio region and the Kuroshio region by adjusting several parameters such as gas exchange rate of carbon dioxide across sea surface and primary production.

1. Introduction

The ocean is considered to affect the condition of atmospheric carbon dioxide which causes global warming because the ocean has high ability to store carbonate matters and exchange carbon dioxide with atmosphere. But carbon dioxide partial pressure of sea water (P_{CO_2}) varies seasonally through the change of its temperature and chemical quality. To clarify the seasonal variation of carbonate system of sea water is very important for better understanding of the global carbon cycle.

HIROTA *et al.* (1991) revealed P_{CO_2} distribution both in winter and in summer in the western North Pacific south of Japan. In their results the P_{CO_2} is low in winter and high in summer compared with partial pressure in air except in equatorial region. Water temperature is considered to cause the seasonal variation of P_{CO_2} there with a small seasonal variation of nutrients.

In the Oyashio region seasonal variations of temperature and chemical quality like nutrients in sea water are both large and P_{CO_2} in the region is considered to reflect the large variation. TAKAHASHI (1989) estimated that the annual net flux of CO_2 through sea surface changes its direction across the 40 °N latitudinal line around the region.

The Intergovernmental Panel on Climate Change (IPCC) says that there is missing CO_2 unexplained in the global CO_2 budget consisting of burning of fossil fuel, residence in air, ocean uptake and deforestization. TSUNOGAI *et.al.* (1993) described that the subarctic region in the northern North

Pacific containing the Oyashio region is potential area for the uptake of missing CO_2. It is an important problem if the Oyashio region and other regions around Japan are emitting or absorbing CO_2. For this problem the seasonal variation of Pco_2 around Japan should be investigated initially.

The purposes of this paper are to estimate Pco_2 in the seas around Japan from the data obtained by the Japan Meteorological Agency (JMA) and four Marine Observatories (MOs) under the JMA and to appeal that comprehensive observations not only in the tropical/subtropical region but subarctic region around Japan including the Oyashio region are necessary for contributing carbon cycle issue through the discussion of the seasonal variation of Pco_2.

2. Data

The JMA and the four MOs have been monitoring the Background Marine Pollution since 1972 along the regular observation lines on the items of temperature, salinity, phosphate and pH, which are closely related to Pco_2. The results are issued as "The Results of the Oceanographical Observations" and "Report of Observation for Monitoring Background Marine Pollution" by the JMA. The data from 1986 to 1990 are used for the analysis in this paper because the condition of indicated pH has been changed since 1986 from the value in situ to that under 25 °C. In Fig. 1 the stations analyzed here are

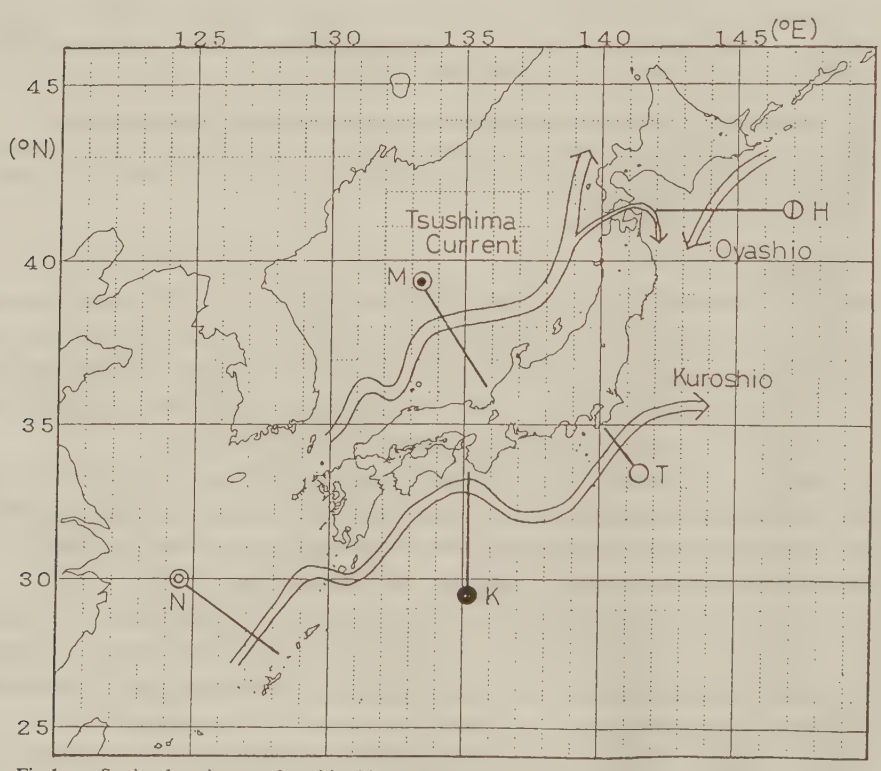

Fig.1 Station locations analyzed in this paper (H, T, K, N and M) and observation lines where the regular surveys on background marine pollution are carried out. Typical sea currents around Japan are also indicated.

shown as well as the typical ocean currents around Japan. Seasonal observations are usually carried out in February for winter, May for spring, July for summer and October for autumn with the exception of June for summer at the station T in Fig. 1

3. Estimation of carbon dioxide partial pressure from pH

Generally speaking, two items should be measured to calculate the carbonate system in sea water among the four items, total carbonate, total alkalinity, P_{CO_2} and pH in addition to temperature and salinity, because the four items are related to each other through the two equations of chemical equilibrium. Unfortunately in the routine Background Marine Pollution observation, only one item, pH, is measured, therefore carbonate system in sea water is not calculated strictly. The P_{CO_2} is, however, estimated with reasonable accuracy as described below.

Distribution of P_{CO_2} in sea water is shown in temperature-pH diagram, Fig. 2 when total alkalinity is 2200 μmol/*l* and changed by ±100 μmol/*l*, where salinity is assumed to be constant, 35 psu. We measured total alkalinity in sea surface water at the station H in Fig.1 in four seasons of 1992 to 1993 based on the method described by the JMA (1970). The results in Table 1 show that the seasonal difference of total alkalinity is quite small within ±10 μmol/*l* in the region. Even taking the seasonal change of salinity into account, the seasonal change of total alkalinity may be ±50 μmol/*l* (±2.5%) at

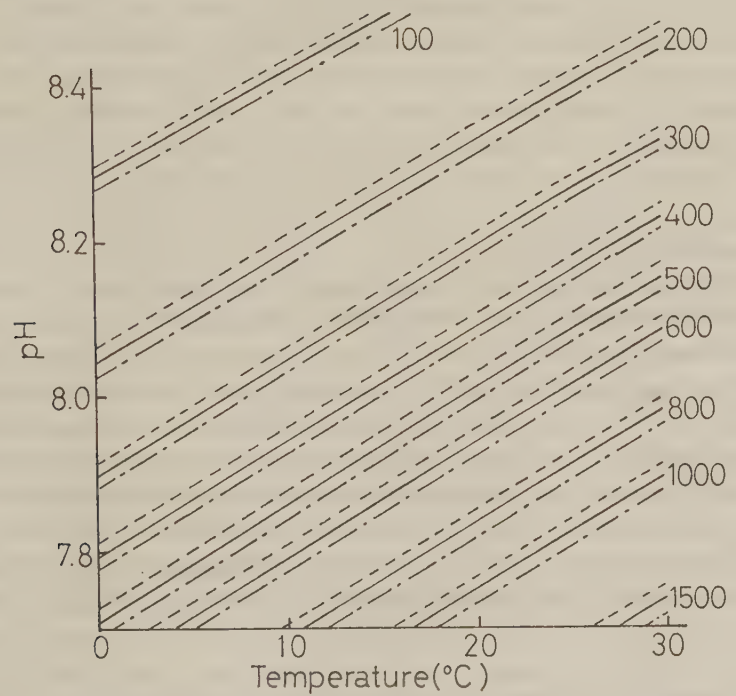

Fig.2 Distribution of P_{CO_2} (ppm) in sea water on the temperature-pH diagram. Total alkalinities (μmol/*l*) are shown in the lines, solid: 2200, broken: 2300 and chain: 2100.

Table 1 Seasonal change of total alkalinity with temperature and salinity in sea surface water observed in 1992 and 1993 at the station H in Fig. 1.

Date	Year	Temp. (℃)	Sal. (psu)	Ta (μmol/l)
8 July	1992	15. 906	33. 659	2237
25 Oct.	1992	14. 342	33. 177	2235
11 Feb.	1993	2. 141	33. 145	2235
23 Apr.	1993	4. 163	33. 504	2243

most in sea surface water of all regions considered here. The change rate of P_{CO_2} is nearly equal to that of total alkalinity based on the equilibrium of carbonate system under the constant pH. Therefore the change of P_{CO_2} may be less than 10 ppm under the present P_{CO_2} (350 ppm). Nearly the same amount of change is caused by the change of 1 °C of temperature or 0.01 of pH, which is always observed seasonally in all areas.

Both temperature and pH generally decrease in winter. The decrease of temperature causes decrease of P_{CO_2} whereas that of pH causes increase of P_{CO_2}. Typical seasonal distributions of temperature and pH are shown in Fig. 3. When temperature changes seasonally without change of pH, the distribution becomes O-A in Fig. 3(a). When pH changes without change of temperature, it becomes O-B. When the two changes occurred in balance or air-sea exchange of CO_2 is very rapid, it becomes O-C. The distribution O-D or O-D' caused by the unbalanced changes of temperature and pH is modified to O-E or O-E' respectively through the air-sea exchange of CO_2. After all, the types of distribution are classified to the three, X, Y and Z in Fig. 3(b). The type X is the case that pH affect P_{CO_2} more than temperature, the type Y that temperature more than pH and the neutral type Z is a intermediate case.

3.1 Temperature-pH diagram

Relations between temperature and pH in surface water in the Oyashio region are plotted in Fig.4. Though the observed values are fairly scattered, picking up the average for five years the normal relation between temperature and pH appears. The type of the seasonal distribution is shown as the inclination in temperature-pH diagram. The seasonal inclination in temperature-pH diagram is rather steep than that of iso-P_{CO_2} lines in Fig. 2, which means P_{CO_2} in winter is higher than in summer.

Relations between temperature and pH in all seas around Japan are also plotted in Fig. 5 with P_{CO_2} under the assumption that total alkalinity is 2200 μmol/*l*. Of course, temperature and pH are both low in winter, but the inclinations are different from each other as well as compared with iso-P_{CO_2} lines. The amplitude of the seasonal variation is the largest in the Oyashio region, followed by the Japan Sea and the East China Sea, and it is small especially in pH in the Kuroshio region such as off Kii Peninsula and off Boso.

3.2 Temperature-P_{CO_2} diagram

The value of P_{CO_2} read in the temperature-pH diagram is plotted in temperature-P_{CO_2} diagram, Fig. 6. The figure indicates clearly the seasonal variation of P_{CO_2} in the seas and the differences among the

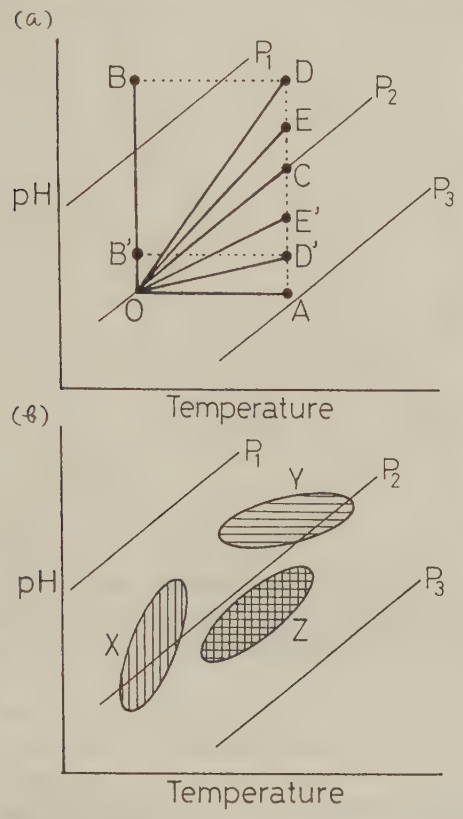

Fig.3 Schematic chart of seasonal variation on temperature-pH diagram. P_1, P_2 and P_3 are isolines of P_{CO_2}. In (a) change of P_{CO_2} is shown when either temperature or pH is changed and both of them are changed. In (b) X and Y show the types of seasonal variation mainly affected by chemical quality and temperature, respectively. Z is the neutral type.

types of its distribution patterns. In winter P_{CO_2} is high only in the Oyashio region and low in other regions. In spring it decreases in all regions around Japan.

Annual mean P_{CO_2} is the highest in the Oyashio region, a little lower in the Japan Sea and the Kuroshio region and the lowest in the East China Sea as shown in Fig. 6.

4. Estimation of carbon dioxide partial pressure from phosphate concentration (PO_4)

Phosphate concentration in sea water is closely related to total carbonate as Redfield revealed. BAES (1983) showed a model where the change of nutrient, total carbonate and total alkalinity are connected with each other through Redfield ratio (1/Rn) and the ratio of calcium carbonate and organic carbon (Ri). Here we use 140 for 1/Rn and 0.25 for Ri according to SIEGENTHALER (1986) and BROECKER (1982) respectively. Applying the relations to the seas around Japan, P_{CO_2} is estimated from the PO_4 concentration and its seasonal variation is discussed.

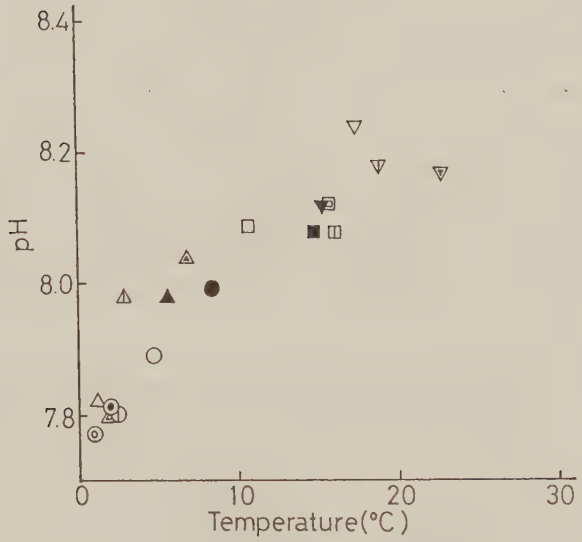

Fig.4 Seasonal variations of temperature and pH at the station H. The marks denote the season, ●:winter, ▲:spring, ▼:summer and ■:autumn. Types of the marks denotes the year, open: '86, split: '87, double: '88, double solid: '89 and solid: '90.

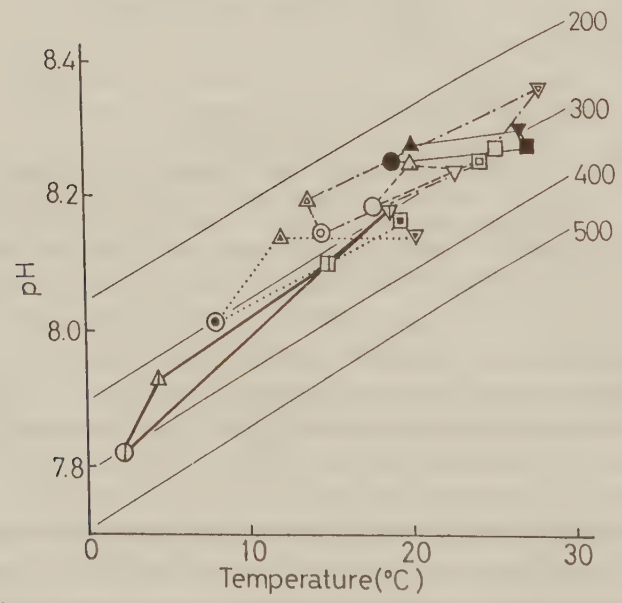

Fig.5 Seasonal variation in each region on temperature-pH diagram. P_{CO_2} (ppm) is also shown when total alkalinity is 2200 μmol/*l*. The marks denote the season, ●:winter, ▲:spring, ▼:summer and ■:autumn. Types of the marks denote the stations shown in Fig. 1, as split: H (Oyashio), double solid: M (Japan Sea), double: N (East China Sea), open: T (Off Boso) and solid: K (Off Kii Peninsula).

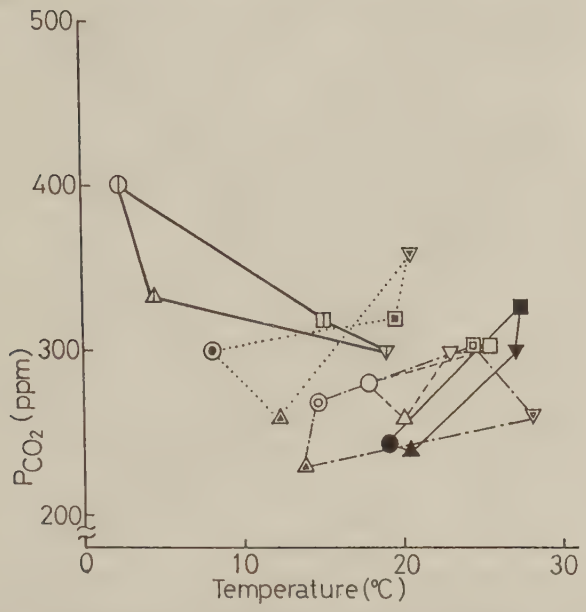

Fig. 6 Seasonal variation of sea water in each region on temperature-P_{CO_2} diagram. P_{CO_2} is calculated from pH and the marks are the same as in Fig. 5.

Now it is assumed that there is sea water with temperature of 15 °C, PO_4 of 0.5 μmol/*l* and total alkalinity of 2200 μmol/*l* in equilibrium with air containing CO_2 of 350 ppm in P_{CO_2}, where salinity is constant, 35 psu. In the assumed water total carbonate and total alkalinity are changed according to the change of PO_4. P_{CO_2} can be calculated when temperature and PO_4 are determined. As the result P_{CO_2} is shown in Fig. 7, a temperature-PO_4 diagram, where total alkalinity is 2200 μmol/*l* but 2300 and 2100 μmol/*l* only for P_{CO_2} of 350 ppm.

The seasonal variations are classified into a water quality type, a temperature type and a neutral type. It should be noted that air-sea exchange of CO_2 is not contained at all in the calculation of P_{CO_2} from PO_4. Neutral type appears only when the effects of temperature and water quality are equal but have opposite sign.

4.1 Temperature-PO_4 diagram

Fig.8 shows normal seasonal variation of temperature and PO_4 in each regions. In all regions temperature decreases with increase of PO_4 in winter and *vice versa* in summer. The inclination of the seasonal variation in the figure is right side down in contrast with temperature-pH diagram and different from each other corresponding to the regions. The range of the seasonal variation is the largest in the Oyashio region, followed by in the Japan Sea and the East China Sea and smallest in the Kuroshio region such as off Kii and off Boso, where the range of PO_4 is especially small.

4.2 Temperature-P_{CO_2} diagram from PO_4

Fig. 9 shows the relation between P_{CO_2} and temperature in a temperature-P_{CO_2} diagram through read-

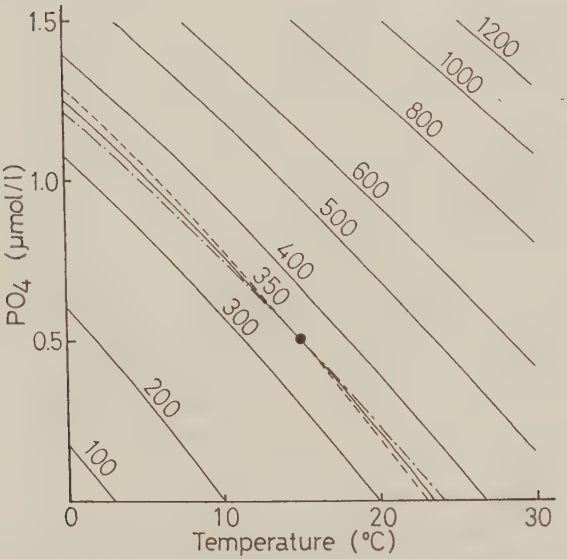

Fig. 7 Distribution of P_{CO_2} in sea water on the temperature-PO_4 diagram. The sea water is assumed to be in chemical equilibrium with air containing 350 ppm P_{CO_2} under 15 °C of temperature, 0.5 μmol/*l* of PO_4 and 2200 μmol/*l* of total alkalinity. Additional lines are for the same condition except for the total alkalinities (μmol/*l*) of 2300 (broken line) and 2100 (chain line) only when P_{CO_2} is 350 ppm.

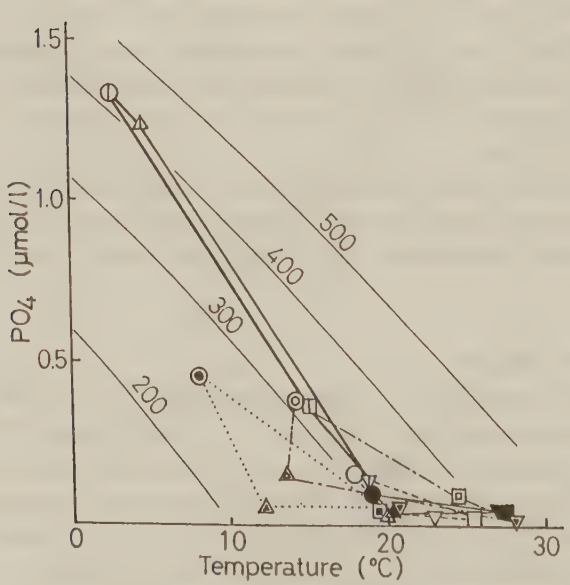

Fig. 8 Seasonal variation of sea water in each region on temperature-PO_4 diagram. P_{CO_2}(ppm) of sea water in equilibrium with air containing 350 ppm CO_2under 15 °C of temperature, 0.5 μmol/*l* of PO_4 and 2200 μmol/*l* of total alkalinity is also shown. The marks are the same as in Fig. 5.

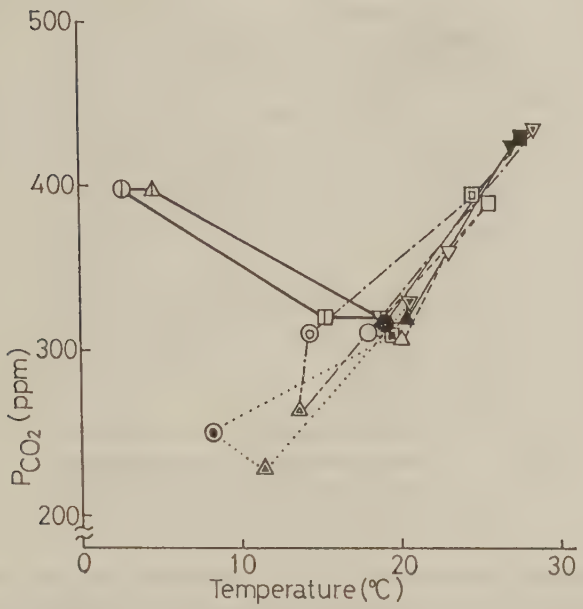

Fig. 9 Seasonal variation of sea water in each region on temperature-P_{CO_2} diagram. P_{CO_2} is calculated from PO_4 and the marks are the same as in Fig. 5.

ing the value of P_{CO_2} in the temperature-PO_4 diagram. The types of the seasonal variation are clearly classified to two. P_{CO_2} is high in summer and low in winter (water quality type) in the Oyashio region and vice versa in the other regions (temperature type).

Decrease of P_{CO_2} in spring is clear in the Japan Sea and the East China Sea but vague in the Oyashio region and the Kuroshio region.

The annual mean level of P_{CO_2} should not be discussed in the estimation from PO_4 because of the assumption of the basic water in some equilibrium shown in Fig. 7. If we assume other conditions for the basic water, the annual mean level will change but the classification of the types of seasonal variation will be still almost the same.

5. A simple model of carbonate system and PO_4

To explain the seasonal variations of P_{CO_2} and other items, a simple model is considered as follows. This model consists of atmosphere and two layers of sea water, which are the surface layer and the deeper layer, as shown in Fig. 10. The P_{CO_2} of the atmosphere is assumed to be constant, 350 ppm. The surface layer varies its depth seasonally, annexes and mixes the chemical matters in the deeper layer only when the surface layer depth gets larger. Temperatures, depths, solar radiations and gas exchange rate of CO_2 in the surface layer are given every month as reasonable values from the observation and the chemicals concentration in the deeper layer are assumed to be constant, where gas exchange rate, the height of air column to be exchanged across sea surface in a unit time, is the inverse value of the residence time of CO_2 in the atmosphere through air-sea exchange. PO_4, total carbonate and total

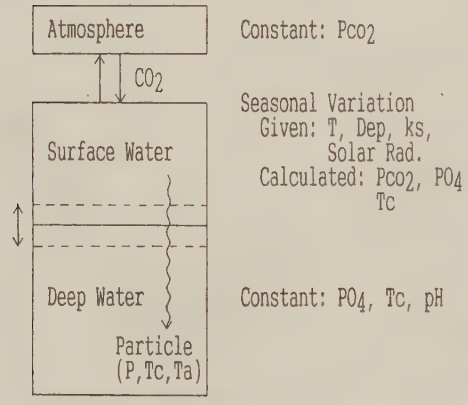

Fig. 10 A model to simulate the seasonal variation of surface water which is connected with atmosphere and deep water.

alkalinity are also assumed to be removed in a definite rate through sinking of a part of particles basically produced by photosynthesis. The equations and conditions in the model are shown in Appendix.

After running of the model for 10 years from the initial stage of the same water of surface layer as the deeper layer, the seasonal variation in a year gets regular. The results are shown in Fig. 11. The difference of seasonal variation of Pco_2 between the Oyashio region (Station H in Fig. 1) and the Kuroshio region (Station K in Fig. 1) is clearly indicated and the results are similar to the estimation from the pH measurement as well as PO_4.

Fluxes used for adjusting the model output to the actual data are shown in Table 2. The result that the residence time of CO_2 in the atmosphere through air-sea exchange in the model is 5 years in the Oyashio region and 10 years in the Kuroshio region is in good agreement with the global average, 750(Gt)/90(Gt/year) = 8 (years) according to the IPCC. Primary productions, 4 gC/m^2day in the Oyashio region and 0.7 in the Kuroshio region are 7-8 times larger than the estimation by KOBLENTZ-MISHKE *et al.*(1970). Removing flux of carbon from the surface layer, whose rate is assumed 10 % of the primary production, are also about 10 times larger in the Oyashio region and twice larger in the Kuroshio region than the global average the IPCC estimated. The reason may be that when surface mixing layer depth gets larger the amount of the mixed nutrients are too large due to sudden increase of nutrient through the boundary between the two layers of the sea water that the primary production with the well known value cannot remove the excess nutrients from the surface layer to get model output in good agreement with the actual data.

6. Discussion

It should be noticed that the Pco_2 around Japan is estimated both from pH and PO_4 but air-sea exchange effect is taken into account only in the estimation from pH but not from PO_4. The reason why the seasonal inclination estimated from pH in a temperature-Pco_2 diagram is smaller than that from PO_4 is air-sea exchange of CO_2 as shown for O-E (O-E') and O-D (O-D') in Fig. 3. The degree of inclination

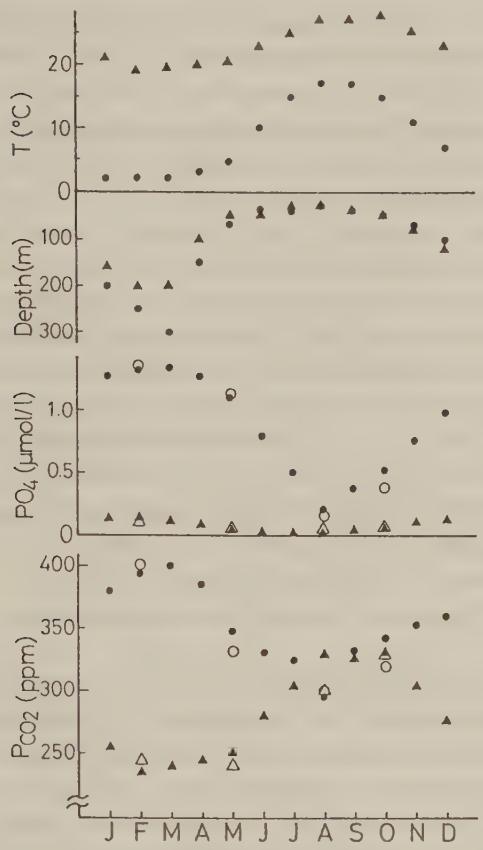

Fig. 11 Seasonal variation in surface water of the model. Temperature and surface mixing depth are input from the observed values and PO_4 and P_{CO_2} are calculated. The regions are ●:Oyashio and ▲:Kuroshio with open marks as observed value.

Table 2 The fluxes input to the model in order to adjust the output to the actual data.

	Oyashio	Kuroshio
Residence Time (Gas Exchange)	5 years (5 m/day)	10 years (2.5 m/day)
Seasonal Ratio in GE	2.3	2.3
Primary Production	0.3 mol/m^{2}day (4 gC/m^{2}day)	0.06 mol/m^{2}day (0.7 gC/m^{2}day)
Seasonal Ratio in PP	5	30

is determined by exchange rate of CO_2 across sea surface and water volume affecting temperature and water quality, that is the thickness of surface mixing layer.

The difference between the seasonal inclinations estimated from pH and PO_4 is small in the Oyashio region and quite large in the Japan Sea and the East China Sea. It suggests that gas exchange rate of CO_2 across sea surface is small or the thickness of mixing layer is large in the Oyashio region. Gas exchange rate of CO_2 across sea surface is dominantly affected by wind speed but annual mean wind speed in the Oyashio region is not so small as in the other regions. Therefore surface mixing layer is expected to be larger in the Oyashio region than the other regions. Actually, in the Japan Sea there is a clear thermocline to prevent vertical mixing of water through it and in the East China Sea mixing is limited due to shallow sea floor around 100 m. On the other hand deep mixing takes place and gets water quality changed very much in winter in the Oyashio region even if large gas exchange occurred.

But these discussion is available only unless new water is mixed side by side, because only vertical process is considered in the present paper. Besides, if the values of Ri and Rn change according to the regions the seasonal variation of Pco_2 estimated by PO_4 may be different from that mentioned above. Comprehensive observation to assure these problems are necessary in the future.

As the IPCC pointed out, about half of the emitted CO_2 by human activities is left in the atmosphere and a part of its budget is not revealed to be called "Missing sink". TSUNOGAI *et al.* (1992) suggest that the ocean uptake of CO_2 in the subarctic region like Oyashio is the possible area to explain the missing sink.

The present study shows the Oyashio region emit CO_2 in winter when wind speed is large and annual budget in the region is possibly emission from sea water to air as TAKAHASHI (1989) said. But it does not deny that the Oyashio region stores missing CO_2. This region is probably source area of CO_2 even before emission of CO_2 by human activity through deep mixing of surface layer in winter. According as the recent CO_2 increase in the atmosphere may reduce the difference between Pco_2 concentrations in sea water and air, emission amount of CO_2 across sea surface may be decreased. Total carbonate in sea water possibly increases due to decrease of emission compared with that at a past time. Whether the increase of the total carbonate can explain the missing CO_2 or not is a problem of future investigation. Anyway, when "Missing sink" is considered, the uptake of CO_2 both in the annual carbon cycle and in the interannual trend should be discussed individually.

On the other hand, the Kuroshio region is considered to be sink because it takes CO_2 up in winter when wind speed is large and air-sea exchange is active.

7. Conclusion

The conclusion in this paper is as follows.

(1) Pco_2 and its seasonal variation are estimated by the two methods, one from pH and the other from PO_4.

(2) In each estimation Pco_2 is high in winter and low in summer in the Oyashio region in contrast with the other regions such as in the Kuroshio region, the Japan Sea and the East China Sea.

(3) In each estimation Pco_2 decreases in spring in all regions around Japan except for in the Oyashio region and the Kuroshio region in the estimation from PO_4.

(4) Annual mean Pco_2 is the highest in the Oyashio region, followed by the one in the Japan Sea

and the Kuroshio region and is the lowest in the East China Sea.

(5) A simple model consisting of atmosphere and two layers of sea water well simulates the seasonal variations in both the Oyashio region and the Kuroshio region by input of the actual seasonal variations of temperature and mixing depth of the surface layer and the concentration of chemical matters in the deeper layer.

8. Future problem

The JMA began the direct measurement of P_{CO_2} by the research vessel, "*Ryofu-Maru*" in 1990 in the western North Pacific but subarctic regions like Oyashio are not included in her survey area. The seasonal variations are so different between the Oyashio and the Kuroshio region that CO_2 observation in subarctic regions is definitely necessary to contribute global carbon cycle study.

Appendix : For a water column of the surface layer

PO_4:

$$P(N) \cdot L(N) = (P(N-1) \cdot L(N-1) + PX \cdot (L(N)-L(N-1))) - F0 \cdot PRO(N) \cdot RN \cdot DN$$

Total Carbonate:

$$C(N) \cdot L(N) = (C(N-1) \cdot L(N-1) + CX \cdot (L(N)-L(N-1))) - F0 \cdot PRO(N) \cdot (1 + RI) \cdot DN + FGAS(N) \cdot DN$$

Total Alkalinity :

$$A(N) \cdot L(N) = (A(N-1) \cdot L(N-1) + AX \cdot (L(N)-L(N-1))) - F0 \cdot PRO(N) \cdot (2 \cdot RI - 0.16) \cdot DN$$

Where

$PX=PD$, $CX=CD$, $AX=AD$ $(L(N) > L(N-1))$

PD,CD and AD mean the values in the deeper layer

$PX=P(N-1)$, $CX=C(N-1)$, $AX=A(N-1)$ $(L(N) \leq L(N-1))$

L(N) : Depth of surface layer at the time N

PRO(N) : Primary production of carbon

FGAS(N) : Gas exchange of CO_2 across the sea surface

F0 : Rmoval rate in the primary production from the surface layer (=0.1)

RI : Ratio of inorganic part to organic one in the removed carbon (=0.25)

RN : Ratio of phosphorus to organic carbon in the removed matter (=1/140)

DN : Time for one step of calculation (=6 days)

References

BAES,C.F.Jr.(1983): The role of the Ocean in the Carbon Cycle.p.31-56., in *Carbon Dioxide*, ed.by W.Bach et al., D. Reidel Publishing Company, Boston.

BROECKER,W.S. and T.-H. PENG (1982) : Tracers in the Sea, Elgidio Press, Lamont-Doherty Geochemical Observatory, Palisachs, New York, 690pp.

HIROTA,M., K.NEMOTO, A.MURATA and K.FUSHIMI (1991) : Observation of carbon dioxide concentration in air and surface sea water in the western North Pacific Ocean. *Oceanogr. Mag.*, **41**, 19-28.
INTERGOVERNMENTAL PANEL ON CLIMATE CHANGE (IPCC) (1990): Climatic Change; The IPCC Scientific Assessment. eds. J.T.Houghton, G.J.Jenkins and J.J.Ephraums, Cambridge Univ. Press, 365pp.
JAPAN METEOROLOGICAL AGENCY (1970) : Manual on Oceanographic Observations. (in Japanese)
JAPAN METEOROLOGICAL AGENCY (1986-1991) : Report of Observation for Monitoring Background Marine Pollution, 1968-1986, No.30-39.
JAPAN METEOROLOGICAL AGENCY (1988-1992) : The Results of the Oceanographical Observations, 1986-1990, No.78-82.
JAPAN METEOROLOGICAL AGENCY (1993) : Marine Climatological Chart of the North Pacific Ocean for 30 year period (1961-1990), 191pp.
KOBLENTZ-MISHKE, J., V.VOLKOVINSKY and G.KAVANOVA (1970) : Scientific Exploration of the South Pacific. Standard Book No.309-01755-6, National Academy of Sciences, Washington, D.C., 185pp.
SHINOHARA,Y. and N.SHIKAMA (1988): Marine Climatological Atlas of the Sea of Okhotsk, Technical Reports of the Meteorological Research Institute, No.23, 57pp.
SIEGENTHALER,U. (1986): Carbon Dioxide: its natural cycle and anthropogenic perturbation. p.209-247., in *The Role of Air-Sea Exchange in Geochemical Cycling*, ed. by P. Buat-Menard., 209-247, D. Reidel Publishing Company, Boston.
TSUNOGAI,S., T.ONO and S.WATANABE (1993): Increase in Total Carbonate in the Western North Pacific Water and a Hypothesis on the Missing Sink of Anthropogenic Carbon. *Journal of Oceanography*, **49**, 305-315.

日本周辺海域における表面海水中の二酸化炭素分圧の季節変化

加納　裕二・林　　和彦
（函館海洋気象台）

海水は季節により水温，水質，さらには二酸化炭素の大気との交換の様子を大きく変化させるので，それらの季節変化の状況を明らかにする事は地球温暖化を引き起こす大気中の二酸化炭素の動向を知る上で重要である．

気象庁と海洋気象台の海洋気象観測船による日本周辺の定点における海洋バックグランド汚染観測の資料を用いて，水温，水素イオン濃度（pH）及びリン酸塩濃度から二酸化炭素分圧を推定し，日本周辺海域での二酸化炭素分圧の季節変化の特徴を調べた．二酸化炭素分圧はpHと全アルカリ度から炭酸物質の化学平衡方程式から計算される．一方，栄養塩，全炭酸及び全アルカリ度の関係を用い，リン酸塩濃度から二酸化炭素分圧を推定することもできる．

どちらの計算結果も，二酸化炭素分圧は，親潮海域では夏季に低く冬季に高いが，その他の海域では全く逆の季節変化をしていることがわかった．二酸化炭素分圧の季節変化の要因として親潮海域では水質の季節変化が重要であるが，その他の海域では水温の季節変化が重要であった．

表面海水中の二酸化炭素分圧の季節変動を説明するため大気，表層海水，深層海水からなるモデルを作成した．フラックスを含むいくつかのパラメータを調節すると，親潮域と黒潮域の二酸化炭素分圧季節変動の違いをはっきりと表現し，実測値とよい一致を示した．

大気と海洋における炭素循環の解明に寄与するためには，本州南方の海域だけでなく親潮を含む日本周辺海域の総合的で詳細な観測が不可欠である．

The Oceanographical Magazine
Vol. 44. Nos. 1-2. pp. 45 to 57, March 1994

Characteristics of interannual variation of water temperature in the East China Sea

Ikuo KANEKO*, Yasushi TAKATSUKI*, Tomoji TASHIRO**
and Xiangping SUN***

* *Marine Department, Japan Meteorological Agency*
1-3-4 Otemachi, Chiyoda-ku, Tokyo 100, Japan
** *Oceanographical Division, Nagasaki Marine Observatory*
11-51 Minamiyamatemachi, Nagasaki 850, Japan
*** *First Institute of Oceanography, State Oceanic Administration*
13 Hongdao Road, Qingdao, China

(Received October 25, 1993: Accepted January 14, 1994)

Abstract: Based on the results by KANEKO and EGUCHI(1987), interannual variability of quasi-biennial and 6-year time scale, which is dominant in sea surface temperature(SST) over the East China Sea(ECS), is studied by the method of cross-spectral analyses. A relationship of the SSTs between the Kuroshio region of the ECS and the tropical Pacific is examined on the quasi-biennial variability. The SST over the northern continental shelf, where the most precedent variability of the 6-year time scale is found, is also analyzed in the correlation with the coastal temperature(CWT) around the ECS and the surface air temperature(AT) in China.

The quasi-biennial variation in the Kuroshio region of the ECS is highly coherent with one in the eastern equatorial Pacific, while is not so coherent with the variation in the western tropical Pacific, the origin region of the Kuroshio. The variation in the Kuroshio region of the ECS is about 8 months behind one in the eastern equatorial Pacific.

The SST variation of 6-year time scale over the northern continental shelf of the ECS is highly coherent with the CWT and AT at Huabei district in China. However, the SST variation leads the CWT and AT variations about 6 months or more, and this is contradictory to the general idea that atmospheric variations directly influence SSTs over shallow marginal seas.

1. Introduction

Weather and fisheries in the East China Sea(ECS), around the Ryukyu Islands and coastal regions of Kyushu are largely affected by temperature variations in the ECS. Development of tropical and extratropical cyclones which pass through the ECS is related to the distribution of sea surface temperature(SST) there(e.g., HANSON and LONG, 1985). Fish catches in the continental shelf region and maricultures in the coastal regions are also influenced by variations of water temperature(e.g., KONDO and TAMAI, 1974; BAIK *et al.*, 1992). An accurate prediction of SST variation is, therefore, required to improve the efficiency of the economical activities in/around the ECS.

It is information about small SST anomalies from normal values that is useful for the economical activities while normal values of SSTs over the sea of mid-latitudes as the ECS contain large seasonal variability. Long-term data of SSTs are, therefore, necessary for precise estimation of normal values

when we calculate and utilize anomalies of SSTs. Since 1950s, the Nagasaki Marine Observatory(NMO), the Japan Meteorological Agency(JMA), has collected and edited the SST, coastal water temperature(CWT) and hydrographic data in/around the ECS to issue warm-season SST forecasts in every spring. The NMO has also continued researches and studies on the SST variability by using these long-term data sets to improve accuracy of the forecast.

As one of such efforts, KANEKO and EGUCHI(1987) made a study on long-term variability of water temperature and salinity in the ECS, focusing upon periodic ones. They showed two dominant peaks in spectral density at quasi-biennial and about 6-year periods by a spectral analysis of SST over the ECS. They also calculated coherence and phase difference of the time series of the SST anomaly referred to the station east off Taiwan and found that at 28-month period, the coherence is high and the phase difference is nearly zero along the Kuroshio path. The phase is delayed from the Kuroshio towards the surrounding regions. SSTs over the tropical Pacific have clear variability of the quasi-biennial oscillation(QBO) time scale (YOSHINO and KAWAMURA, 1987; KAWAMURA, 1988). It is, therefore, natural to build up an hypothesis that the quasi-biennial variation found in SSTs over the ECS is the one carried from the tropical Pacific through heat advection by the Kuroshio. About a relation between the variations in the ECS and in the tropical Pacific, DING and YOSHINO(1988) found the characteristic SST decreases over the Kuroshio region before El Nino events. El Niño events should also be paid attention when we focus on the quasi-biennial variability in the ECS because LAU and SHEU(1988) proposed the idea that El Niño/Southern Oscillation can be considered as the amplitude modulation of the QBO.

On the 6-year variation, KANEKO and EGUCHI(1987) found that high coherence zone exists along the Kuroshio as well as the quasi-biennial variation, but the variation in the Kuroshio region is 30 degrees, about 6 months, behind one over the northern continental shelf. Power-spectral density at 6-year period is high over the northern continental shelf while it is low in the Kuroshio region. They thought that these phenomena are related to the rapid response of shallow shelf water to forcing by atmospheric variations.

By their study, characteristics of the periodic variability in the central and southern ECS became made clear, but a relation with large scale variability both in the ocean and the atmosphere is not yet investigated. Long-term data of water and air temperature near by China, and those in the tropical Pacific are necessary to put their studies forward. During the Japan-China Joint Research Programme on the Kuroshio(JRK), we have gathered Chinese data with the support of the China State Oceanic Administration(SOA). In this study, we focus on the quasi-biennial and 6-year periodic variations and clarify the relationships of them between the ECS and factors which have effects on the variations in the ECS. We make some suggestions for further study to identify the source of these variability in the ECS.

2. Data Analysis

2.1 Data

All of the data used in this study are monthly averaged ones. Their durations are shown in Figure 1. Japanese data are

(a) SST at 1 degree grid points in the ECS from 1953 to 1989. They were compiled by the Nagasaki Marine Observatory.

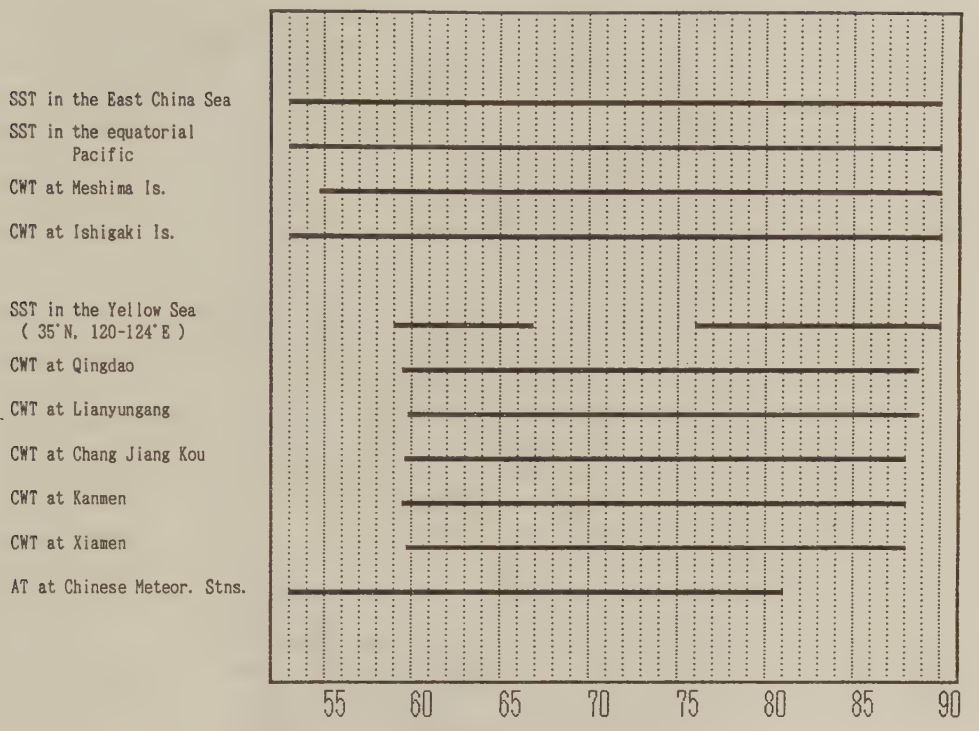

Fig. 1 Data used in this study and their durations.

(b) SST in the El Niño monitoring areas of the equatorial Pacific from 1953 to 1989. They were compiled by the El Niño Monitoring Center of the JMA.

(c) Coastal water temperature(CWT) measured at Meshima Island west off Kyushu from 1954 to 1989. The data were obtained by the Japan Maritime Safety Agency.

(d) CWT measured at Ishigaki Island from 1953 to 1989, by the JMA.

Around the ECS several CWT stations have been maintained by Japanese governmental organizations, but the data at only two stations, Meshima Island and Ishigaki Island, are available as long-term data since 1950s because the old-fashioned method of bucket sampling has been maintained at these stations.

Chinese data are as follows;

(a) SST at the area along 35°N in the Yellow Sea from 1959 to 1966 and from 1976 to 1989, compiled by the Qingdao Marine Environmental Forecasting Observatory of the SOA.

(b) CWT at Qingdao, Lianyungang, Chang Jiang Kou, Kanmen and Xiamen from 1959 to 1988, obtained by the SOA.

(c) Air temperature(AT) at Chinese meteorological stations from 1953 to 1980.

The locations of the stations and the areas of these data are shown in Figure 2 and also in the inset of Figure 4. The SST data at the grid points enclosed by the polygons in Figure 2 are averaged in each area to yield the areal time-series. They are compared with other SST, CWT or AT time-series.

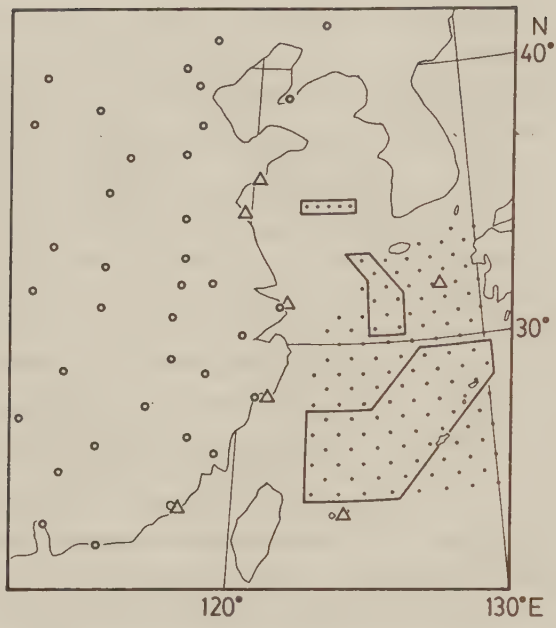

Fig. 2 Station location charts in the ECS. Dots indicate SST grid stations, open triangles CWT stations, and open circles AT stations. The areas enclosed by polygons are called "35°N in the Yellow Sea", "Northern continental shelf" and "Kuroshio region", respectively, from north.

2.2 Analytical procedure

These data are processed in the same way as one by KANEKO and EGUCHI(1987). The normal values and the monthly anomaly time-series are calculated from the original monthly time-series. The power and cross spectra are computed from the monthly anomaly time-series by using FFT algorithm. Hanning window is applied four times to the FFT output for smoothing, and the number of equivalent degrees of freedom is 16. The low-pass and band-pass filters used in this study are all Fourier-Lanczos type, which has smooth transfer function.

3. Results and discussions

3.1 Quasi-biennial variation

We compared the quasi-biennial SST variation at the grid points in the ECS with that in the western tropical Pacific since the previous study suggests that the Kuroshio transfers the quasi-biennial variation to the ECS. The quasi-biennial SST variation in the southern ECS is significantly correlated with one in the western tropical Pacific(Fig.3). However, coherence in the central and northern ECS is lower than 95% confidence limit.

Among four areas in the tropical or equatorial Pacific, the quasi-biennial SST variation in the eastern equatorial Pacific, the area C, is most correlated with one of the Kuroshio in the ECS(Fig.4). Figure 5

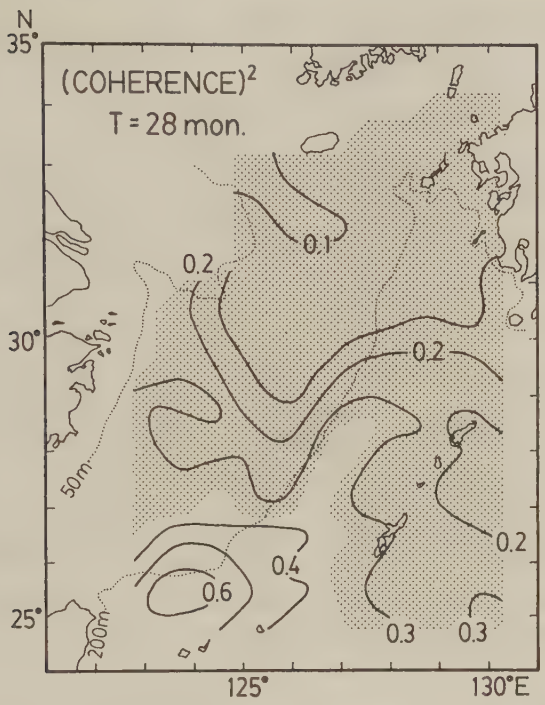

Fig. 3 Distribution of (coherence)^2 in the ECS for 28-month period SST variation. The reference area, the western tropical Pacific, is shown in Figure 4 as the area A.

shows the distributions of coherence and phase lag referred to the eastern equatorial Pacific. High coherence zone spreads along the Kuroshio path. The phase in the Kuroshio is constant and about 100 degree, 8 months, behind that in the eastern equatorial Pacific.

The power-spectral density of the SST anomaly in the eastern equatorial Pacific has a clear peak at the period between 40 and 50 months(Fig.6(b)). The peak period corresponds to the mean interval of El Niño events, which have been observed 9 times during the period from 1953 to 1989. Only a small peak, which is not significantly separated from the main peak, is found at the quasi-biennial period. However, the correlation between the SST variations in the Kuroshio region of ECS and in the eastern equatorial Pacific is higher at the quasi-biennial period than at any other periods(Fig.6(c)).

Though there is no doubt that the quasi-biennial SST variability in the ECS has some connection with one in the eastern equatorial Pacific, we believe that more examinations of the results from the spectral analysis are indispensable for this case. It is because the quasi-biennial variability of SST is, at present, not recognized as an oscillation of which forcing and exact period are elucidated. We should also pay attention to a relationship between the quasi-biennial variability and El Niño events, considering the result by LAU and SHEU(1988). For these reasons, we draw the time series of the SST variations of which quasi-biennial components are extracted by a band-pass filter and make peak-to-peak comparisons at maxima or minima of the time series. The band-pass filter used here transmits variations at the

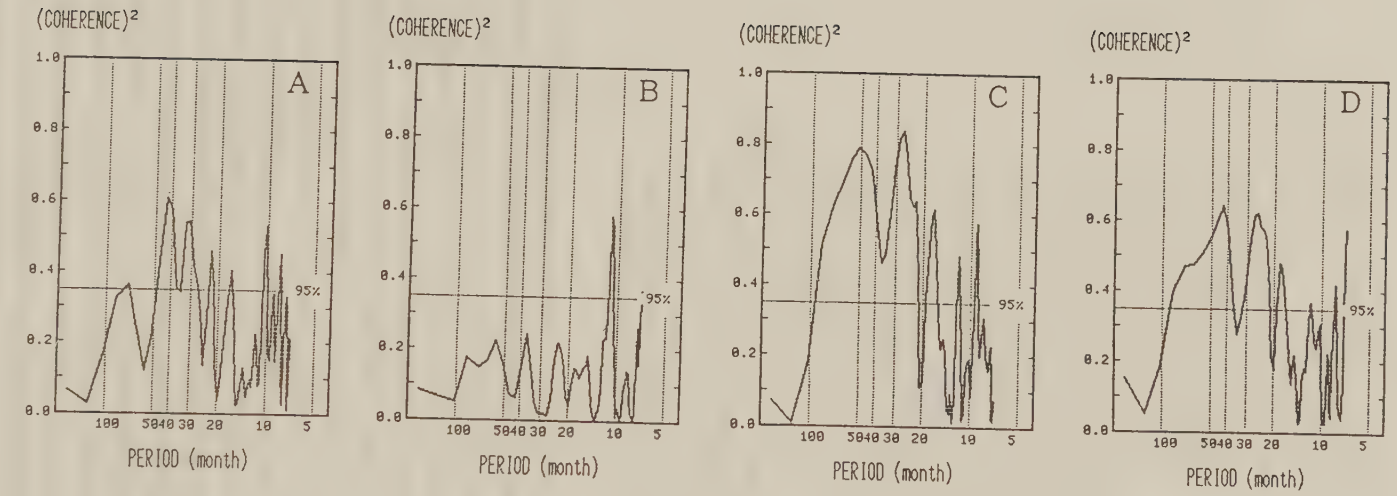

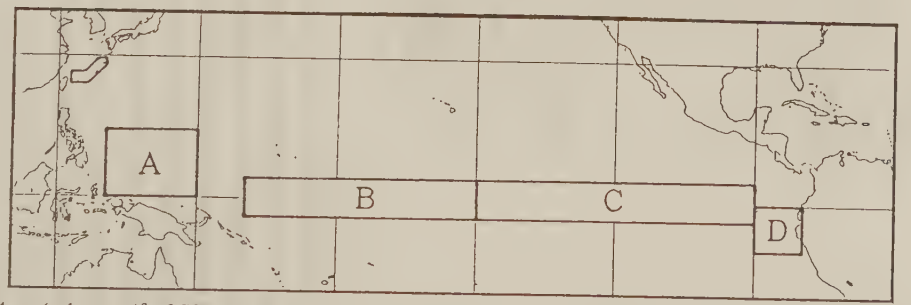

Fig. 4 (coherence)² of SST variation between each area of the equatorial Pacific and the Kuroshio region in the ECS. Locations of the areas are shown in the chart.

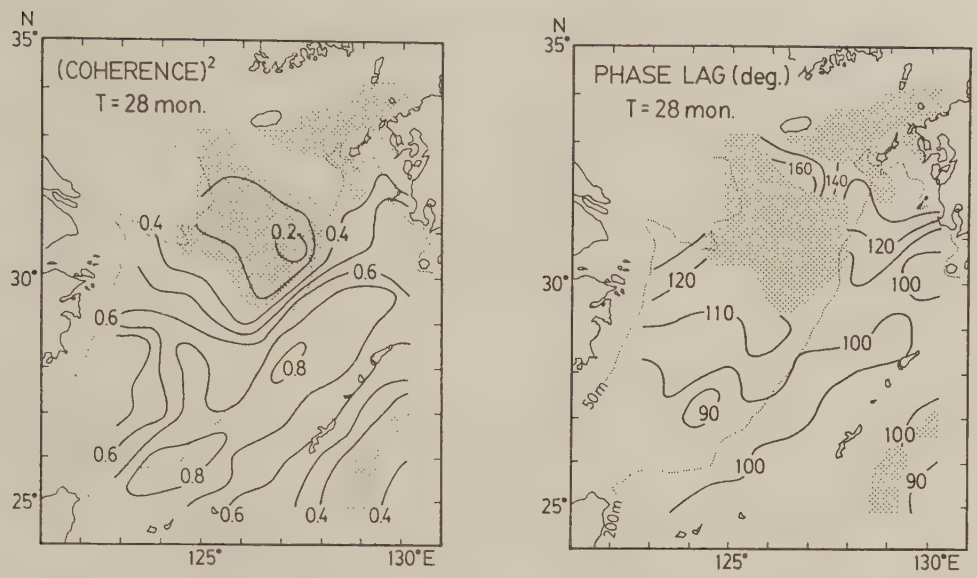

Fig. 5 Distributions of (coherence)^2 and phase lag in the ECS for 28-month period SST variation. Regions where coherence is lower than 95% confidence limit are hatched. The reference area, the eastern equatorial Pacific, is shown in Figure 4 as the area C.

periods between 20 and 35 months.

Figure 7 shows the filtered SST time series in the Kuroshio region of the ECS and in the eastern equatorial Pacific. Periods of El Niño events are indicated by 9 bars in the lower part of the figure. El Niño events correspond to the periods when the quasi-biennial component in the eastern equatorial Pacific become large positive, except in 1974. In 1974, the magnitude of original SST anomaly was small, and this year is not recognized as the period of El Niño event. We can interpret that the dominant component, of which period is about 45 months, is negative and canceled the quasi-biennial variation in 1974 when we inspect the phase of the 45 month component though this component is not shown in Figure 7. At any rate, our results obtained from the analysis of SST time series reconfirm the result by LAU and SHEU(1988), that occurrences of large ENSOs generally coincide with large QBOs in global precipitation.

The quasi-biennial variation in the Kuroshio region of the ECS follows one in the eastern equatorial Pacific when the amplitude in the eastern equatorial Pacific is large. DING and YOSHINO(1988) showed that SST anomaly in the Kuroshio tends to be negative before El Niño events. Their result can be clearly understood when we pay attention to the relation of the two quasi-biennial variations.

The quasi-biennial variation in the ECS is clearly correlated with one in the eastern equatorial Pacific and may be called as "oceanic QBO" in a similar manner that YOSHINO and KAWAMURA(1987) called the SST variations of 22-28 month period in the equatorial Pacific. We should investigate in future how the quasi-biennial variation in the eastern equatorial Pacific affects the SST in the Kuroshio region of the ECS. The quasi-biennial variation of SST leads in the Kuroshio region(Fig. 5), and besides a

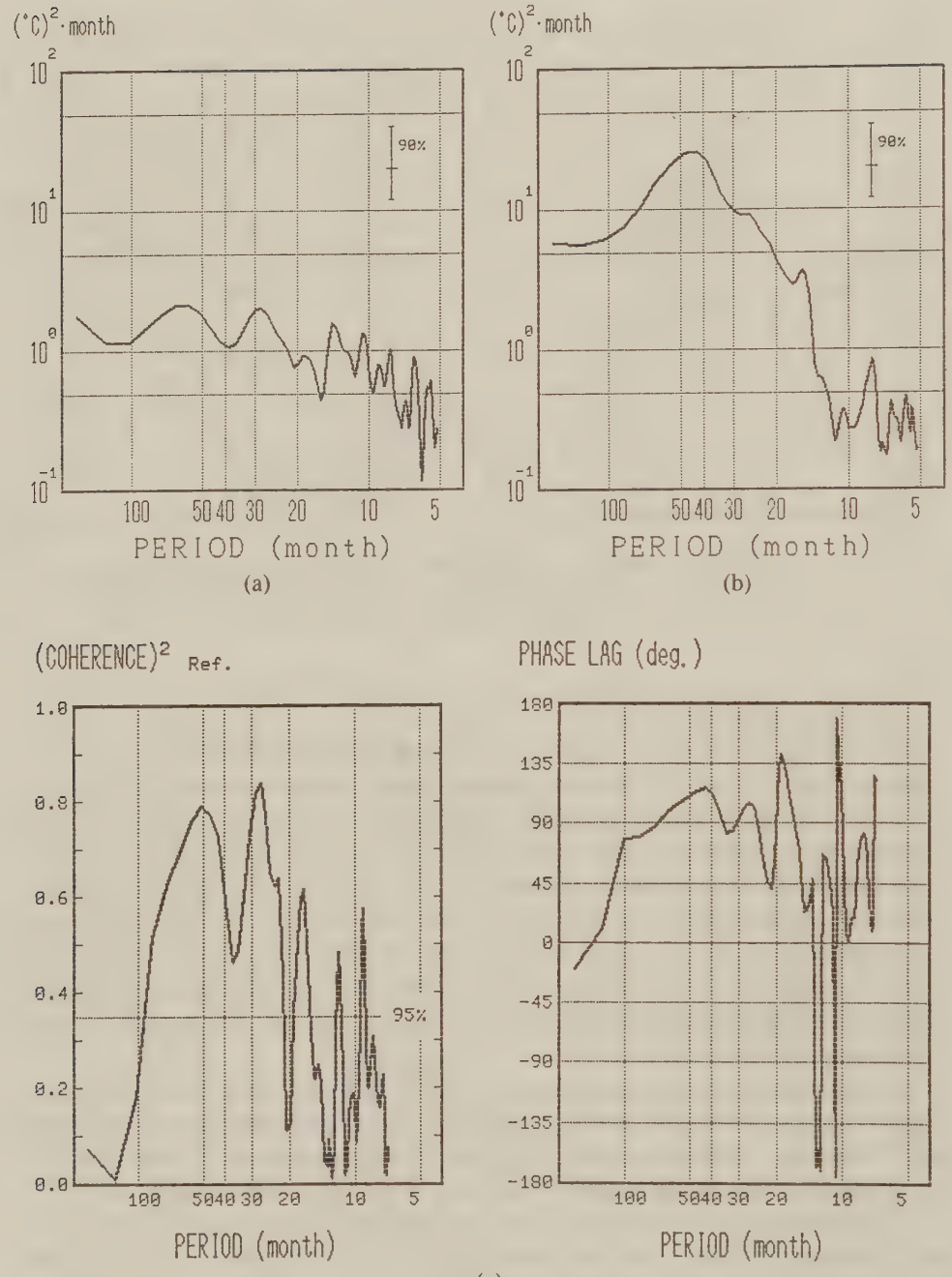

Fig. 6 Power spectra of SST variation in the Kuroshio region of the ECS (a) and the eastern equatorial Pacific (b), and their correlation (c).

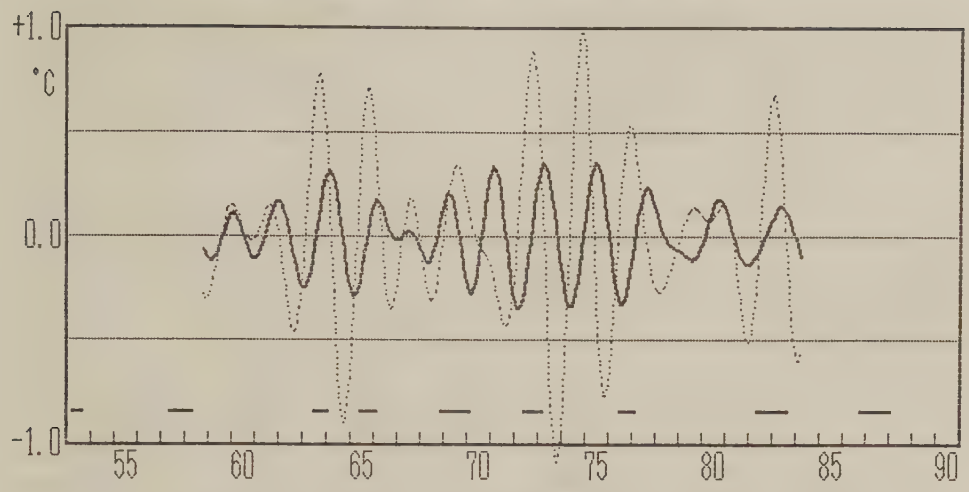

Fig. 7 Comparison of band-pass filtered SST time-series in the two areas. Thick line corresponds to the Kuroshio region of the ECS, and dotted line the eastern equatorial Pacific (area C). Short bars in the figure indicate periods of El Niño events.

similar variation is found in the sub-surface layer of the hydrographical section crossing the Kuroshio in the ECS (KANEKO and EGUCHI, 1987). It is, therefore, proper to think that the Kuroshio already obtains the variability before entering the ECS through the Ishigaki Strait. We will be able to determine where and how the variability is strengthened or injected in the Kuroshio when we have the time-series of SST, CWT and air-sea heat exchange around Taiwan, the Philippines and the North Equatorial Current.

3.2 6-year period variation

As for the other period, 6 years, the correlations between the AT variations at the meteorological stations in China and the SST variation over the northern continental shelf are calculated and mapped in Figure 8, since atmospheric influence is suggested from the study by KANEKO and EGUCHI(1987). The area of the northern continental shelf shown by a polygon in Figure 8 is determined from the power and phase distributions in their paper. Over the Great Plain of China, Huabei Pingyuan, the AT variations are highly coherent with the SST variation over the northern continental shelf. However, the AT variations over the Huabei Pingyuan are about 30 degrees, 6 months, behind the SST variation over the northern continental shelf, which result is contrary to our expectation.

The variability in the Yellow Sea or western ECS is, therefore, investigated to find out an origin of the precedence in the SST variation over the northern continental shelf. Owing to a lack of long time-series of SST there, we have to utilize the time-series of CWTs though they may contain local variability which is difficult to be evaluated and eliminated. The CWT variations at Lianyungang and Meshima Is. are highly coherent with the SST variation over the northern continental shelf, but they are as much as 50 degrees, 10 months, behind the SST variation over the northern shelf(Table. 1). In Figure 9, these

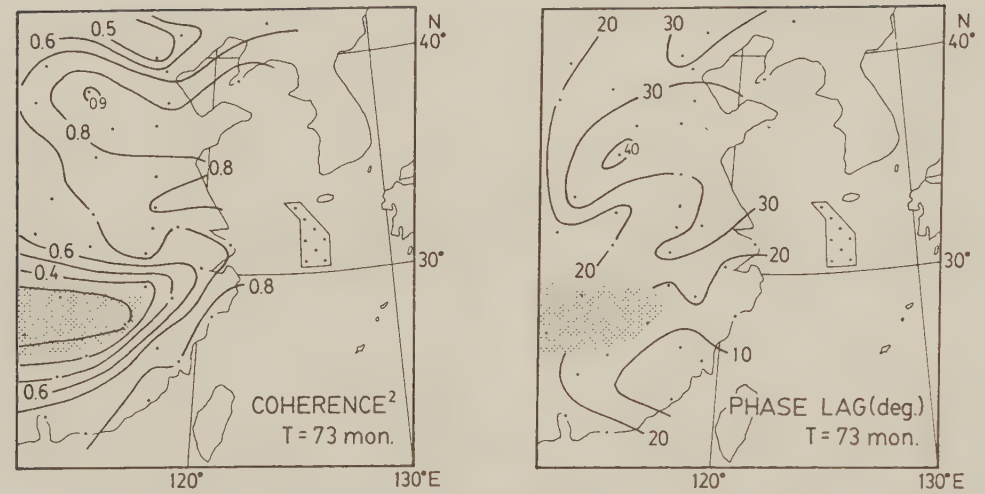

Fig. 8 Distribution of (coherence)^2 and phase lag in China for 73-month period AT variation. Regions where coherence is lower than 95% confidence limit are hatched. Location of the reference area, the northern continental shelf, is indicated by a polygon.

time-series are compared after applying the low-pass filter which transmits variations longer than 45-month period. The CWT variations at two stations are evidently behind the SST variation on the northern shelf except at the minimum in 1980, when phase differences are too small to be evaluated.

The data set of SST in the Yellow Sea compiled by the Qingdao Marine Environmental Forecasting Observatory is the only one available as historical time-series though it has a serious blank of observation from 1966 to 1975. The divided two time-series are too short to apply spectrum analyses nor low-pass filter. However, we want to get as much information as possible from these data since we can not find out any other continuous data in the northern ECS or Yellow Sea. As is shown in Figure 6(a), the quasi-biennial and 6-year period SST variations are dominant and power in the periods between the two peaks is weak over the ECS. The 6-year period variation can be clearly recognized in the SST time-series applied by 29-month running mean to remove the quasi-biennial component(Fig. 10). The variation in the Yellow Sea seems to be behind during the period from 1960 to 1965, but the phase difference is small since 1977. This result is similar to that obtained from the CWT data. The both results as a whole indicate the precedence of the SST variation over the northern continental shelf, but we can not conclude now that this phenomenon is inherent in the sea over the northern continental shelf without researching the temperature variability at the western coast of Korea, of which data may be used as a substitute for those in the Yellow Sea.

4. Concluding remarks

For the quasi-biennial time scale, the SST variation in the ECS has strong correlation with one in the eastern equatorial Pacific, while it has not so strong correlation with one in the western tropical Pacific. We, thereby, have to revise our hypothesis that the western boundary current directly transfers the

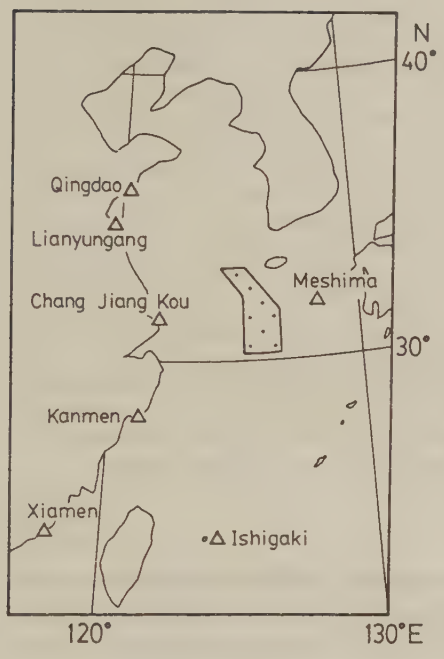

Table 1 (coherence)^2 and phase lag of CWT time-series referred to SST time-series on the northern continental shelf. Locations of the CWT stations and the reference area are shown in the chart.

CWT Station	(Coherence)^2	Phase ± 95% C.L. (deg.)
Meshima	0.80	+47 ± 20
Ishigaki	0.34	+12 ± 70
Qingdao	0.63	+53 ± 31
Lianyungang	0.81	+54 ± 19
Chang Jiang Kou	0.51	+31 ± 41
Kanmen	0.66	+50 ± 29
Xiamen	0.46	+ 3 ± 47

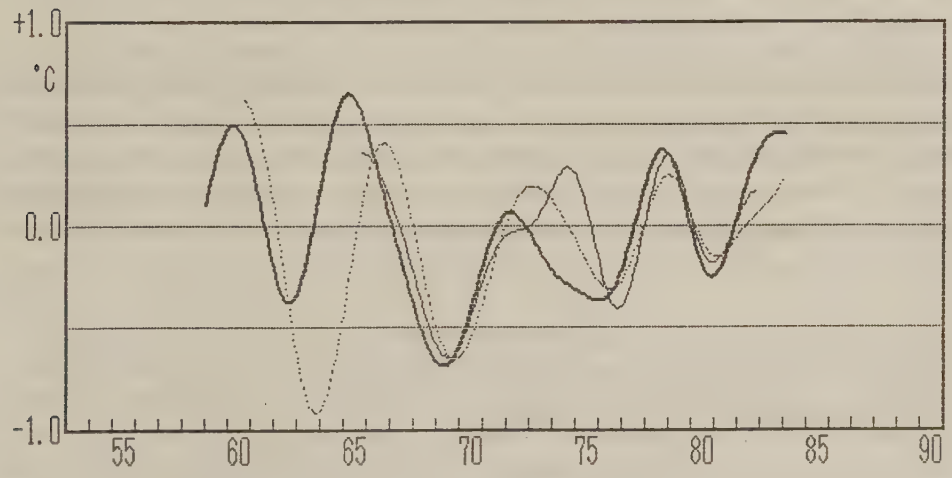

Fig. 9 Comparison of low-pass filtered SST/CWT time-series. Thick line corresponds to the northern continental shelf, thin line Lianyungang, and dotted line Meshina. Locations of the area and stations are shown in the inset of Table 1.

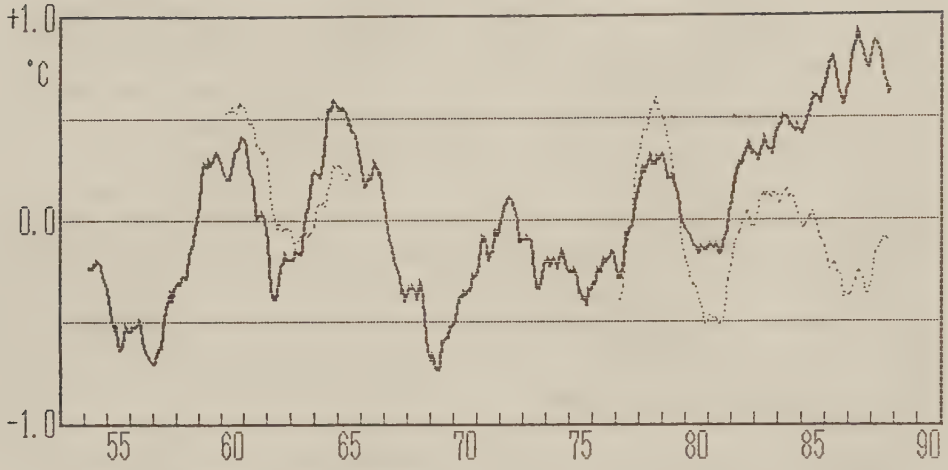

Fig. 10 Comparison of running-meaned SST time-series in the two areas. Thick line corresponds to the northern continental shelf, and dotted lines the 35°N in the Yellow Sea. Locations of the areas are shown in Figure 2.

variation from the equatorial region to the ECS. We speculate some intermediate process that receives the variation in the eastern equatorial Pacific and injects it into the Kuroshio in the region south off the ECS. The effect of El Niño phenomena on the Kuroshio and the ECS is suggested by the investigation about the quasi-biennial variability. Characteristics of the variations in SST, CWT and air-sea heat exchange should be investigated in the region south off the ECS to clarify where the Kuroshio acquires the quasi-biennial variability.

The SST variation of 6-year period over the northern shelf of the ECS is highly coherent with the CWT or AT variation at Huabei district in China. However, the idea that local forcing of atmosphere mainly raise the SST variation over the northern continental shelf is doubtful because the SST variation on the northern continental shelf precedes the CWT or AT variation. A lack of solar radiation and wind velocity data of long term over the sea prevents us to estimate the heat exchange time-series in the past 30 years. For the present, we have no idea what mechanism generates the peculiarity of the 6-year variation over the northern continental shelf.

Acknowledgement

The authors thank Wang Deyuan, senior engineer of the National Oceanographic Data Center, and Tang Mingyi, senior engineer of the North China Sea Marine Forecasting Center for their kind help to the authors in collecting the Chinese data. Thanks are extended to Takeshi Uji and an anonymous reviewer for their criticisms and helpful comments. This study is supported by a grant from the Japan Science and Technology Agency for the Japan-China Joint Research Programme on the Kuroshio(JRK).

References

BAIK, C. I., J. H. PARK and K. D. CHO(1992): The Variations of Fishing Conditions of Yellow croaker Pseudosciaena polyactis Bleeker in Relation to the Oceanographic Conditions of Korean Waters. *Bull. Fish. Res. Dev. Agency* (Republic of Korea), **46**, 69-80.

DING, L. and M.YOSHINO (1988) : Relationship between Sea Surface Temperature in the Kuroshio region and El Niño Phenomena. *Report of Environmental Research Center, Univ. of Tsukuba*, **12**, 1-5 (in Japanese).

HANSON, H. P. and B. LONG (1985) : Climatology of Cyclogenesis over the East China Sea. *Mon. Wea. Rev.*, **113**, 697-707.

KANEKO, I. and I. EGUCHI (1987) : Interannual Variation of Sea Surface Temperature in the East China Sea. 6 and 2-year periods. *Umi to Sora*, **63**, 127-138 (in Japanese).

KAWAMURA, R. (1988) : Quasi-Biennial Oscillation Modes Appearing in the Tropical Sea Water Temperature and 700 mb Zonal Wind. *J. Meteor. Soc. Japan*, **66**, 955-965.

KONDO, M. and K.TAMAI (1974) : Oceanographic variations and Fishery conditions in the East China Sea. *Suisan Kaiyou Kenkyuu Kaihou*, **25**, 165-175 (in Japanese).

LAU, K.-M. and P. J. SHEU (1988) : Annual Cycle, Quasi-Biennial Oscillation, and Southern Oscillation in Global Precipitation. *J. Geophys. Res.*, **93**, 10975-10988.

YOSHINO, M. and R. KAWAMURA (1987) : Periodicity and Propagation of Sea Surface Temperature Fluctuations in the Equatorial Pacific. *Beitr. Phys. Atmosph.*, **60**, 283-293.

東シナ海の水温経年変動特性

金子　郁雄・高槻　靖（気象庁海洋気象部）
田代　知二（長崎海洋気象台）
孫　湘平（中国国家海洋局第一海洋研究所）

金子・江口（1987）の研究結果をふまえて，東シナ海の海面水温で卓越する準2年及び6周期の変動について，クロススペクトル解析による研究を行った．準2年周期変動については，黒潮域と太平洋熱帯域の海面水温との相関を調査した．6年周期変動については，周辺の沿岸水温及び中国大陸の気温との相関について解析した．

準2年周期変動については，東シナ海黒潮域での変動は，太平洋熱帯域の海面水温の変動と東部で相関が高く，黒潮源流にあたる西部とは相関が低いことがわかった．東シナ海黒潮域の準2年海面水温変動は，東部赤道太平洋より8か月遅れている．

北部大陸棚上で目立つ6年周期変動は，華北地方の沿岸水温及び気温の6年周期変動との相関が高い．しかし，北部大陸棚上の変動の位相の方が，沿岸水温及び気温の変動の位相より6カ月またはそれ以上先行しており，水深が浅い縁辺海では大気の変動が先に現れ，これが直接海面水温に影響するであろうという一般的な予想に反する結果である．

The Oceanographical Magazine
Vol. 44. Nos. 1-2. pp.59 to 75, March 1994

Distributions and behaviors of chemical substances in the East China Sea and Yellow Sea

Masanao IMAI, Katsuhiko FUSHIMI, Jun-ichi OHYAMA
Marine Department, Japan Meteorological Agency
1-3-4 Otemachi, Chiyoda-ku, Tokyo 100, Japan
and
Kan OGAWA
Maizuru Marine Observatory
901 Shimofukui, Maizuru 624, Japan

(Received December 7, 1993; Accepted January 14, 1994)

Abstract: We have carried out chemical observations since 1986 through 1989, mainly along the meridian of 123°E and 124°E (31°30'N - 36°30'N) which ranged from the East China Sea to the Yellow Sea. We analyzed the data obtained by these observations and summarized the result as follows:

In the area of this study, lithium and boron have positive correlation with salinity, therefore behave as conservative elements derived from the open sea. Barium and copper have negative correlation with salinity, therefore behave as conservative elements derived from land.

In autumn, in the southern part of this area, the ratio of phosphate-phosphorus to nitrate-nitrogen (PO_4-P/NO_3-N) is similar to the Redfield Ratio, but in the Yellow Sea Cold Water (YSCW), the ratio is larger than the Redfield Ratio. The relationships between nutrients and Apparent Oxygen Utilization (AOU) in the YSCW, and the vertical profiles of nutrients in theYSCW are examined in order to understand the large value of PO_4-P/NO_3-N ratio. But the large value of the ratio in the YSCW can be explained neither by selective regeneration of PO_4-P from organic matter nor by the input of dissolved PO_4-P in interstitial water into sea water. In winter, vertical mixing reachs the bottom in all part of this area, and the YSCW is disappeared. In all part of this area the ratio of PO_4-P to NO_3-N was similar to the Redfield Ratio.

1. Introduction

In the study for "Understanding the purification mechanism and its ability in the Kuroshio", to clarify the process that substances are taken in the Kuroshio and the quality of the Kuroshio water is changed by them, is one of the important research tasks. It has been reported that the concentration of phosphate-phosphorus in the Kuroshio water is increased by mixing with coastal water in the East China Sea (SAGI and ARAKAWA, 1982). On the study of behavior of substances in the Kuroshio water, therefore, chemical characteristics of coastal water (the East China Sea water and the Yellow Sea water in this study) must be understood.

In the East China Sea and Yellow Sea, the continental estuary water, the Kuroshio water and the Yellow Sea warm current water mix each other, and peculiar water masses are formed, so chemical characteristics are complicated throughout the year.

We carried out the investigation and analysis in order to understand the chemical characteristics of the East China Sea and Yellow Sea.

2. Materials and methods

Since 1986 through 1989, we have carried out the observations on board the R/V *Ryofu Maru* which belongs to the Japan Meteorological Agency mainly in autumn and winter, mainly along the meridian of 123°E and 124°E (31°30'N - 36°30'N). Locations of observation stations are shown in Fig. 1 in November, 1986; February and October, 1987; January, April and August, 1988; October, 1989.

The chemical components analyzed in this study, and the measurement methods are shown in Table 1.

A samples of sea water were filtered by glass fiber filter (GF/F) for the measurements of nutrients, and by nuclepore filter (0.4μm) for the measurements of other elements. The filtrate and the particulate substances on a filter were subjected to a chemical analysis.

Fig. 1 Oceanographical observation stations.

Table 1 Chemical components analyzed in this study, and measurement methods

Chemical components	Measurement method
Phosphate-phosphorus (PO_4-P)	Absorption spectrophotometry
Nitrate-nitrogen (NO_3-N)	"
Silicate-silicon (SiO_2-Si)	"
Total phosphorus (T-P)	Potassium persulfate decomposition, Absorption spectrophotometry
Total nitrogen (T-N)	" , "
Paticulate phosphorus	" , "
paticulate nitrogen	" , "
Lithium (Li)	Flame spectrophotometry
Boron (B)	ICP spectrometry
Barium (Ba)	"
Copper (Cu)	Solvent extraction, Atomic absorption spectrometry
Cadmium (Cd)	" , "

3. Results and discussion

3.1 Oceanic conditions

The distributions of water temperature, salinity, dissolved oxygen, phosphate-phosphorus and nitrate-nitrogen along the meridian of 123°E in November 1986 (autumn) are shown in Fig. 2. In this section, a vertical mixing reached the 30m depth, and below the 30m depth stratification was established by the existence of the Yellow Sea Cold Water (YSCW) which has low temperature and high salinity. In the southern part of this area (south of 33°N), the vertical mixing reached the bottom, and the concentrations of nutrients were high values. Especially at the station on 32°N, the concentrations were very high. In the northern part of this area (north of 34°N), they were low values in the surface mixed layer, and high values were observed in the YSCW below 50m depth. The reason of this nutrients distribution in the northern part was considered that nutrients were removed from the surface mixed layer by the assimilation of plankton and/or by the adsorption on particles,and the successive regeneration from the settling particles in the YSCW.

The distributions of water temperature, salinity, dissolved oxygen, phosphate-phosphorus and nitrate-nitrogen along the meridian of 123°E in February 1987 (winter) are shown in Fig. 3. Three months had passed since the season of former observation. Water temperature had fallen, and the vertical mixing reached the bottom at all part of this section. The distribution of nutrients indicated that the vertical mixing prevailed in this season.

The distributions of water temperature along the meridian of 123°E in October (autumn) 1987, January (winter), April (spring) and August (summer) 1988 are shown in Fig. 4. In autumn 1987, the vertical mixing reached the 30m depth, and below the 30m depth stratification was established, and below the 50m depth the YSCW existed. This situation was same as in last autumn. In winter 1988, the vertical mixing reached the bottom at all part of this section like as in winter 1987. In spring 1988, the stratification had not established yet. In summer 1988, the clear stratification existed, and extended over the southern shallow area.

In this area, the seasonal variation was observed in the nutrients distribution as mentioned above. In the warm season, the YSCW appeared in the Yellow Sea (the Yellow Sea : the area north of the line which join the Changjiang River mouth to the Cheju Island (Fig. 1)). In winter the Kuroshio water

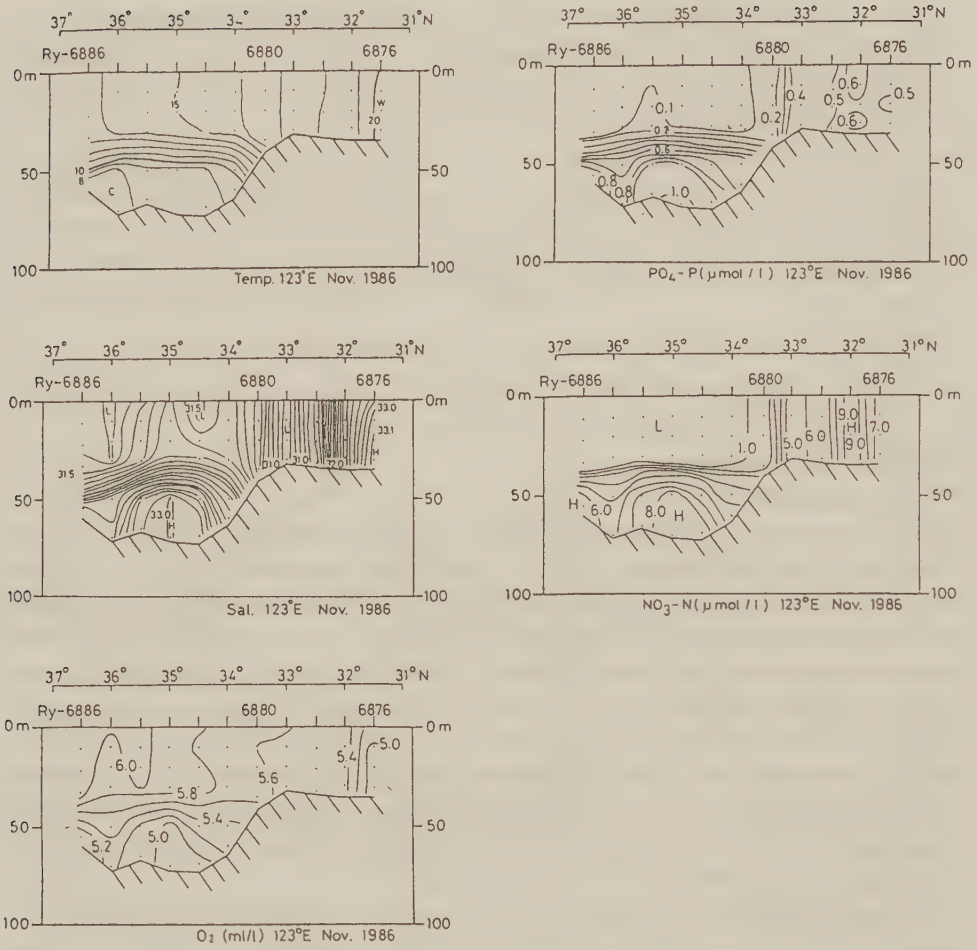

Fig. 2 Water temperature, salinity, dissolved oxygen, phosphate-phosphorus and nitrate-nitrogen along the meridian of 123°E in November 1986.

enters the central part of the Yellow Sea, and mixes with the continental estuary water around itself, and is changed in the quality by the air-sea heat exchange. This water mass is caught in the deeper part in the Yellow Sea (ocean basin) when the stratification begins to form in the warm season. This water mass is named "the Yellow Sea Cold Water", and it has lower temperature and higher salinity than around sea water. The YSCW exists in the warm season, and it disappears by the vertical mixing in winter (KONDO, 1985, TASHIRO *et al.*, 1989).

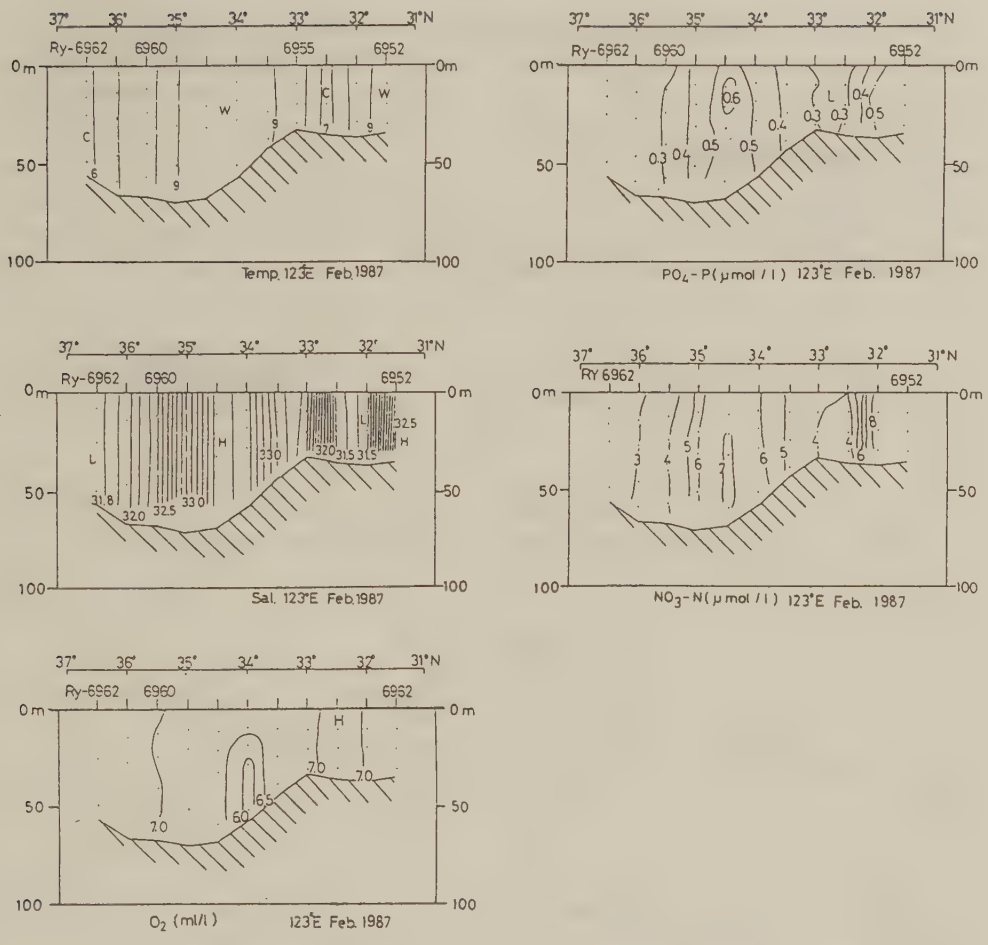

Fig. 3 Water temperature, salinity, dissolved oxygen, phosphate-phosphorus and nitrate-nitrogen along the meridian of 123°E in February 1987.

3.2 The relations between salinity and various chemical components

3.2.1 Lithium, boron, barium and copper

In this area, we measured various chemical components, and investigated the relation to salinity distribution.

The relations of lithium, boron, barium and copper to salinity in October 1987 are shown in Fig. 5. Lithium and boron had positive correlations with salinity respectively. In this area, lithium and boron behaved as conservative elements derived from the open sea water. These elements have the proper as a indicator of the open sea water in the mixing process between the open sea water which contain the Kuroshio water and the continental estuary water. Barium and copper had negative correlations to salinity respectively. In this area, barium and copper behaved as conservative elements derived from

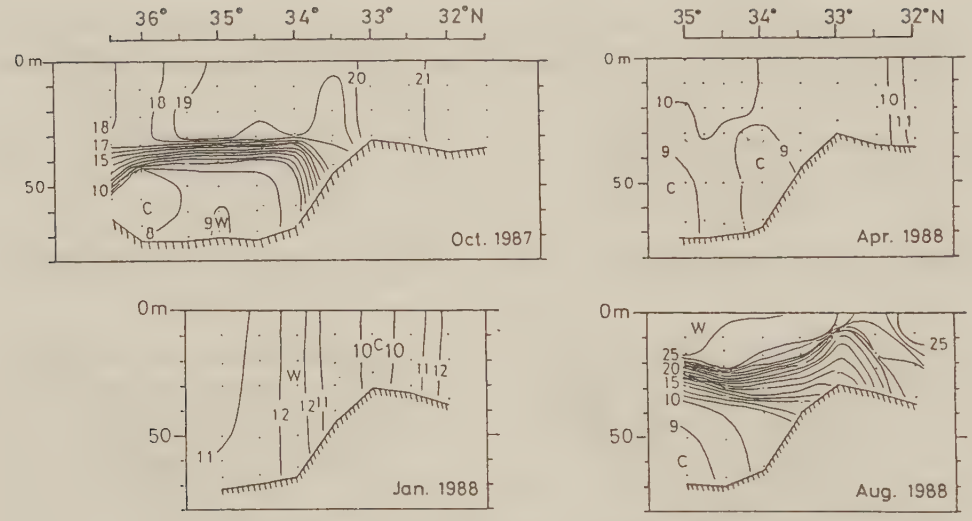

Fig. 4 Water temperature along the meridian of 123°E in October 1987, January, April and August 1988.

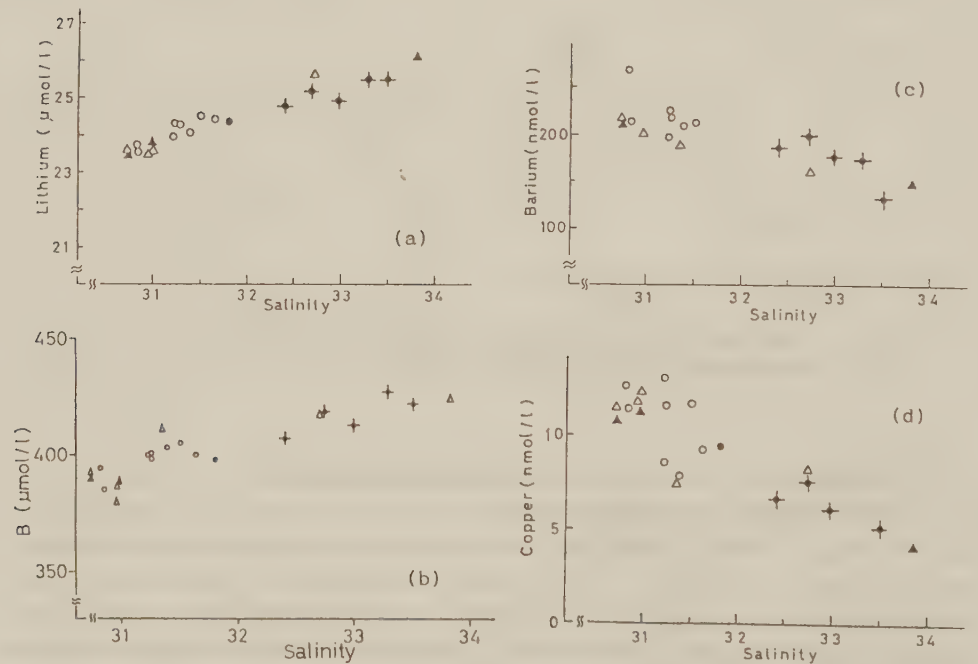

Fig. 5 The relations between salinity and various elements (October 1987).
(a)Lithium, (b)Boron, (c)Barium, (d)Copper.
○ : surface(north of 34°N), ● : subsurface(north of 34°N),
✦ : the Yellow Sea Cold Water,
△ : surface(south of 33°N), ▲ : Subsurface(south of 33°N).

land. These elements have linear relationship with salinity, therefore it is sugested that these elements are supplied from land and diluted simply with the open sea water.

3.2.2 Silicate-silicon

The relations between salinity and silicate-silicon along the meridian of 123°E in October 1987 (autumn) are shown in Fig. 6.

In the northern part of this area (north of 34°N) where the YSCW existed, silicate-silicon had positive correlation to salinity. The reason of this relation was considered that silicate-silicon was removed from the surface mixed layer of low salinity by the assimilation of plankton and/or by the adsorption on

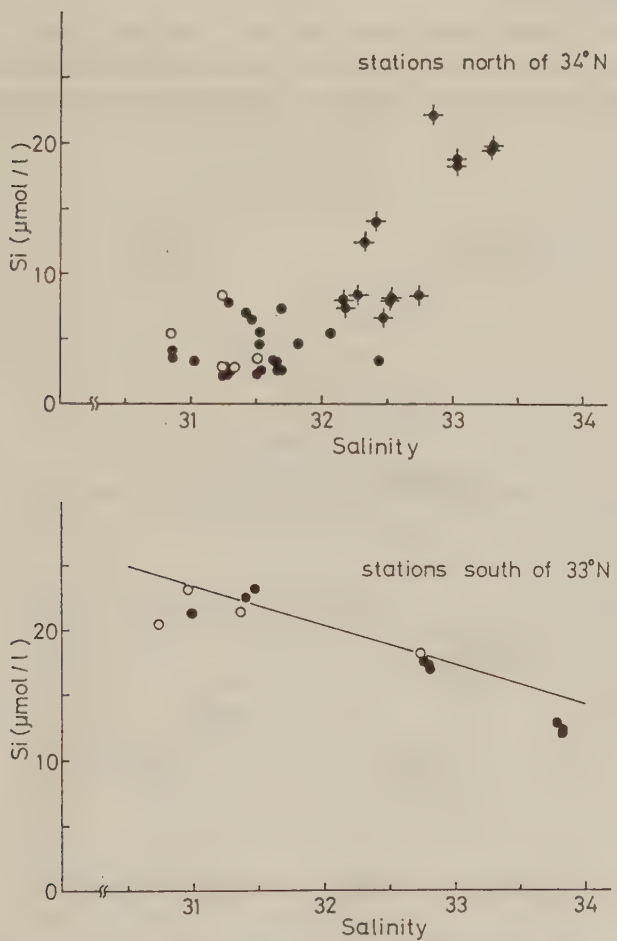

Fig. 6 The relations between salinity and silicate-silicon along the meridian of 123°E in October 1987.
Upper:north of 34°N, Lower:south of 33°N.
○ : surface, ● : subsurface,
✦ : the Yellow Sea Cold Water.

particles, and regenerated from the settling particles in the YSCW which had high salinity.

On the other hand, in the southern part of this area (south of 33°N) silicate-silicon had negative correlation to salinity. The straight line in this figure is similar to the correlation which was reported by Dr. Huang *et al.* (1983) at the inshore region near the Changjiang River mouth in November 1981. In the southern part of this area, silicate-silicon seemed to behave as the conservative component derived from land.

3.2.3 Nitrate-nitrogen

The relations between salinity and nitrate-nitrogen along the meridian of 123°E in October 1987 and 1989 (autumn) are shown in Fig. 7. In this study, the concentration of nitrate-nitrogen included the concentration of nitrite-nitrogen.

In the northern part of this area, nitrate-nitrogen had positive correlation to salinity like in the case of silicate-silicon. On the contrary, in the southern part of this area, nitrate-nitrogen had negative correlation to salinity like silicate-silicon, so that nitrate-nitrogen seemed to behave as the conservative

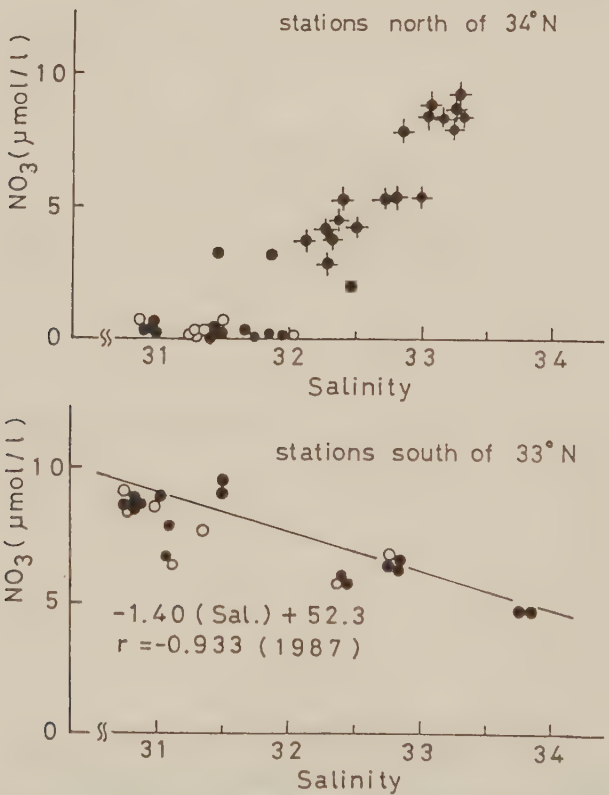

Fig. 7 The relations between salinity and nitrate-nitrogen along the meridian of 123°E in October 1987 and October 1989. Upper:north of 34°N, Lower:south of 33°N.
○ : surface, ● : subsurface,
✦ : the Yellow Sea Cold Water.

component derived from land.

3.2.4 Phosphate-phosphorus

The relations between salinity and phosphate-phosphorus along the meridian of 123°E in October 1987 and October 1989 (autumn) are shown in Fig. 8.

In the northern part of this area, phosphate-phosphorus had positive correlation to salinity like silicate-silicon or nitrate-nitrogen. But in the southern part of this area, the concentration of phosphate did not change against the salinity change. It is suggested that the behavior of phosphate-phosphorus was different from that of silicate-silicon or nitrate-nitrogen in the southern part of this area.

In the area of study, the behavior of nutrients was different from that of other elements such as lithium or etc..

3.3 Relations between nutrients

The relation between nitrate-nitrogen and silicate-silicon in November 1986 (autumn) is shown in

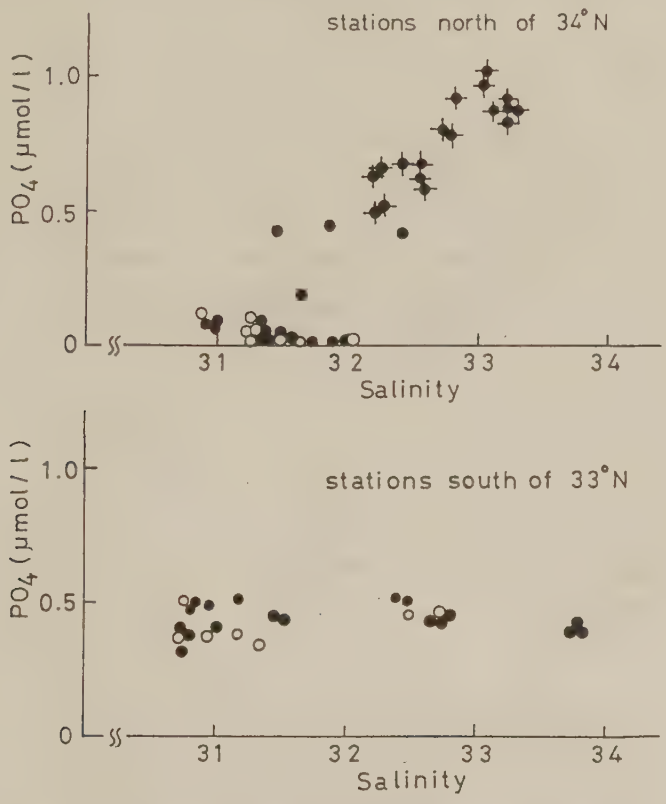

Fig. 8 The relations between salinity and phosphate-phosphorus along the meridian of 123°E in October 1987 and October 1989. Upper:north of 34°N, Lower:south of 33°N.
○ : surface, ● : subsurface,
✦ : the Yellow Sea Cold Water.

Fig. 9. There was a good positive correlation between nitrate-nitrogen and silicate-silicon. It suggested that the behavior of both components was similar.

The relation between phosphate-phosphorus and silicate-silicon in November 1986 (autumn) is shown in Fig. 10. This relation was similar to that between nitrate-nitrogen and silicate-silicon. But in the YSCW, the concentration of phosphate-phosphorus was high as compared with silicate-silicon.

The relation between phosphate-phosphorus and nitrate-nitrogen in November 1986 (autumn) is shown in Fig. 11. There was a positive correlation between phosphate-phosphorus and nitrate-nitro-

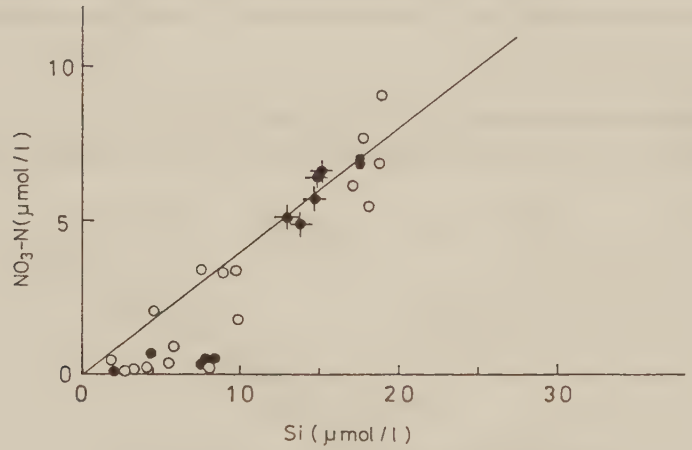

Fig. 9 The relations between nitrate-nitrogen and silicate-silicon in November 1986.
○ : surface, ● : subsurface,
✦ : the Yellow Sea Cold Water.

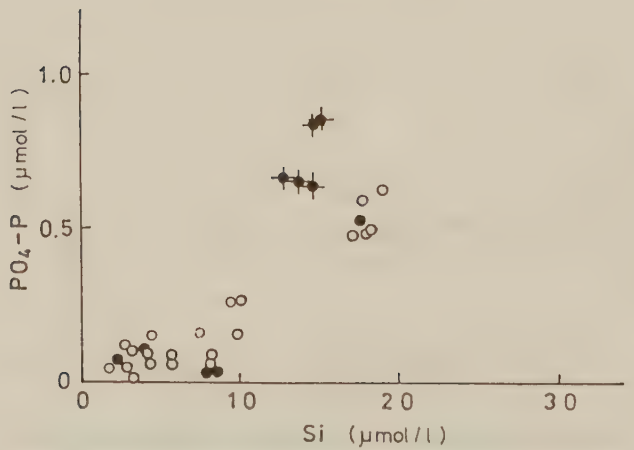

Fig.10 The relations between phosphate-phosphorus and silicate-silicon in November 1986.
○ : surface, ● : subsurface,
✦ : the Yellow Sea Cold Water.

gen. The data, except for that of the YSCW, distributed near the straight line with the slope of 1/15 that was close to the Redfield Ratio of 1/16. But all the data from the YSCW distributed far above this straight line. In autumn, in the YSCW, the concentration of phosphate-phosphorus was in excess as compared with that of nitrate-nitrogen or silicate-silicon. An excess of phosphate-phosphorus was found only in the YSCW, and the existence of an excess phosphate-phosphorus seems to be the characteristic of the YSCW.

The relations between phosphate-phosphorus and nitrate-nitrogen in February 1987 (winter) are shown in Fig. 12. The YSCW disappeared as a result of the whole vertical mixing of water in winter.

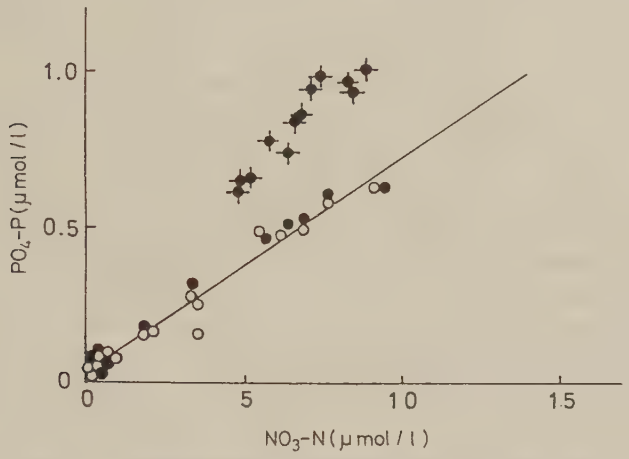

Fig.11 The relations between phosphate-phosphorus and nitrate-nitrogen in November 1986.
○ : surface, ● : subsurface,
✦ : the Yellow Sea Cold Water.

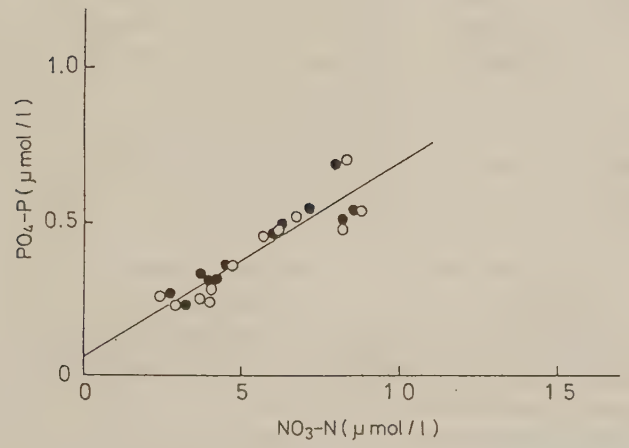

Fig.12 The relations between phosphate-phosphorus and nitrate-nitrogen in February 1987.
○ : surface, ● : subsurface.

There was a good positive correlation between phosphate-phosphorus and nitrate-nitrogen, and every datum distributed near the straight line with a slope of 1/15.9 which was very close to the Redfield Ratio. In winter, the excess of phosphate-phosphorus could not be found at any part of this area. It suggests that phosphate-phosphorus was added in excess into the YSCW when the formation of the YSCW or after the formation of the YSCW.

The relations between phosphate-phosphorus and nitrate-nitrogen in October 1987 (autumn), January (winter) and August (summer) 1988 are shown respectively in Fig. 13. All straight lines in these

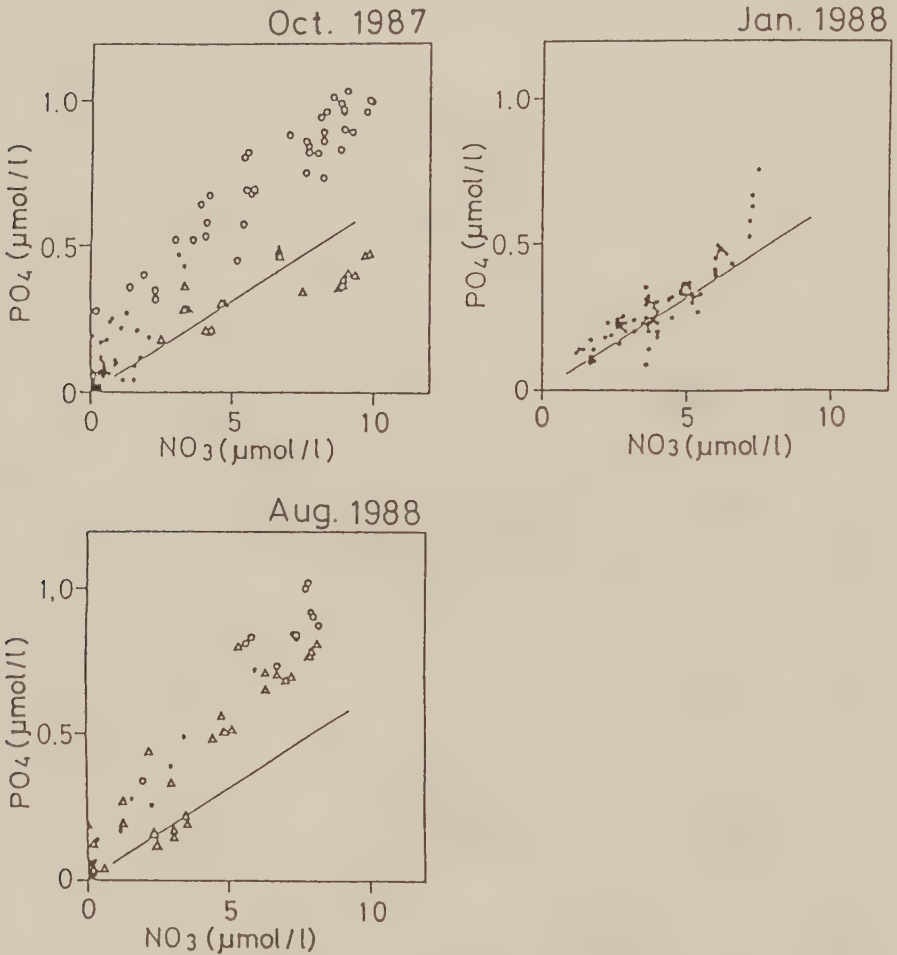

Fig.13 The relations between phosphate-phosphorus and nitrate-nitrogen in October 1987, January and August 1988.
October 1987 and August 1988
○ : the Yellow Sea Cold Water, △ : south of 33°N,
● : the other.
January 1988
● : the whole area.

figures have the slope of 1/16 which is the Redfield Ratio. In autumn the data of the YSCW distributed separately from the data of the southern part of this area. The data, except for that of the YSCW, were close to the Redfield Ratio but in the YSCW concentrations of phosphate-phosphorus were high as compared with nitrate-nitrogen. The similar situation was observed in the last autumn (November 1986). In winter, the data at all part of this area had the close correlation to the Redfield Ratio. The similar situation was also observed in the last winter (February 1987). In the summer of 1988, there was a good positive correlation between phosphate-phosphorus and nitrate-nitrogen, and the data of the YSCW were not separate from the data of the southern part of this area, and the slope was larger than the Redfield Ratio. This means that phosphate-phosphorus existed in excess as compared with nitrate-nitrogen in summer, too.

3.4 The cause of excess of phosphate-phosphorus in the YSCW

In the YSCW, the ratio of phosphate-phosphorus to nitrate-nitrogen was larger than the Redfield Ratio.

It was considered that the increase of inorganic nutrients was caused by a decomposition of an organic matter (LIN and SONG, 1981, SUGIURA, 1970). The relations between AOU (Apparent oxygen utilization) and nutrients in the YSCW were examined in order to understand the process to be able to change the ratio of phosphate-phosphorus to nitrate-nitrogen. The relations between AOU and nutrients in the YSCW are shown in Fig. 14. In summer and autumn, a linear relationship existed between AOU and nutrients. The value of AOU(ml/*l*)/phosphate-phosphorus(μmol/*l*) ratio and AOU(ml/*l*)/nitrate-nitrogen(μmol/*l*) ratio in the YSCW were calculated by using an observed data. The values of the ratio were 0.30 and 3.89 respectively, and these values were similar to those in the open sea (0.33, 4.2). This result indicated that the large value of phosphate-phosphorus/nitrate-nitrogen ratio in the YSCW could not be explained by the selective regeneration of phosphate-phosphorus from an organic matter.

Moreover, it was considered that the excess of phosphate-phosphorus was caused by the elution of phosphate-phosphorus from the interstitial water in a bottom sediment into sea water. The vertical profiles of nutrients in the YSCW were examined for the same purpose. The vertical profiles of nutrients at observation stations where the YSCW existed are shown in Fig. 15. It was reported that the vertical profile of manganese concentration indicated the elution of manganese from a bottom sediment into sea water in the YSCW (NORIKI *et al.*, 1988). But in our observation, a clear vertical gradient which indicated the elution of nutrients from a bottom sediment into sea water, was not found.

3.5 The distribution of phosphorus and nitrogen in various forms

As aforesaid, the behavior of phosphate-phosphorus against salinity was quite different from that of nitrate-nitrogen against salinity in the area south of 33°N. Therefore, we researched not only an inorganic form but also the other forms of phosphorus and nitrogen such as organic and particulate forms for further study on the behavior of these elements in this area.

The distributions of various forms of phosphorus and nitrogen in the area south of 33°N in October 1987 and October 1989, and the observation stations are shown in Fig. 16. The concentrations of dissolved organic form were calculated as differences between the dissolved total and dissolved inor-

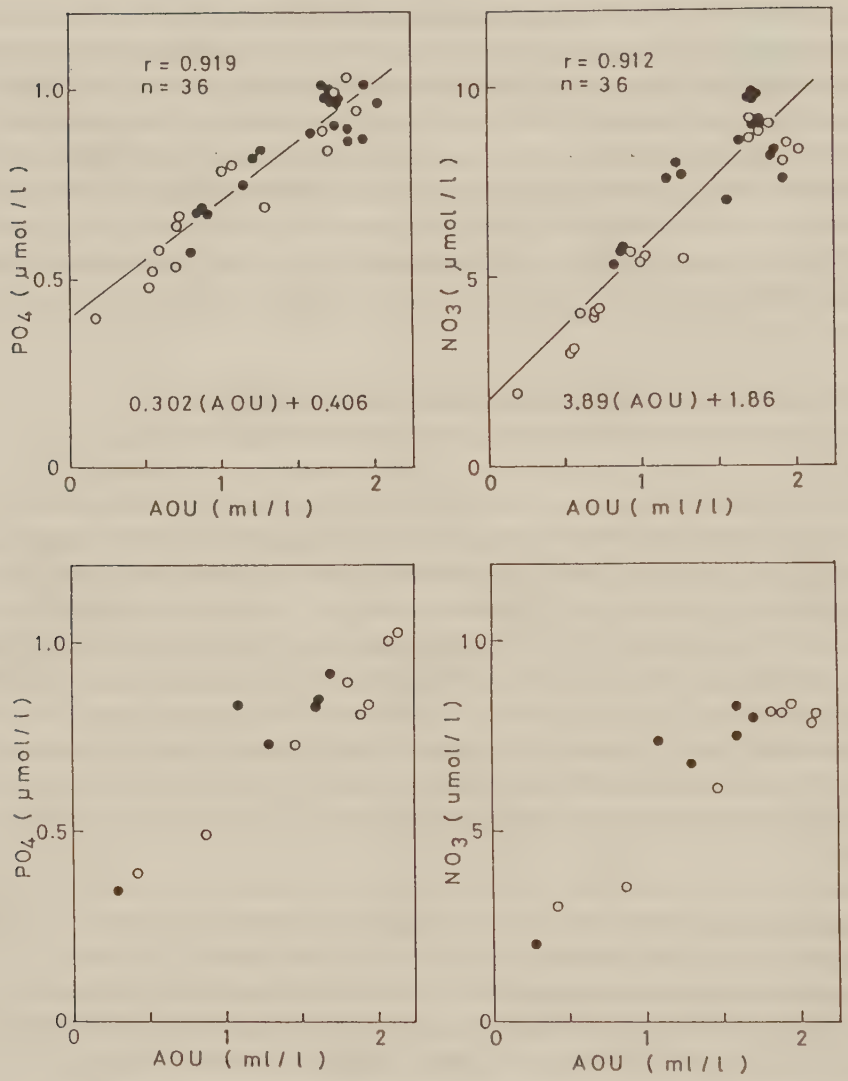

Fig.14 The relations between AOU and nutrients in the Yellow Sea Cold Water.
Upper: October 1987, Lower: August 1988.
○ : 123°E, ● : 124°E.

ganic forms. We call the group of stations at 123°E and 123°30'E, "a", at 124°E and 124°30'E, "b", east of 125°E, "c" respectively. We calculated the mean values of dissolved inorganic-, dissolved organic- and particulate form of phosphorus and nitrogen at each group of stations. We took the total concentration at group "a" as 100%. The mean values of salinity were 31.812 at "a", 31.522 at "b" and 31.821 at "c" respectively. Therefore the mean mixing ratios of open sea water with coastal water were almost the same at all groups of stations.

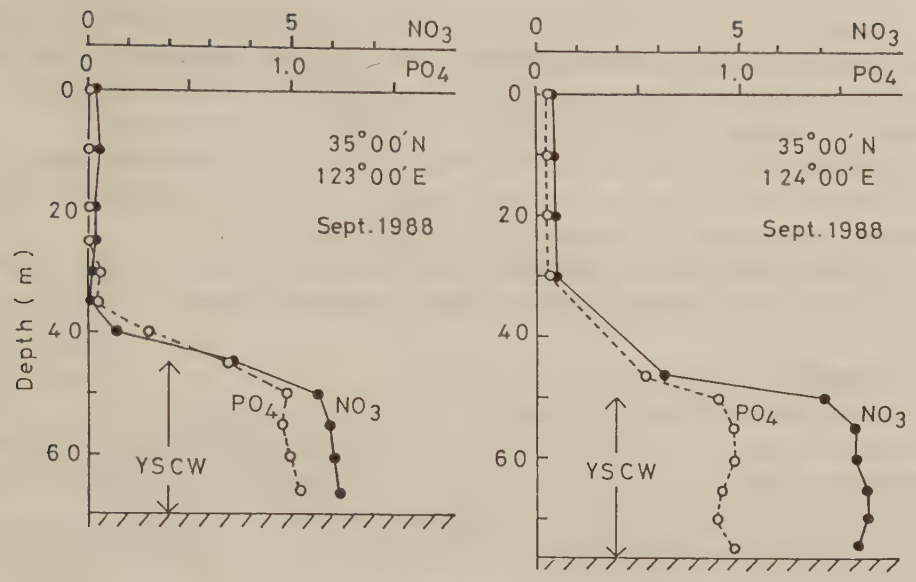

Fig.15 Vertical profiles of phosphate-phosphorus and nitrate-nitrogen (September 1988).

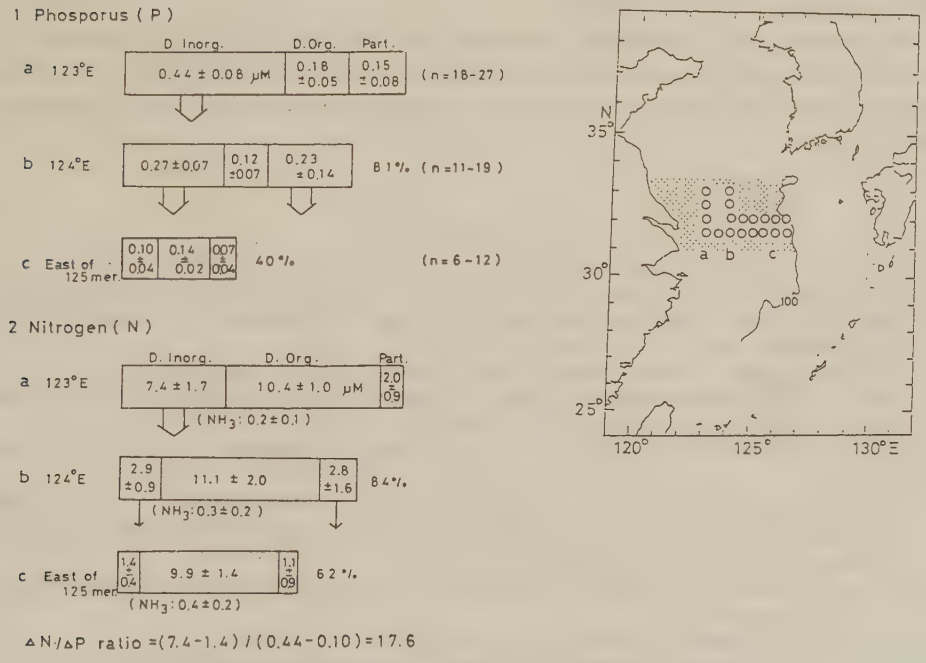

Fig.16 Distributions of dissolved inorganic form (D.Inorg.),dissolved organic form (D.Org.) and Particulate form (Part.) of phosphorus and nitrogen in the area south of 33°N in October 1987 and October 1989, and observation stations.

Phosphorus and nitrogen might be supplied from the coastal area (EDMOND *et al.*, 1981). The total concentration decreased taking distance far from the coastal area. The concentration of a dissolved inorganic form decreased at a large rate. However the concentration of a dissolved organic form almost never changed. The concentration of a particulate form decreased from "b" to "c".

As regarding phosphorus, the dissolved inorganic form amounted to 57% of the total at stations "a". The ratio decreased as far from the coast, and at stations "c", the dissolved inorganic form became almost the same concentration as the dissolved organic and the particulate form.

As regarding nitrogen, the dissolved organic form amounted to 52% of the total at stations "a". The rate increased as far from the coast, and it became 66% of the total at "b", 80% at "c".

4. Conclusion

We have clarified following results in this study.

In the area of this study, lithium and boron have positive correlation with salinity, therefore behave as conservative elements derived from the open sea. Barium and copper have negative correlation with salinity, therefore behave as conservative elements derived from land.

The correlation between salinity and nutrients in the area north of 34°N was different from that in the area south of 33°N.

In the YSCW, phosphate-phosphorus existed in excess as compared with nitrate-nitrogen or silicate-silicon respectively. An excess of phosphate-phosphorus was not brought by the selective regeneration from the oxidation of the organic matter.

In the area south of 33°N, phosphorus and nitrogen which might be supplied from the coastal area, firstly decreased in the dissolved inorganic form as far from the coast, and successively decreased in the particulate form. The concentrations of the dissolved organic form almost never changed in the whole studied area.

References

EDMOND, J. M., E. A. BOYLE, B. GRANT and R. F. STALLARD (1981) : DeepSea Res., 28, 1339-1374.

HUANG, S., J. YANG, W. JI, X. YANG and G. CHEN (1983) : Silicon, Nitrogen and Phosphorus in the Changjiang River Mouth Water. *Proceedings of International Symposium on Sedimentation on the continental Shelf, With Special Reference to the East China Sea*, **1**, 241-250.

KONDO, M.(1985): Study on oceanic conditions at fishing ground in the East China Sea and Yellow Sea-1 (Distribution of average water temperature and salinity in the 50m depth and the bottom layer). *Bulletin of Seikai Region Fisheries Research Laboratory*, **62**. (in Japanese)

LIN, J. and W. SONG(1981) : Basic characteristics of the Yellow Sea Cold Water Mass. *Ocean study*, **4**, 1-16. (in Chinese)

NORIKI, S., M. MIYAGAWA and S. TSUNOGAI (1988): Elution of manganese from sediment on the continental shelf in the East China Sea and Yellow Sea and transfer to the open sea. *Abstract of the 1988 spring meeting of the Oceanographical Society of Japan*, 236-237. (in Japanese)

SAGI, T. and S. ARAKAWA (1982) : Budget of the phosphorus in the East China Sea. *KER annual contribution*, **5**, 188-191. (in Japanese)

SUGIURA, Y. (1970) : Ocean and Chemistry. Kyoritsu-Shuppan, Tokyo. (in Japanese)

TASHIRO, T., T. URASHIMA and T. SHIMIZU (1989) : Formation, movement and mixing process of the Yellow Sea Cold Water. *KER annual contribution*, 85-95. (in Japanese)

東海及び黄海における化学物質の分布と挙動

今井　正直・伏見　克彦・大山　準一
（気象庁海洋気象部）

小川　　完
（舞鶴海洋気象台）

1986～1989年に，東海及び黄海において123°Eと124°Eに沿った観測線（31°30'N～36°30'N）を中心に観測を行なった．

この海域においては，リチウム（Li）とホウ素（B）は外洋起源の元素としての保存性を示し，バリウム（Ba），銅（Cu）は陸起源の元素としての保存性を示した．

秋季には，海域の南部では硝酸対窒素に対するリン酸態リンの比（PO_4-P/NO_3-N）はレッドフイールド比に近いが，黄海冷水中ではレッドフイールド比よりも大きかった．PO_4-P/NO_3-Nの比が大きい原因を調べるために黄海冷水中の栄養塩とＡＯＵの相関及び黄海冷水中の栄養塩の鉛直分布を調べた．しかし，原因と考えられた有機物からのPO_4-Pの選択的な分解や，海底からのPO_4-Pの溶出はみられなかった．

冬季になるとこの海域の全域で海底まで鉛直混合が起こり，黄海冷水は消滅した．PO_4-P/NO_3-Nは全域でレッドフイールド比に近かった．

平成6年3月31日発行

編集兼
発行人　気象庁
JAPAN METEOROLOGICAL AGENCY
東京都千代田区大手町1－3－4
3-4, Otemachi-1, Chiyoda-ku, Tokyo, 100

印刷所　内外印刷株式会社
東京都中央区八丁堀2－22－8